8-2014

Building Envelope Failure Assessment of Residential Developments Subjected to Hurricane Wind Hazards

James Grayson
Clemson University, jmgrays@g.clemson.edu

BUILDING ENVELOPE FAILURE ASSESSMENT OF RESIDENTIAL DEVELOPMENTS SUBJECTED TO HURRICANE WIND HAZARDS

A Dissertation
Presented to
the Graduate School of
Clemson University

In Partial Fulfillment
of the Requirements for the Degree
Doctor of Philosophy
Civil Engineering

---

by
James Michael Grayson
August 2014

Accepted by:
Dr. Weichiang Pang, Committee Chair
Dr. Scott D. Schiff
Dr. Nigel B. Kaye
Dr. Firat Y. Testik

ABSTRACT

An unfortunate global precedent has been set by hurricane wind hazard events that illustrate the importance of building resilient coastal communities. Although community resilience is heavily dependent upon the socioeconomic response of the community before, during, and after a hazard event, it is also dependent on the vulnerability of the community to a disaster. Therefore, one way that structural engineers can assist communities in becoming more resilient is to investigate and implement methods that mitigate the "initial shock" experienced by a residential development subjected to a hazard event.

The focus of this research was to develop a mechanics-based building envelope failure assessment model for light-frame wood construction subjected to hurricane wind hazards, and then assess the performance of a residential development to a 700-year mean recurrence interval hurricane wind event. A component-based approach was taken to develop an integrated building envelope model based on previous research of individual component capacities. Key modules of the building envelope failure assessment model include a hurricane simulation module, a probabilistic three-dimensional wind-borne debris trajectory module, a debris generation module, and a wind-borne debris impact-tracking module.

The developed building envelope failure assessment model is capable of providing the time evolution of building envelope damage experienced by the individual buildings within a residential development, and is implemented to investigate how the building stock within a low-rise residential development reacts to various levels of vulnerability.

A typical South Carolina (SC) residential development was selected and modeled within the developed building envelope failure assessment model to illustrate how an actual residential development may perform when subjected to hurricane wind hazards. Initially, the building envelopes were assumed constructed using low-capacity building components and techniques to simulate a vulnerable development. Vulnerability was reduced progressively within the residential development by increasing the percentage of homes retrofitted against hurricane wind hazards using currently available retrofit techniques, such as roof sheathing attachment supplemented with closed-cell spray foam, the installation of wind-resistant roof shingles, and the installation of window impact protection. Results confirm that a fully retrofitted residential development demonstrates a more robust performance with the fully retrofitted residential development exhibiting an approximately 49% increase in the final building envelope survival over the unretrofitted residential development. These results have the ability to assist government officials, developers, designers, and homeowners with the information necessary to build more resilient and better-prepared communities exposed to hurricane wind hazard events. There is also the potential for this research to provide insurance companies with the information necessary to set insurance premiums within hurricane–prone regions – which is becoming increasingly more important as more of the global population continues to settle in wind hazard-prone areas.

DEDICATION

I dedicate this work to my wife, Carmen, and my sons, Matthew and Nathan.

ACKNOWLEDGEMENTS

I would like to thank Dr. Weichiang Pang for his guidance, patience, and advice – on life and research. I truly believe that I would not have reached this goal with any other advisor. I would like to thank my committee members, Dr. Scott D. Schiff, who has provided unlimited knowledge and experience during my research and education, Dr. Nigel B. Kaye, who has provided me with invaluable feedback during our research discussions, and Dr. Firat Y. Testik for assisting me when I needed it most. I am grateful for the contributions that each of you has made during my time at Clemson University, and I sincerely hope that we have many more opportunities to collaborate in the future.

A special thank you is reserved for Fangqian (Abby) Liu, Bin Pei, and Saurabh Prabhu whose friendship and assistance have been invaluable to me. I will never be able to repay any of you for your contributions. Additionally, I would like to thank the Clemson University Cyberinfrastructure Technology Integration (CITI) group for their assistance in utilizing the Palmetto Cluster during the course of this research.

Finally, I would like to thank my family for their unwavering support over the long course of my undergraduate and graduate studies. At times, it seemed like a never-ending journey, but you were always there for me when I needed it most – reminding me to give my best – and supporting me even when it seemed that my best was not good enough.

SPONSORS

This material was prepared as a result of work sponsored by the South Carolina Sea Grant Consortium (SCSGC) with National Oceanic and Atmospheric Administration (NOAA) financial assistance award NA10OAR4170073, and the National Science Foundation (NSF) Graduate Research Fellowship under Grant No. 2008430. The statements, findings, conclusions, and recommendations are those of the author and do not necessarily reflect the views of the SCSGC, NOAA, or NSF.

CO-AUTHORSHIP

- Parts of Chapters 1, 2, and 6 have been published in the following paper:

  Grayson, J.M., Pang, W., and Schiff, S. (2013a). "Building envelope failure assessment framework for residential communities subjected to hurricanes." *Eng. Struct.* 51, 245-58.

- Parts of Chapters 1, 3, and 6 will be submitted for publication in the following paper:

  Grayson, J.M., Pang, W., and Schiff, S. "Consideration of exogenous wind-borne debris in a mechanics-based building envelope failure assessment model." *Probab. Eng. Mech.* (in preparation).

- Parts of Chapters 1, 4, 5, and 6 will be submitted for publication in the following paper:

  Grayson, J.M., and Pang, W. "The influence of hurricane wind hazard mitigation retrofits on residential development performance." *J. Archit. Eng.*, special section on housing and residential building construction (in preparation).

TABLE OF CONTENTS

Table of Contents (continued)

Page

LIST OF TABLES

List of Tables (continued)

Table Page

LIST OF FIGURES

List of Figures (continued)

Figure Page

List of Figures (continued)

Figure Page

List of Figures (continued)

Figure Page

List of Figures (continued)

Figure Page

1 INTRODUCTION

1.1 Motivation for More Resilient Communities to Hurricane Wind Hazards

Community resilience is a topic that has gained considerable momentum over the past decade. This momentum is driven predominantly by an increase in socioeconomic losses due to disasters experienced in many areas around the world. A significant portion of these losses can be attributed to natural hazards, with many areas at significant risk for extreme tropical wind events (i.e., hurricanes, typhoons or cyclones – henceforth referred to as hurricanes). Therefore, it is crucial that steps be taken to ensure that these socioeconomic losses are reduced through appropriate strategies worldwide.

Pielke et al. (2008) estimates that the average annual normalized damages that can be attributed to hurricane damage in the United States (U.S.) are $10 billion (2005 U.S. dollars). These significant average annual losses coupled with the continued increase in the U.S. coastal population, with approximately 39% of the population living in coastal shoreline areas (U.S. Census Bureau 2011; NOAA 2011), warn of a severe future in which the damages attributed to hurricanes in the U.S. have the potential to increase significantly. This future may very well become a reality unless changes are made that address the rate of population growth in hurricane-prone regions, the improvement and implementation of building standards and codes, and/or the consideration of other mitigating factors that will effectively reduce these damages (Pielke et al. 2008). Based on this outlook, it is evident that more research is needed that promotes more resilient communities in U.S. areas at risk from hurricane events.

1.2 Identified Resilience Research Needs

The National Science Board (NSB) released *Hurricane warning: The critical need for a national hurricane research initiative* in 2007, which reveals that, despite the advances in hurricane research over the previous decade, there is still relatively little know about the most important aspects of hurricanes. The NSB (2007) builds a focus on hurricane science and engineering that could provide near–term benefits, such as protecting lives and property, and reducing the economic impact of hurricanes, and long-term benefits that will increase the resilience of the U.S. to hurricanes through improved building standards and a greater understanding of hurricane risk by the public. A high priority is assigned to developing a better understanding of the interaction of hurricanes with engineered structures, noting that current risk prediction models are highly parameterized and overly simplified. Additionally, the NSB states that assessing and improving the resilience of the built and social infrastructure is extremely important to response and recovery efforts, noting that additional studies are needed to identify and prioritize the most cost-effective mitigation strategies and improvements.

Gaynor and Simiu (2007) recognize the importance of developing loss estimation methodologies on the community scale, noting that the majority of losses during hurricane events occur once the building envelope of a structure is breached allowing wind and wind-driven rain to enter. They conclude that the performance of the built environment is a significant factor in determining the overall resiliency of the community, while recognizing that community resilience is also heavily dependent on societal factors. The National Science and Technology Council (2008) reiterates many of

the findings of Gaynor and Simiu (2007) while further identifying that improved structural design and the implementation of non-structural mitigation measures will increase the resiliency of a community.

The National Research Council (NRC) provides a vision of the characteristics of a resilient community in the year 2030 (NRC 2012). These characteristics identify a community in which the public and private sectors work cooperatively towards a risk management strategy that includes structural and nonstructural risk-reduction measures and tools. Such tools might include codes, standards, and guidelines that drive the critical structural functions of resilience and investment in risk-based pricing of insurance.

The National Institute of Standards and Technology (NIST) (McAllister 2013) provide a research needs assessment that is focused on developing guidelines and standards that promote a more resilient physical infrastructure. Short-term activities (i.e., within three to five years) recommended by NIST identify technical gaps from reviews of past disaster and existing model codes and standards, define resilience terminology for the built environment to help communicate new concepts, and develop guidance for community resilience planning. Long-term activities (i.e., greater than three to five years) should seek to develop risk-based performance goals for resilient communities, develop tools and metrics to support quantitative technical assessment, policy development, and decision making, and develop guidelines on risk-based performance goals and criteria for inclusion in standards for voluntary reference.

1.3 Definition of Community Resilience

Resilience is generally thought of as an ability to recover from a sudden shock to a system, or in this case a community. Buckle et al. (2000) conclude that resilience is a quality of the people, agencies, and infrastructure of a community that reduces vulnerability, but further stipulate that resilience is not merely the absence of vulnerability, but rather the ability to mitigate or prevent losses before damage occurs, and to manage recovery and maintain normal living conditions after damage occurs. This definition of resilience is significant in that it suggests that the current coastal community paradigm of "build-disaster-rebuild" is no longer a viable model in preparing for the future, especially considering that forecasted hurricane events could potentially increase in intensity (Emanuel 2013; HUD 2013; Liu and Pang 2013). It seems that it would be much more effective to replace the current paradigm with the more resilient "build-event-recover" model (Ewing and Synolakis 2011), in which the community exhibits enough resilience to absorb the hazard event so that the damages incurred by the community do not degenerate to disaster levels as illustrated in Figure 1.1.

1.4 Resilience of Residential Communities to Hurricane Wind Hazards

It is evident from the damage incurred by coastal communities during extreme hurricane events, such as Hurricane Hugo, Hurricane Andrew, Hurricane Katrina, Hurricane Sandy, and most recently Typhoon Haiyan, that if populations are going to continue to live in coastal areas then coastal communities must become more resilient to extreme hurricane events. The development of resilient residential coastal communities

will rely on the identification of cost effective mitigation practices that reduce the socioeconomic losses experienced by coastal communities subjected to extreme hurricane events.

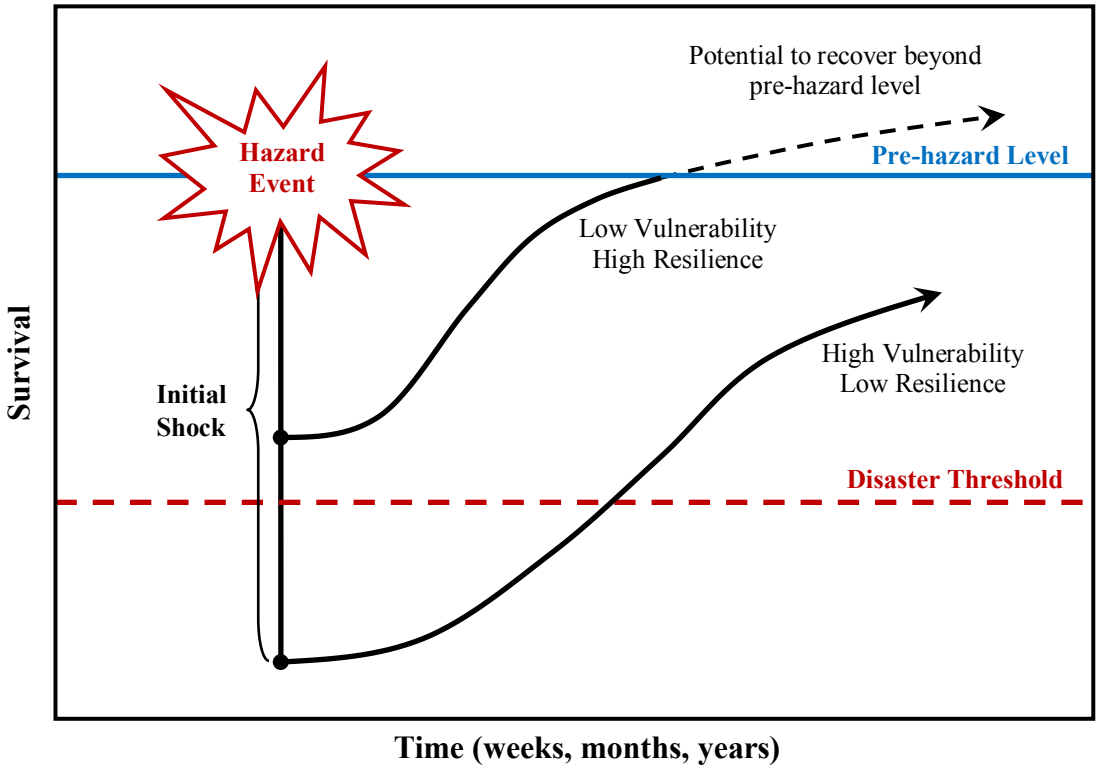

Figure 1.1: Graphical definition of community resilience. Figure is adapted from the U.S. Agency for International Development (2007).

There have been very few studies that directly investigate the resilience of a community to hurricane wind hazards. Tokgoz (2012) presents a comprehensive resilience study developed for single or multiple buildings within a community for single hurricane events. A two-parameter type III smallest extreme value (Weibull) distribution is used to generate the range of wind speeds for each category of hurricane considered (i.e., Saffir-Simpson Hurricane Wind Scale categories one, two, and three) coupled with

damage curves that were estimated from the HAZUS-MH technical manual (FEMA 2003). Tokgoz (2012) modifies previous earthquake resilience research to provide the base definition of resilience as the functionality of a system (e.g., Bruneau et al. 2003; Bruneau and Reinhorn 2007) and then define the functionality of that system (e.g., Cimellaro et al. 2010) in order to assess the resilience of the community to the hurricane wind hazard.

1.5 Research Objectives

A significant issue with attempting to quantify the hazard resilience of a community from the perspective of structural engineering is that community resilience is heavily dependent on socioeconomic factors that determine the recovery time of a community after exposure to a hazard event. Current hazard resilience studies assume simplified recovery functions in order to estimate the recovery time of a community subjected to a hazard event (e.g., Cimellaro et al. 2010; Tokgoz 2012). However, the intent of this research is not to estimate the resilience of a community to hurricane wind hazards based on assumed recovery functions, but rather to investigate how mitigating the initial shock experienced by a residential development can prevent a hurricane wind hazard event from becoming a hurricane wind disaster event. The representation of the community building stock on a more detailed component level than is available from current hurricane wind damage assessment models is useful for incorporating the community recovery process. The detailed damage and subsequent recovery information will provide the ability to perform community life-cycle resilience assessments while considering scenarios such as

the occurrence of back-to-back hazard events (i.e., another hazard event occurring before community recovery is completed from the first hazard event) which may be more difficult with less detailed and/or less flexible damage assessment models.

This investigation addresses the performance of residential developments subjected to hurricane wind hazards and is accomplished through two main objectives. The first objective is the development of a mechanics-based building envelope failure assessment (BEFA) model. The BEFA model is capable of quantifying the damage incurred by individual building envelopes due to direct wind pressure loading and wind-borne debris impact within a residential development on a more detailed scale than many current hurricane damage assessment models. The BEFA model utilizes previous peer-reviewed research as a foundation for the model and is modular in nature to facilitate the expansion of the model as new resilience research or updated information becomes available.

The second objective is the implementation of the BEFA model to investigate the influence that the percentage of homes retrofitted within a residential development has on the response of the residential development to a design-level hurricane event. This objective illustrates the response of the residential development to the initial shock inflicted by a hurricane wind hazard event, and further demonstrates how mitigation can prevent a hazard event from becoming a disaster event. This objective is significant in that it determines the amount of damage from which the residential development must recover, which is critical information needed to assess the resilience of a community exposed to hurricane wind hazards.

2 BUILDING ENVELOPE FAILURE ASSESSMENT FRAMEWORK FOR RESIDENTIAL DEVELOPMENTS SUBJECTED TO HURRICANES

2.1 Introduction

Wind-related disasters are typically among the costliest natural disasters to occur in the U.S. each year. With the majority of residential structures in the U.S. consisting of light-frame wood construction, coupled with an ever growing U.S. coastal population, it is intuitive that there has been and will continue to be an exponential increase in socioeconomic losses due to hurricanes and other strong wind events. Post-hurricane damage assessments have illustrated that the bulk of losses experienced by residential structures during a hurricane is attributed to damage to the building envelope, typically due to wind-borne debris impact. Traditionally, this exterior envelope has not been designed by structural engineers (Rosowsky and Schiff 2003), and as such, extensive damage to building envelopes has been observed after every major hurricane to make landfall in the U.S.

Many studies have sought to quantify residential damage incurred during extreme wind events (e.g., Gurley et al. 2005; Li and Ellingwood 2009; Lin 2010; Pinelli et al. 2004; Vickery et al. 2006b; Yau et al. 2011). However, few studies within the public domain develop an integrated assessment model that can explicitly track and apply the consequences of cumulative damage to the building envelope due to applied wind pressure and wind-borne debris impacts. In addition, many current studies are relegated to using a static building inventory when in reality the building stock within a region (e.g., residential development, county, state) can change significantly over time (Jain and

Davidson 2007). The subsequent discussion represents the foundation research that is utilized in some capacity during the development of the proposed building envelope failure assessment (BEFA) framework.

Twisdale et al. (1996) developed an integrated risk assessment model to investigate the wind-borne debris impact risk of residential structures. This model utilizes numerical models to simulate the hurricane windfield and the wind-borne debris generation, trajectory, and impact to estimate the overall (i.e., mean) wind-borne debris risk of a residential area of interest. The HAZUS-MH model (Vickery et al. 2006a; 2006b) is a multi-hazard loss prediction model (i.e., earthquakes, floods and hurricanes) that utilizes a simplified version of the Twisdale et al. (1996) wind-borne debris risk model as part of its wind load model to assess the aggregate damage of an individual structure exposed to time-dependent hurricane wind speeds and directions. The Florida Public Hurricane Loss Projection Model (FPHLPM) (Gurley et al. 2005) is a hurricane loss prediction model capable of predicting annualized or storm-specific hurricane-induced losses of residential structures for zip code delineated areas within Florida. The FPHLPM is a component-based vulnerability model similar to the HAZUS-MH model; however, the FPHLPM averages the structural performance of an individual structure for specific wind directions at a pre-determined wind speed without considering aggregate damage.

Li and Ellingwood (2006; 2009) use a first-order reliability analysis to develop building component fragilities and identify uncertainties in structural system capacities and demands during extreme wind events. The resulting limit states are useful in quantifying expected losses to residential construction, and in developing and evaluating

mitigation techniques that may aid in risk management. Lin (2010) and Yau et al. (2011) extend the vulnerability model concept initiated by HAZUS-MH and the FPHLPM through an integrated vulnerability model (Lin et al. 2010) that explicitly accounts for the correlation between wind-borne debris damage and wind pressure damage. The integrated vulnerability model was developed by coupling a pressure-damage model devised from the component-based model of the FPHLPM with the wind-borne debris risk model developed by Lin and Vanmarcke (2008; 2010). Dao et al. (2012) present a methodology for assessing the probability of damage to windows within a residential housing development subjected to a hurricane. A significant aspect of the study performed by Dao et al. (2012) is that it investigates the relationship between the timing of the building envelope breech as the hurricane passes by and the subsequent losses experienced by the building. Recently, Herbin and Barbato (2012) have presented a methodology for developing fragility curves for building envelope components and protection systems subjected to wind-borne debris impact. These fragility curves are developed through finite element modeling and Monte Carlo simulation with the results specifically developed for use within a performance-based wind-engineering framework.

It is crucial that subsequent research into building envelope failures due to hurricane wind hazards continues to build upon these previous studies in order to determine which areas of the building envelope are critical to protect when faced with an approaching hurricane. This chapter proposes a modular framework that expands upon current research by providing the user with the flexibility to investigate an unlimited number of "what if" scenarios with the goal of providing a useful tool that can be utilized either pre-

or post-construction to aid officials, developers, architects, designers, and homeowners in mitigating the losses experienced during such an event.

2.2 Overview of the Building Envelope Failure Assessment (BEFA) Framework

The proposed BEFA framework is best broken down into three phases (see Figure 2.1). This is a necessary step in the evolution of the framework to ensure that it performs as computationally efficient as possible. It is crucial that the subject of efficiency is considered within a framework that incorporates a greater level of detail, especially if a simpler model would achieve reasonable results in a shorter timeframe. However, it is beneficial to pursue a more intricately detailed framework as it is essential in investigating the influence of various attributes (e.g., building orientation and location, number of stories, gable vs. hip roofs, etc.) common to residential developments.

The pre-processing phase begins with the user defining all parameters related to the area of interest (i.e., residential development). These parameters include, but are not limited to: the selection of the type of hurricane event (i.e., historical or synthetic), the spatial and temporal window of the area of interest, orientation and dimensions of the individual buildings, probabilistic and/or deterministic capacities of components, and the impact resistances of the vulnerable components (i.e., windows and doors). From the user-defined parameters, the Building Module constructs the area of interest into a data file that can be passed into the processing phase. The compilation of the data files outside of the processing phase reduces the computational overhead considerably, and it provides

the user the flexibility to compile any number of input files and/or databases in advance of the simulations.

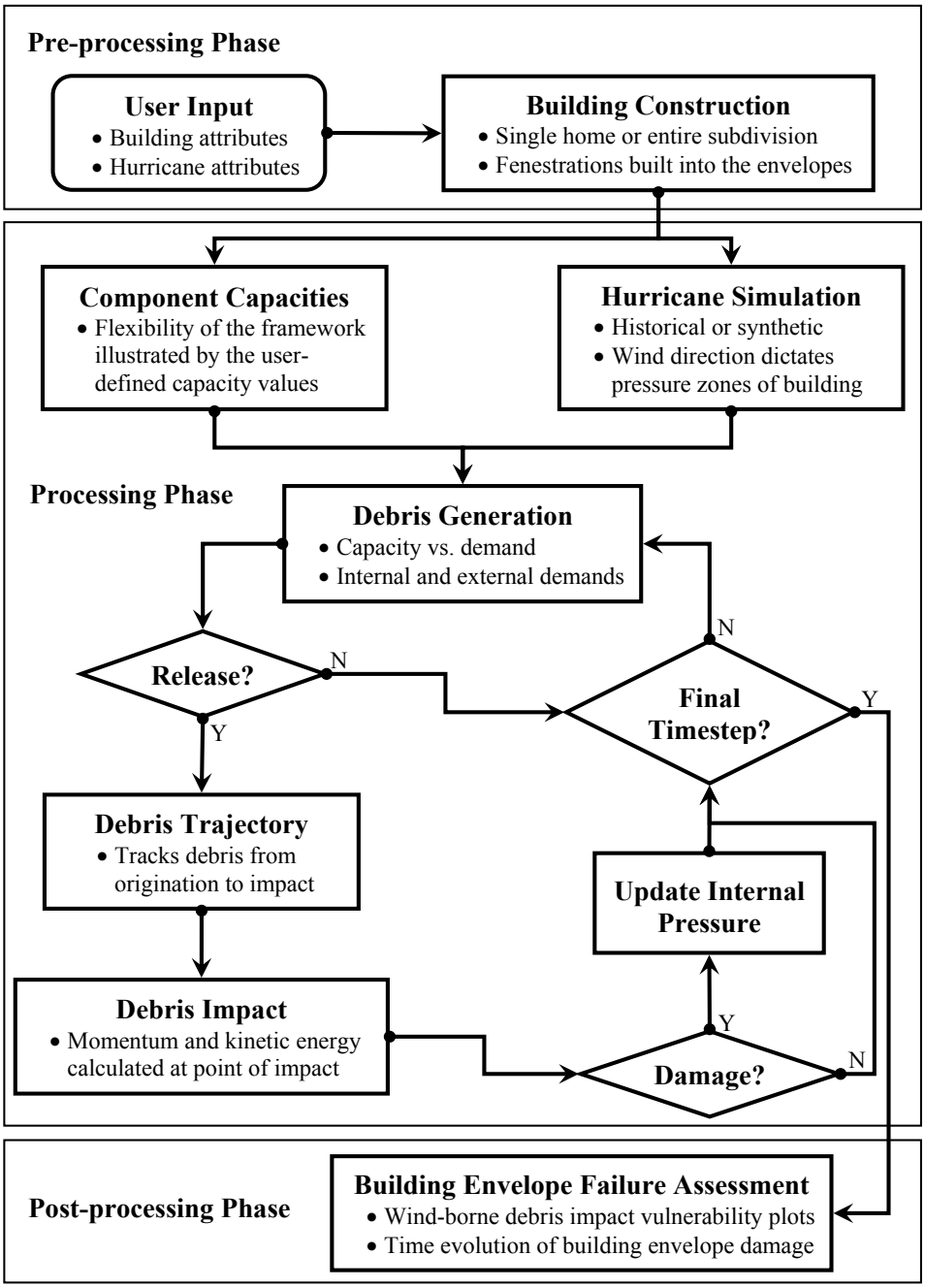

Figure 2.1: Flowchart of the building envelope failure assessment (BEFA) framework.

The processing phase is comprised of the Monte Carlo simulation engine used to perform the building envelope failure assessment. It is during this phase that the residential development is subjected to the historical or synthetic hurricane(s) selected by the user. The building component resistances are sampled from their respective distributions, derived either from test data or from analytical studies, and the simulation then proceeds into an iterative loop that evaluates the area of interest at each time step. The peak wind gust speed experienced by each building within the area of interest is determined from the generated mean wind speeds from the Hurricane Simulation Module. These peak gust wind speeds are used to calculate the peak wind pressures experienced by the individual homes. These calculated peak wind pressures are applied to each building within pressure zones based on building orientation, wind direction, and the building enclosure classification. The Debris Generation Module compares the wind and impact loads (i.e., demands) to the assigned component resistances (i.e., capacities) and determines if wind-borne debris are generated from the individual building envelopes at each time step. If there is a release of wind-borne debris, the information is passed to the Debris Trajectory Module, which is driven by a three-dimensional (3D) probabilistic wind-borne debris trajectory model (Grayson 2011; Grayson et al. 2012) that tracks the path of the individual debris released. Any wind-borne debris trajectories that occur are passed to the Debris Impact Module and assessed for impacts and/or damage to the vulnerable components. If damage to the building envelope does occur, the information is passed back to the Debris Generation Module to determine if an adjustment in the enclosure classification, and by extension the internal pressure for a particular building, is

warranted and the simulation proceeds to the next time step. After completion of the last time step of the user-defined temporal window, output files are generated for analysis in the post-processing phase.

The post-processing phase encompasses all analysis other than that required to update the framework during a particular simulation. Due to the computational requirements of a simulation, any extraneous analysis performed during the simulation causes a significant reduction in computational efficiency. The output files provide information for each time step of the user-defined temporal window, including, but not limited to: the amount and type of debris released from each building, impacts created by the debris released from each building, the source and impacted buildings for a particular piece of debris, and the aggregate damage to the individual building envelopes.

Within the three phases of the framework (i.e., pre-processing, processing, and post-processing), each phase contains individual modules tasked with a specific portion of the simulation. The modular nature of the framework allows for easier updating and validation as more realistic test data, such as that obtained from full-scale test facilities (e.g., the Institute for Business and Home Safety, and the "Three Little Pigs" Project at the University of Western Ontario (Kopp et al. 2012)), are made available.

2.2.1 Building Module

The Building Module is capable of generating rectangular plan, gable and hip roof structures of one or more stories (see Figure 2.2). This module is utilized outside of the simulation (i.e., in the pre-processing phase) to reduce the computational time required to

perform the simulations, and is capable of creating house models that consist of roof and wall sheathing, roof covering, and roof planks (e.g., truss members and fascia boards). Wall covering (e.g., vinyl siding, brick veneer, etc.) is not accounted for explicitly in the framework, other than to assume that a brick veneer or masonry wall does not generate debris or allow for the release of wall sheathing. Other types of wall covering (e.g., vinyl siding), are assumed too flexible to create appreciable damage if they were to become airborne and are considered to be adequately removed from the building model before wind speeds generate the pressures required to remove wall sheathing (Reinhold et al. 2000).

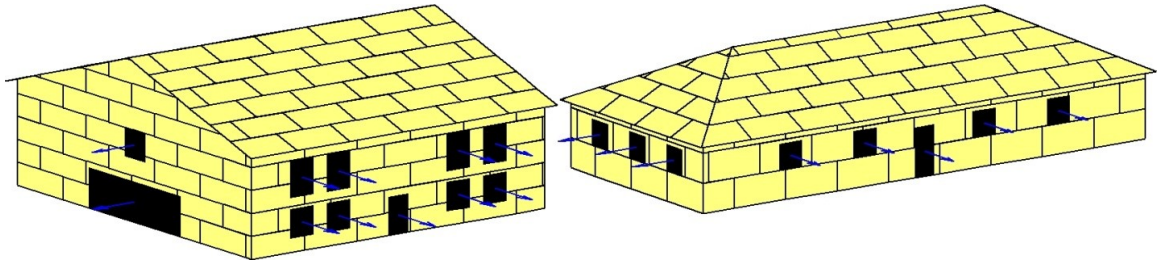

Figure 2.2: Multi-story, rectangular plan (left) gable and (right) hip roof structures modeled within the BEFA framework. Normal vectors are shown for the vulnerable components.

Roof covering within the framework is treated differently than is typical in several current vulnerability models; for example, the FPHLPM does not consider individual roof covering pieces, but rather the roof covering is modeled as aggregate sections assigned the same area as the underlying roof sheathing (Gurley et al. 2005). The FPHLPM (Gurley et al. 2005) ascertained that modeling the individual pieces of roof covering would not add to the overall accuracy of that particular model. However, the intent of this model is to assess the damage incurred to building envelopes from wind-borne debris

impacts within a residential development setting by specifically investigating a more detailed representation of the area of interest; therefore, this framework does consider individual pieces of roof covering (e.g., tiles or shingles based on user input). In order to facilitate the inclusion of the overlapped roof covering within the framework, an assumption is necessary to determine what roof covering parameters are used for calculations in the event that an individual piece of roof covering becomes airborne. Due to the limited amount of roof covering failure research available, the simple assumption is made that only the exposed area of the roof covering is available for failure and subsequent debris flight (i.e., the lapped portion of attachment of the roof covering is not considered for release).

The release of roof fascia boards (0.025 m x 0.152 m) and truss members (0.051 m x 0.102 m) as wind-borne debris within the framework is based on modifications to the fascia and truss component assumptions of the Twisdale et al. (1996) model. Roof fascia boards are available for injection into the wind field as a function of the roof edge sheathing (i.e., the flat eave and gable eave roof sheathing) with a 50% chance of injection following a roof edge sheathing failure. For truss member failures, Twisdale et al. (1996) conservatively assumes that all gable-end truss members are available for release when only one gable-end roof-sheathing panel remains attached to the truss. However, it seems reasonable that the availability of truss members as wind-borne debris is dependent not only on the gable-end roof sheathing, but also on the gable-end wall sheathing (i.e. the sheathing that is directly attached to the truss at the gable-end). It also seems highly unlikely that all truss members become available for release after only one

gable-end roof sheathing panel remains. Therefore, the BEFA framework modifies the assumptions of Twisdale et al. (1996) to include truss member release as a function of the gable-end roof and wall sheathing. Truss members become available for release within the BEFA framework as certain criteria are met (e.g., a section of top chord becomes available for release as roof and wall sheathing near the top chord are removed). Once it is determined that a roof fascia or truss member is available for release, it is assumed that there is a 50% chance of injection of the member into the wind field, which is an assumption necessary because of a lack of documented statistical information on the release of roof members affected by a loss of sheathing.

Assumptions were not made within Twisdale et al. (1996) regarding the release of truss members from hip roof structures, and truss member failure results for gable roof structures were reported with fascia boards in a combined "roof planks" category. However, fascia boards comprise a larger percentage of the total number of roof planks released from a structure; therefore, it is assumed that the number of actual truss member failures is low for gable roof structures. Due to the geometric configuration of a hip roof structure and the assumed low incidence of truss member failures of gable roofs reported by Twisdale et al. (1996), it is assumed within the BEFA framework that truss members of hip roof structures are not available for injection into the wind field at this time.

Vulnerable components within the BEFA framework (e.g., windows, doors, and garage doors) are checked for pressure and impact failures at each time step of the simulation, and the results utilized to update the enclosure classification, and by extension the internal pressure coefficients, of each house model. The BEFA framework

is capable of investigating the influence of the internal pressurization through the utilization of deterministic internal pressure coefficients (e.g., ASCE 7 2010), or probabilistic internal pressure coefficients (e.g., peer-reviewed research such as Ellingwood and Tekie 1999) depending upon user input. However, compartmentalization of the interior of the house structure and its influence on variations in internal pressure is not taken into account at this time.

2.2.2 Hurricane Simulation

The Hurricane Simulation Module is capable of simulating historical or synthetic hurricane events, and the user has the ability to investigate the influence of the hurricane on the residential development at a specific temporal window centered at the residential development of interest. The data used to simulate the hurricane surface wind fields within the BEFA framework depend on the user selection of a synthetic or historical hurricane, and for historical hurricanes, the year of hurricane formation. Historical hurricanes formed after 1993 are included in the National Oceanic and Atmospheric Administration-Hurricane Research Division (NOAA-HRD) hurricane wind analysis system (H*Wind) with a select few hurricane surface wind field analyses available prior to 1994 (Powell et al. 2010). The surface wind analyses provided by H*Wind consist of real-time analyses conducted on a 6-hour cycle that estimate the surface wind field for a tropical event using a time-to-space compositing technique that is useful for filling in data coverage gaps (Powell et al. 2010). Historical hurricanes that formed prior to 1994 and are not available in the H*Wind database require calculation of the gradient wind

field using data obtained from the National Hurricane Center (NHC) North Atlantic hurricane database (HURDAT) before conversion to the surface wind field. Synthetic hurricane, H*Wind, and HURDAT files typically provide data in increments of six hours; therefore, a simple linear interpolation of parameters is performed to define the mean surface wind field of the hurricane in 10-minute increments.

The calculation of the gradient wind field for historical hurricanes formed prior to 1994 is based on the work of Georgiou (1985), which provides a method to calculate the mean over-water gradient balance wind field $\left(\bar{V}_g\right)$ presented in Eqn. 2.1 and the corresponding wind direction $\left(\theta_g\right)$ at the point of interest presented in Eqn. 2.2.

$$\bar{V}_g = \frac{1}{2}\left(V_t \sin(\alpha) - fr\right) + \left[\frac{1}{4}\left(V_t \sin(\alpha) - fr\right)^2 + \left(\frac{B\Delta p}{\rho}\right)\left(\frac{Rmax}{r}\right)^B e^{-\left(\frac{Rmax}{r}\right)^B}\right]^{\frac{1}{2}} v \qquad 2.1$$

$$\theta_g = \theta + \alpha + \beta \qquad 2.2$$

where V_t is the hurricane translation speed, r is the radius from the hurricane eye to the point of interest, α is the angle from the hurricane heading $\left(\theta\right)$ to the radius r, f is the Coriolis parameter, Δp is the hurricane central pressure difference, *Rmax* is the radius-to-maximum winds from the hurricane eye, B is the Holland pressure profile exponent parameter, ρ is the air density, and β is equal to 90 degrees in the Northern Hemisphere. If *Rmax* and the B parameter are not available for a specific hurricane, Vickery et al. (2000) provide Eqns. 2.3 and 2.4 to estimate these parameters:

$$\ln Rmax = 2.636 - 0.00005086\Delta p^2 + 0.0394899\psi + \varepsilon_{R\max} \qquad 2.3$$

$$B = 1.38 + 0.00184\Delta p - 0.00309Rmax + \varepsilon_B \quad 2.4$$

where, ψ is the latitude of the hurricane eye, and ε is the standard deviation between the predicted and observed values for a Gaussian distribution with zero mean. The value of ε varies depending upon the location of the storm (i.e., above or below 30°N); therefore, the reader is referred to Vickery et al. (2000) for information regarding appropriate values of ε. Assuming that the mean over-water balance wind speed calculated with Eqn. 2.1 is the mean gradient wind speed, Table 2.1 provides conversion factors collated by Lee and Rosowsky (2007) to convert the mean gradient wind speed to the 10-minute mean surface wind speed $\left(\bar{V}_{600s}\right)$ using Eqn. 2.5.

$$\bar{V}_{600s} = G_{g-s}\bar{V}_g \quad 2.5$$

Little research has been performed on the spatial variation of 3-second wind speed gusts within a residential development; however, according to Harper et al. (2010), the probabilistic nature of gusts will have some variance about the expected gust value. Therefore, the 10-minute mean surface wind speed for each time step obtained from the synthetic or H*Wind files, or from the HURDAT calculations is multiplied by a gust factor ($G_{3s,\ 600s}$) equal to 1.66 (Harper et al. 2010) to convert it to the 3-second gust wind speed $\left(\bar{V}_{3s}\right)$.

Table 2.1: Gradient-to-surface wind speed conversion factors $\left(G_{g-s}\right)$ (Lee and Rosowsky 2007)

Location	Wind from ocean gradient-to-mean	Wind from land gradient-to-mean
Zone 1 [a]	0.45	0.45
Zone 2 [b]	0.50	0.45
Zone 3 [c]	0.65	0.50
Zone 4 [d]	0.65	0.65

[a] Inland airports more than 10 km from the coast
[b] Airport within 10 km of the coast
[c] Sites adjacent to the sea
[d] Off-shore sites

Spatial variation of the 3-second wind gusts from house to house is simulated by extending the assumption stated by Harper et al. (2010) that the maximum 3-second wind gusts of a surface wind follow a type I (Gumbel) distribution. A coefficient of variation (COV) equal to 0.10 is selected through comparisons of the Hurricane Simulation Module output for Hurricane Hugo with the envelope of peak gusts relative to the eye track of Hurricane Hugo presented by Powell et al. (1991). The peak 3-second gust wind speed $\left(\hat{V}_{3s}\right)$ is sampled for each house within the residential development for every 10-minute time step and compiled into an *m* x *n* peak 3-second gust wind speed output matrix. Within the gust wind speed output matrix, *m* is the number of time steps of the simulation plus one (e.g., an 8-hour temporal window divided into 10-minute increments yields 49 data points) and *n* is the number of houses within the residential development. Sampling the peak 3-second gust wind speed for each house in this manner does not take into account any correlation that may exist between the observed house-to-house peak

gusts; therefore, research is currently underway to quantify the correlation of the spatial variation of wind speeds within a residential development (Pang et al. 2012).

2.2.3 Debris Generation

The peak 3-second gust wind speed output matrix obtained from the Hurricane Simulation Module is utilized to generate modified component & cladding (C&C) wind pressures from ASCE 7 (2010). The C&C velocity pressure in Eqn. 2.6 and the design wind pressure in Eqn. 2.7 are modified according to the FPHLPM (Gurley et al. 2005) to represent the realistic wind pressures that a structure experiences during an extreme wind event rather than using design wind pressures.

$$q_h = 0.613 K_h \left(\hat{V}_{3s} \right)^2 \tag{2.6}$$

$$p = 0.8 q_h \left[GC_p - GC_{pi} \right] \tag{2.7}$$

where the factor of 0.8 incorporated by the FPHLPM is used to remove the factor of safety built into the design code provisions in order to replicate realistic wind pressures, q_h is the velocity pressure at mean roof height, K_h is a terrain exposure coefficient determined from ASCE 7 (2010) from building height and exposure category, GC_p is the external pressure coefficient with built-in gust factor, and GC_{pi} is the internal pressure coefficient with built-in gust factor. To replicate realistic wind pressures, the BEFA framework utilizes the same assumption as the FPHLPM (Gurley et al. 2005) of an effective wind area of 0.9 m^2 in the selection of the C&C external pressure coefficients for all components.

The application of the wind pressures obtained from Eqn. 2.7 onto an individual building requires that the components be assigned to pressure zones similar to those modified by the FPHLPM (Gurley et al. 2005) from ASCE 7 (2010). Figure 2.3 illustrates eight separate wind cases utilized to identify which of the modified pressure zones are effective for a particular wind direction. It should be noted that wind cases shown in Figure 2.3 are the same for a hip roof structure.

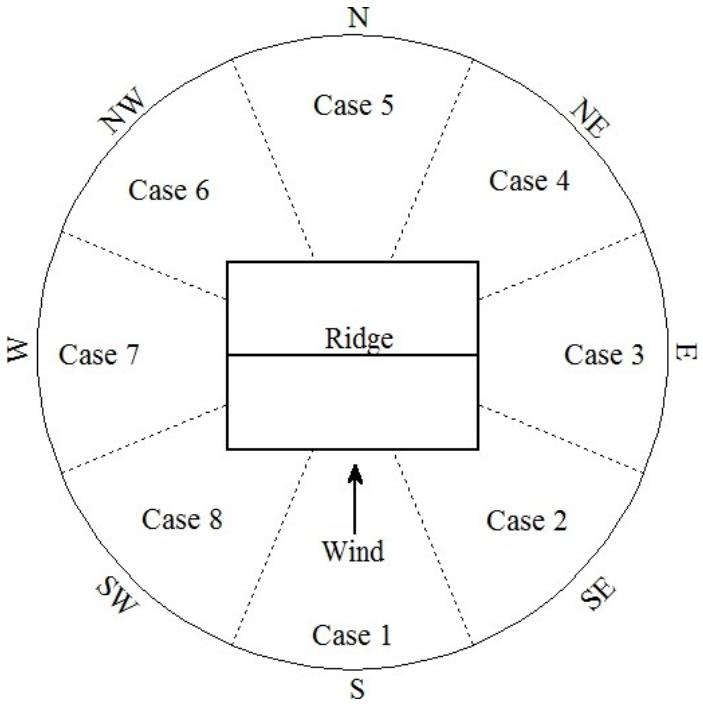

Figure 2.3: Wind cases used to identify the effective modified wind pressure zones. An example wind direction for case 1 is as shown.

Figure 2.4 illustrates the modified pressure zones for wind cases perpendicular to the building ridge (wind cases 1 and 5), parallel to the building ridge (wind cases 3 and 7), and the cornering winds (wind cases 2, 4, 6, and 8). Component pressure resistances (capacity) are compared to the calculated wind pressures (demand) within their respective modified pressure zone to determine which members have failed and potentially become

wind-borne debris. Once a building component is determined to have failed, the Debris Generation Module checks to determine if any secondary debris is released due to the initial component failure (e.g., truss member release due to sheathing failure). The surface area of the building envelope remaining is updated based on the type of component failure, and all pertinent information for a failed building component is then passed to the Debris Trajectory Module.

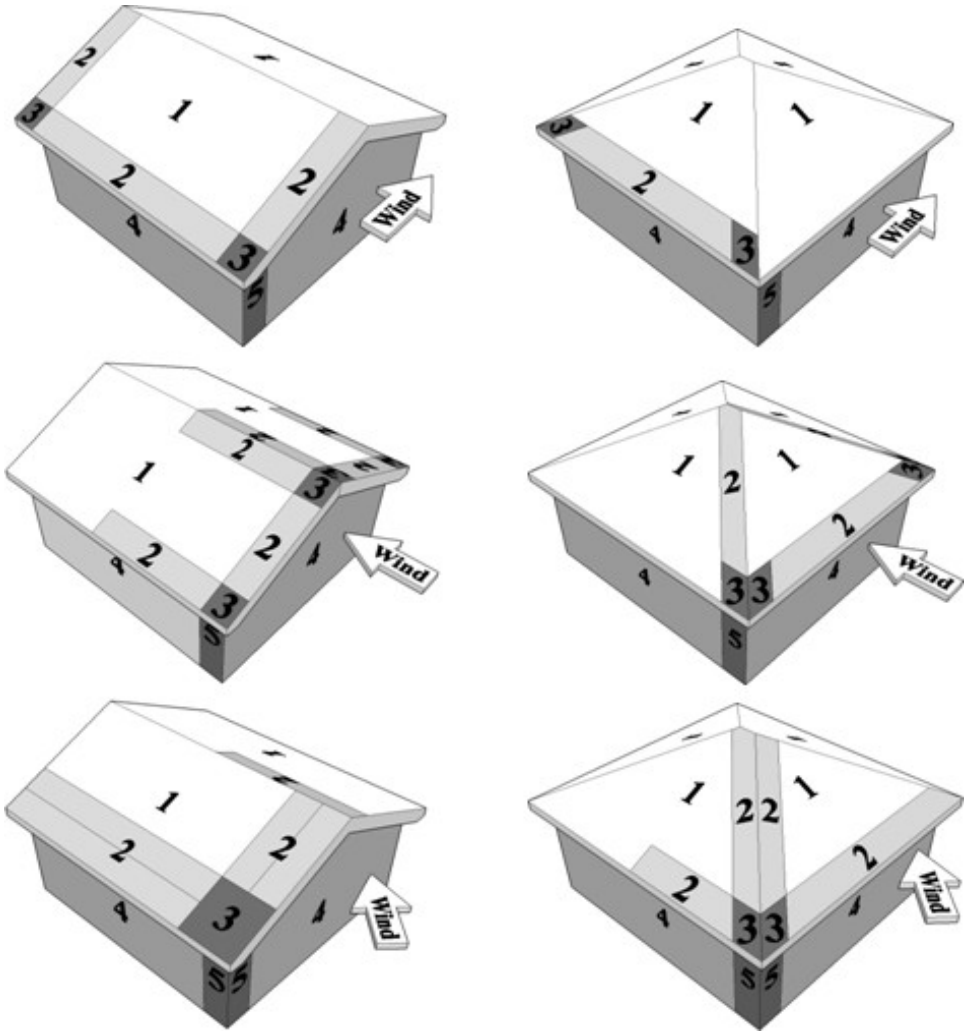

Figure 2.4: Modified wind pressure zones utilized within the BEFA framework for (left) gable roof structures, and (right) hip roof structures. Figure is adapted from Gurley et al. 2005.

Internal pressurization of an individual building is determined based on the enclosure classifications of ASCE 7 (2010), in which an open building is classified as a building with each wall at least 80% open:

$$A_o \geq 0.8A_g \tag{2.8}$$

where, A_o and A_g are the total area of the openings in a wall and the gross area of a wall receiving positive pressure, respectively, and a partially-enclosed structure is classified as a building that complies with the following conditions:

$$A_o > 1.10A_{oi} \tag{2.9}$$

$$A_o > \min\left(0.37\,\mathrm{m}^2, 0.01A_g\right) \tag{2.10}$$

$$A_{oi}/A_{gi} \leq 0.20 \tag{2.11}$$

where, A_{oi} and A_{gi} is the sum of the areas in the building envelope not including A_o, and the sum of the gross surface areas of the building envelope not including A_g (i.e. sum of gross areas not exposed to positive pressure), respectively. It should be noted that openings are classified within the BEFA framework as actual perforations within the building envelope (e.g., sheathing loss, window failure, etc.) and not potential openings in the building envelope as in the case of design (e.g., unprotected windows or doors, etc.). Failed roof and wall sheathing from uplift, and vulnerable component failure from pressure or debris impact are tracked at each time step to determine if a change in the building enclosure classification, and consequently the internal pressure coefficients

(GC_{pi}), is warranted based on the wind direction at a particular time step and the results of Eqns. 2.8 to 2.11.

2.2.4 Debris Trajectory

The Debris Trajectory Module is driven by a mechanics-based three-dimensional (3D) probabilistic debris trajectory model (Grayson 2011; Grayson et al. 2012) capable of providing relevant debris trajectory information (i.e., linear and rotational position, velocity, and acceleration) needed to track wind-borne debris. The probabilistic debris trajectory model is based on recent deterministic 6-degree-of-freedom (6DoF) wind-borne debris trajectory models that are modified to incorporate the aleatoric uncertainty associated with wind-borne debris flight. The authors quantified this aleatoric uncertainty through parametric studies of coefficients of variation (COV) utilizing the Monte Carlo simulation method to sample the debris flow angles (i.e., the debris angle of attack and tilt angle) of the deterministic wind-borne debris trajectory model from a Gaussian distribution. Location statistics (i.e., the mean, standard deviation, and coefficient of skewness) were calculated for the probabilistic wind-borne debris trajectories obtained from the Monte Carlo simulations and compared to the location statistics of physical test data provided by the University of Western Ontario to identify the appropriate COVs necessary to provide reasonable probabilistic wind-borne debris trajectories. As a true 6DoF model, the probabilistic debris trajectory model can potentially be more computationally intensive to implement than some current simplified debris trajectory models. However, the opportunity to gain greater insight into the debris impact protection

required in a residential development subjected to hurricane wind hazards far outweigh the computational costs that may be required. Figure 2.5 provides an example of the probabilistic wind-borne debris trajectory model by illustrating two trajectories of a 1.22 m x 2.44 m x 0.013 m piece of roof sheathing with identical initial conditions.

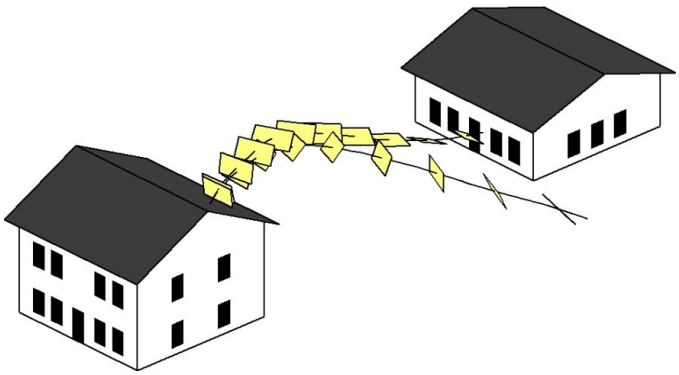

Figure 2.5: An example of the wind-borne debris trajectories for a typical roof-sheathing panel possessing identical initial conditions obtained from the probabilistic wind-borne debris trajectory model. Position and orientation of the sheathing are illustrated at every third time step (Δt = 0.03 seconds) for clarity.

2.2.5 Debris Impact

The Debris Impact Module is utilized to determine if any of the wind-borne debris released from a building during a particular time step has impacted either itself or another building within the area of interest. All relevant debris trajectory information is obtained from the Debris Trajectory Module at the time of impact to any roof sheathing, wall sheathing, or vulnerable building component of the building envelope. There has been some debate pertaining to whether linear momentum or kinetic energy is a better indicator of damage to building envelope components from wind-borne debris impact; however, Holmes (2010) concludes that both linear momentum and kinetic energy are

relevant quantities of measuring damage dependent upon the situation of the impact. Therefore, the Debris Impact Module calculates both linear momentum and kinetic energy of the debris at the time of impact. The quantity used to determine if a particular building envelope component fails due to wind-borne debris impact is dependent upon how the impact capacity of that type of component is defined by the user during the pre-processing phase.

The Debris Impact Module requires the most computational resources compared to the other modules of the BEFA framework; therefore, the Debris Impact Module only checks impacts to the roof and wall sheathing, and vulnerable components at this time to reduce the computational time required during a simulation. This assumption precludes the framework's ability to determine if further debris is created from building components that have a tendency to fragment into numerous pieces upon impact by wind-borne debris (e.g., roof tiles). Computational resources are maximized by assessing if any part of a wind-borne debris trajectory is within a volume representing each of the individual buildings within the residential development. Wind-borne debris trajectories contained within this volume are checked systematically at each time step to determine at what point an investigated wind-borne trajectory intersects the plane of any particular building envelope component. The normal vector of the impacted building envelope component is compared to the wind-borne debris trajectory to determine if an impact has occurred from the outside in rather than from the inside out of a building envelope. A wind-borne debris trajectory is checked until the first instance of impact to a building envelope. Once the initial impact is determined, it is assumed that the original wind-

borne debris trajectory will change due to the impact and is no longer valid. All pertinent information of the initial impact is recorded, such as the translational and rotational position and velocity, and the Debris Impact Module then proceeds to the next wind-borne debris trajectory and reiterates the previous process until all wind-borne debris trajectories have been assessed for impact.

2.3 BEFA Framework Example and Discussion

An example of the BEFA framework is presented that focuses on illustrating the building envelope damage incurred by a representative South Carolina (SC) residential development subjected to Hurricane Hugo. Figure 2.6 identifies the path of Hurricane Hugo in relation to the SC coastline, and illustrates the selection of three points of interest (POI) based on the hurricane eye track and estimated *Rmax*, which was approximately 43 km from the center of the eye of Hurricane Hugo at 0530 UTC.

The representative SC residential development was evaluated at these three POIs to facilitate qualitative verification that the BEFA framework performs as expected during a hurricane event, and in the development of a debris vulnerability envelope that illustrates the usefulness of the framework in assessing the wind-borne debris impact vulnerability of a planned or as-built residential development. For this example, a 12-hour temporal window centered at the point of interest was more than adequate to ensure that the simulation results were not influenced by unrealistic initial conditions (e.g., a large debris release at the initial time step due to an instantaneous application of wind pressure). However, to keep the illustrations concise, the results are presented for an 8-hour window

centered on the point of interest (i.e., 0130-0930 UTC) without any loss of pertinent information.

Table 2.2 displays the components, their capacities, and the pressure coefficients utilized in this example for four separate cases of roof and wall sheathing attachment. Cases 1-3 increased the fastener size used to attach the roof and wall sheathing to the structure from a 6d common smooth-shank nail to an 8d common smooth-shank nail, respectively (Lee and Rosowsky 2005). Case 4 was a retrofit of case 1 that utilizes closed-cell sprayed polyurethane foam (ccSPF) on the underside of the roof sheathing fastened with 6d common smooth-shank nails (Datin et al. 2011). These four separate cases are presented to illustrate the flexibility of the BEFA framework in comparing potential mitigation techniques. It should be noted that the values in Table 2.2 are not "hard-wired" into the BEFA framework. The building stock of the framework is flexible in that building parameters are determined by the user during the pre-processing phase of the simulation; therefore, the framework is capable of incorporating deterministic and/or probabilistic capacities and their associated distributions that have been identified by other research studies investigating the behavior and performance of various building envelope components.

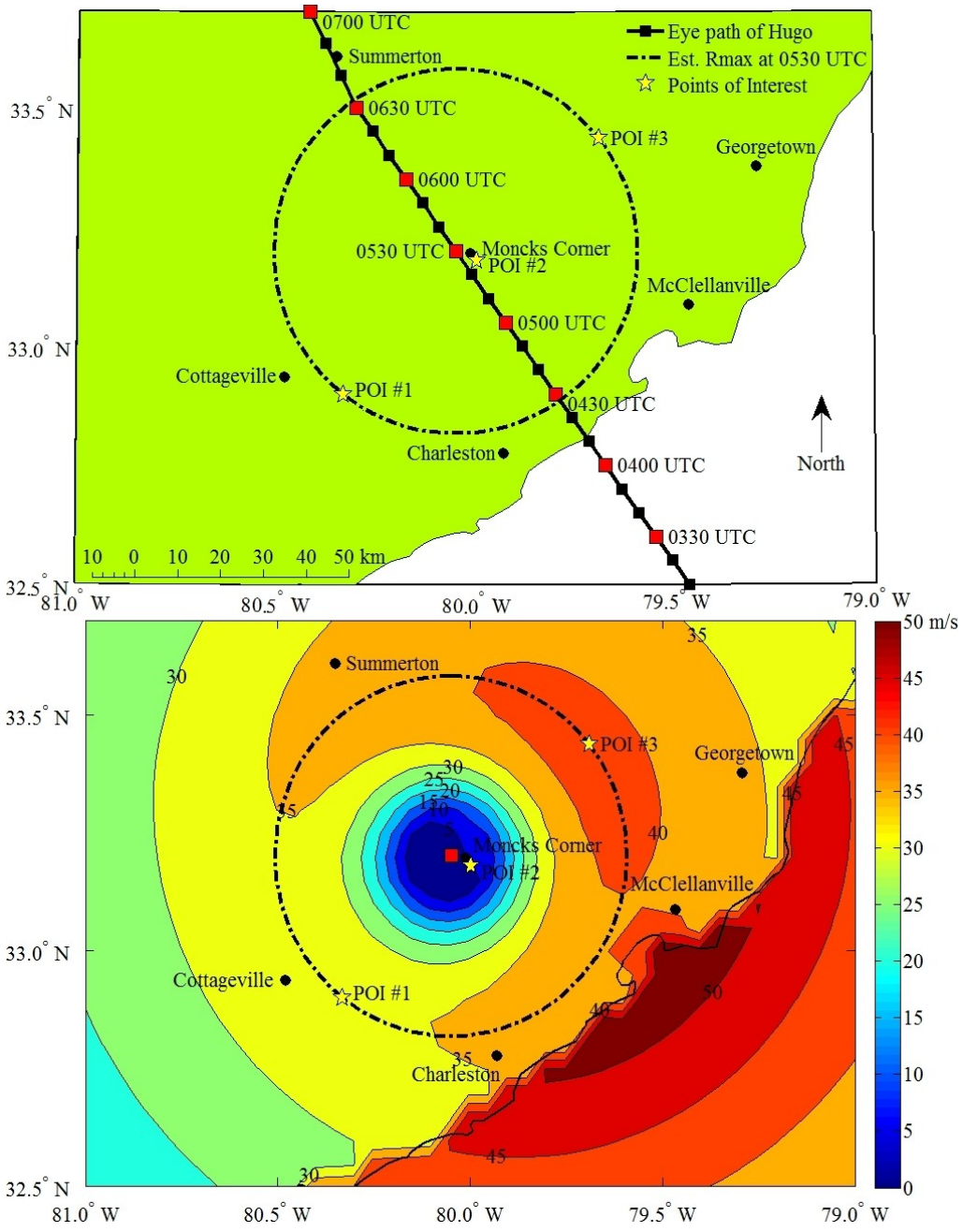

Figure 2.6: (Top) Selection and identification of three points of interest (POI) for the evaluation of a representative SC residential development subjected to Hurricane Hugo. (Bottom) Mean wind speed contours for Hurricane Hugo illustrating the reasoning in selecting these three particular POIs.

Table 2.2: User-defined parameters for the presented BEFA framework example.

Case	Building Component			Mean	COV	Distribution	Reference
1	Roof Sheathing	6d Nails[a]	Full Sheet[d]	1.20	0.150	Normal	Lee and Rosowsky (2005)
			Half Sheet[e]	1.53			
	Wall Sheathing		Full Sheet[d]	1.20			
			Half Sheet[e]	1.53			
2	Roof Sheathing	8d Nails[b]	Full Sheet[d]	2.76	0.200	Normal	Lee and Rosowsky (2005)
			Half Sheet[e]	3.51			
	Wall Sheathing	6d Nails[a]	Full Sheet[d]	1.20	0.150		
			Half Sheet[e]	1.53			
3	Roof Sheathing	8d Nails[b]	Full Sheet[d]	2.76	0.200	Normal	Lee and Rosowsky (2005)
			Half Sheet[e]	3.51			
	Wall Sheathing		Full Sheet[d]	2.76			
			Half Sheet[e]	3.51			
4	Roof Sheathing	6d[a] + ccSPF[c]	All Panels	10.7	0.184	Lognormal	Datin et al. (2011)
	Wall Sheathing	6d Nails[a]	Full Sheet[d]	1.20	0.150	Normal	Lee and Rosowsky (2005)
			Half Sheet[e]	1.53			
All Cases	Roof Covering	Shingles		3.35	0.400	Normal	Gurley et al. (2005)
	Doors[f]	Front		4.79	0.200	Normal	Gurley et al. (2005)
		Back		4.79	0.200		
	Garage Doors[f]	Two-car garage		2.49	0.200	Normal	Gurley et al. (2005)
	Windows[f]	Small		5.00	0.200	Normal	Gurley et al. (2005)
		Medium		3.33	0.200		
		Tall		2.50	0.200		
		Picture		1.78	0.200		
	GC_p[g,h]	ASCE 7-10 Figures 30.4-1 and 30.4-2A-C				Deterministic	ASCE (2010)
	GC_p[i,h]	Open		+/-0.00		Deterministic	
		Partially Enclosed		+/- 0.55		Deterministic	
		Enclosed		+/- 0.18		Deterministic	

[a] Smooth shank; 2.87 mm diameter x 50.8 mm long; 150 mm/300 mm nailing schedule
[b] Smooth shank; 3.33 mm diameter x 63.5 mm long; 150 mm/300 mm nailing schedule
[c] closed-cell sprayed polyurethane foam
[d] Full sheet measures 1.22 m x 2.44 m
[e] Half sheet measures 1.22 m x 1.22 m
[f] Resistance values given are for unprotected openings
[g] Based on an effective area of 0.9 m2
[h] Values are dimensionless

Figures 2.7 and 2.8 represent the surface wind profiles and mean wind directions experienced by the representative SC residential development during Hurricane Hugo at the three POIs identified in Figure 2.6. The results in Figure 2.7 agree reasonably well with the peak surface gust envelopes presented by Powell et al. (1991).

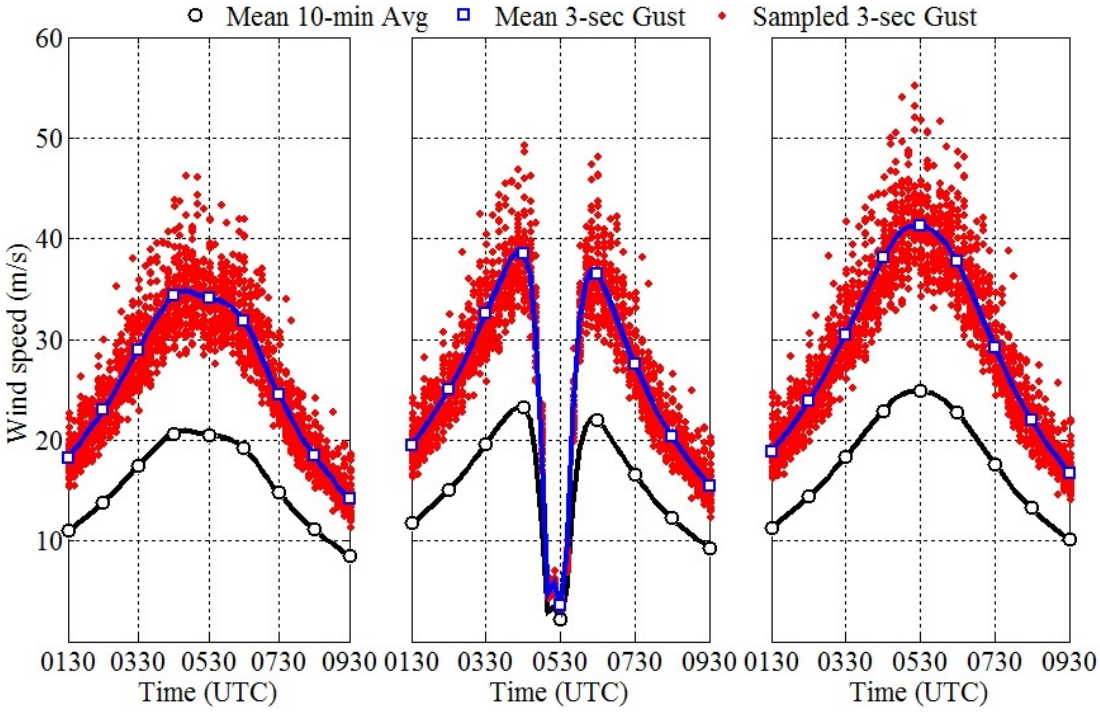

Figure 2.7: Wind velocity profiles for Hurricane Hugo at (left) POI #1 at the SW *Rmax*, (center) POI #2 at the eye path, and (right) POI #3 at the NE *Rmax*.

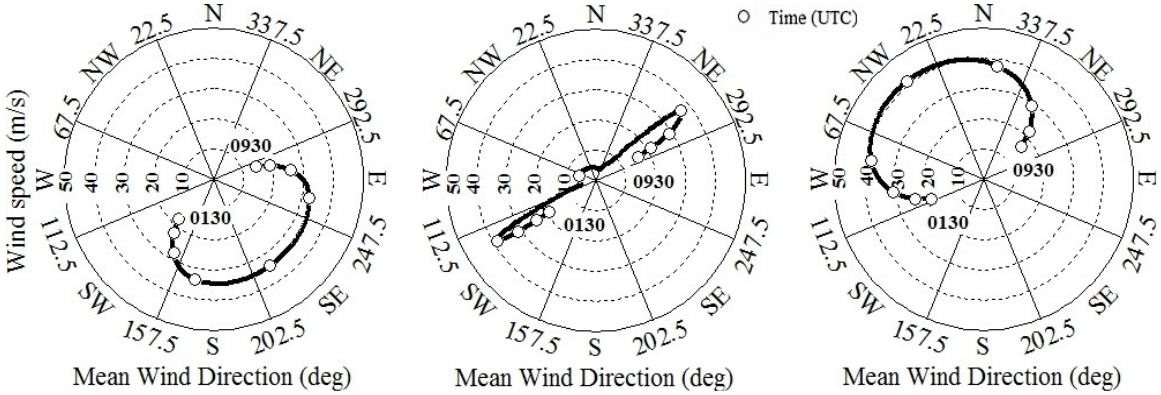

Figure 2.8: Wind direction plots for Hurricane Hugo at (left) POI #1 at the SW *Rmax*, (center) POI #2 at the eye path, and (right) POI #3 at the NE *Rmax*.

Figure 2.9 provides a basic layout of the representative residential development within the BEFA framework with an example of the wind-borne debris field released at POI #3 for a time step corresponding to 0350 UTC. The direction of the wind was essentially from right to left (east to west as shown in Figure 2.8); therefore, note the variation of the wind-borne debris trajectories and landing locations provided by the 3D probabilistic wind-borne debris trajectory model.

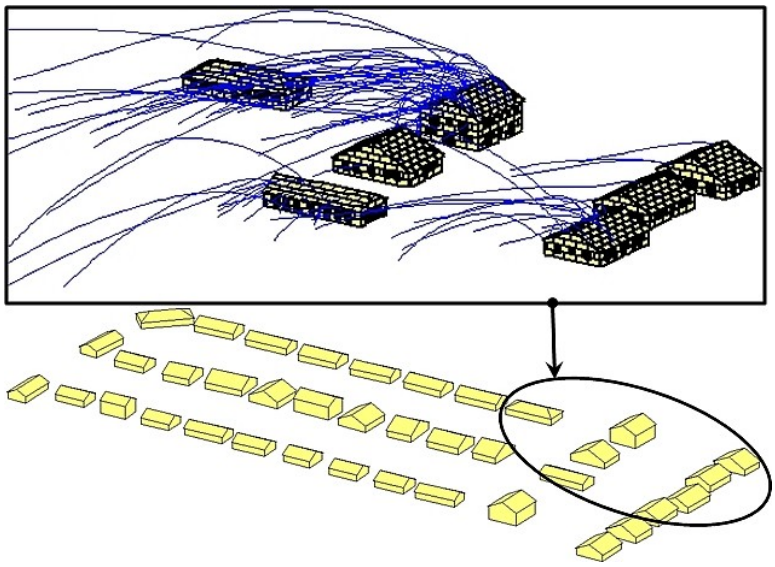

Figure 2.9: Representative South Carolina residential development.

Figure 2.10 illustrates the time evolution and component composition of the wind-borne debris released as a percentage of total debris for case 1 (see Table 2.2) at the three POIs during the passage of Hurricane Hugo. There was an initial release of roof covering at the lower wind speeds, with a gradual increase in the release of roof sheathing as the wind speed increased. The failed roof covering depicted in Figure 2.10 is the roof covering that failed due to direct uplift pressure and does not consider roof covering that left the structure attached to roof sheathing, as it does not directly contribute to the wind-

borne debris field. The substantial increase in the release of wall sheathing at POI #3 (see top of Figure 2.10) was indicative of the higher wind speeds experienced at the northeast *Rmax* compared to the other POIs. Based on initial intuition, there appeared to be some anomalies with the data as presented in Figure 2.10. Firstly, there was significantly less debris released at higher wind speeds than previously seen at lower wind speeds, and secondly, it seems implausible that there should be a significant increase (or spike) in the debris released after a steady decline in debris even while the wind speed continued to increase. This is because the amount of debris released is not just a function of wind speed and component resistance, but also of wind direction and component availability.

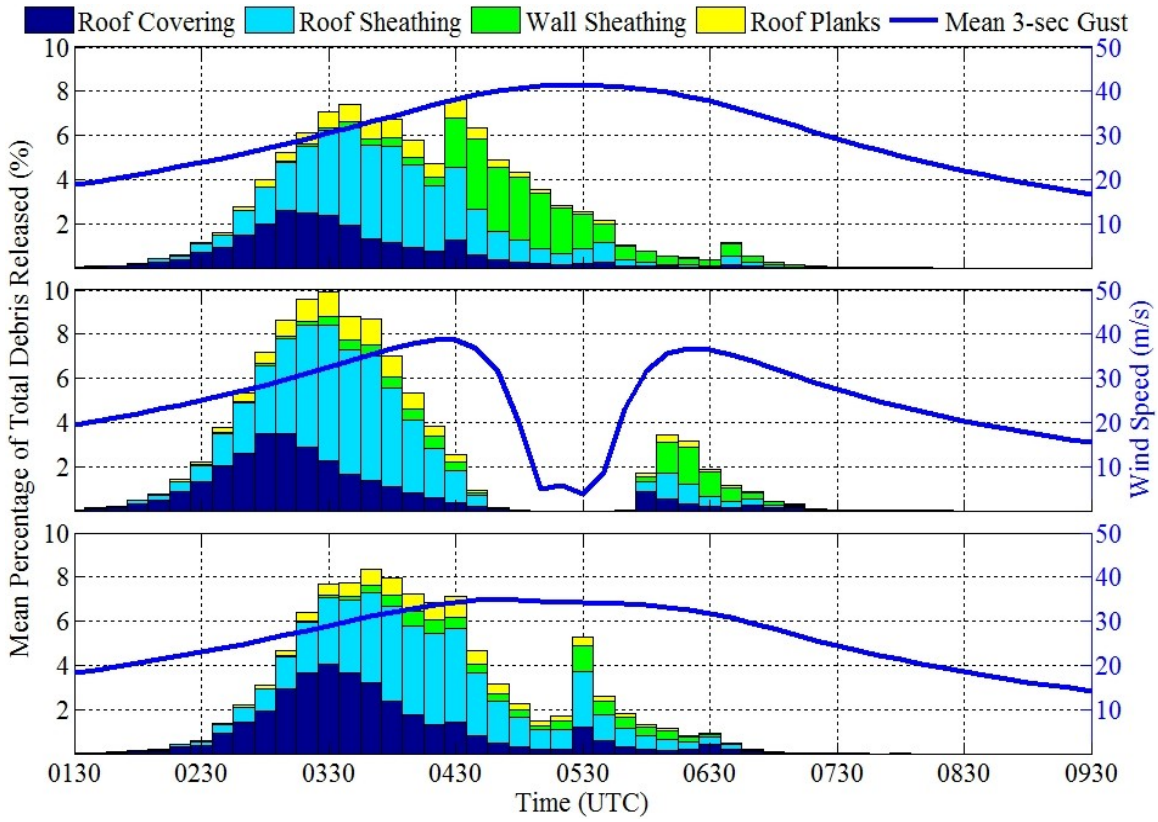

Figure 2.10: Time evolution of debris as a percentage of the total debris released during case 1 simulations at (top) POI #3 at the NE *Rmax*, (center) POI #2 at the eye path, and (bottom) POI #1 at the SW *Rmax*.

Figure 2.11 isolates the time evolution of debris released at POI #3 for cases 1 and 2 (see Table 2.2) to illustrate how initial intuition can be misleading when assessing the time evolution of damage to structures subjected to hurricane wind hazards. The first scenario regarding the reduced amount of debris released at the maximum wind speed is addressed by comparing the timing of the debris release for cases 1 and 2. It is seen that as the uplift capacity of the roof sheathing increased with the increased fastener size (i.e., case 2), there was a shift in the debris released towards the higher wind speed. The maximum debris release will not necessarily coincide with maximum wind speed for two potential reasons. The first reason is simply due to a lack of components available for release (e.g. roof sheathing in case 1). The second reason is that increasing the capacity of a building component can shift the mean resistance of a particular component beyond the mean demand capable of being produced by a particular hurricane event (i.e., the roof sheathing in case 2).

The second scenario is addressed by overlaying the time evolution of the changes in wind direction (see Figure 2.11), and thereby the subsequent change in wind pressure zones, with the debris released during the passage of the hurricane. It should be noted that the wind cases illustrated in Figure 2.11 were for the majority of the buildings within the residential development; however, the change in wind direction for all buildings regardless of the wind case occurred at the same intervals throughout. As the wind direction transitioned with the passage of the hurricane, the modified wind pressure zones applied to the buildings transitioned as well, which increased the external wind pressures

(e.g., uplift) on other areas of the buildings and contributed to a subsequent increase in the amount of wind-borne debris released during a particular time step.

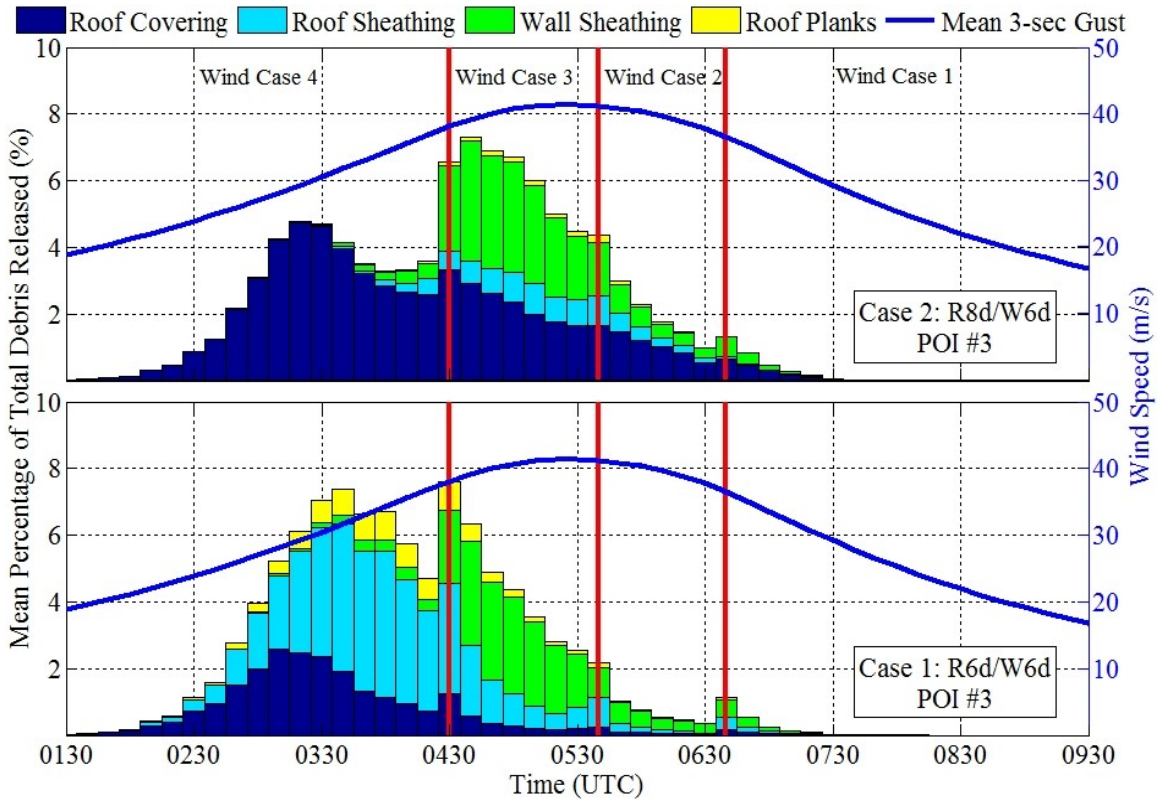

Figure 2.11: Time evolution of debris as a percentage of the total debris released for case 2 (top) and case 1 (bottom) at POI #3 at the NE *Rmax*. Vertical red lines delineate the wind cases (see Figure 2.3) experienced by the development.

In both situations, it is important to identify that the failure of the building envelope components is not just a function of the capacity of the building component and the demand created by wind pressure as intuition would have us assume (e.g., higher wind speeds lead to higher amounts of debris). Rather the BEFA framework has helped to illustrate through time evolution that the timing of building envelope component failure is also subject to the wind direction and remaining components available for failure. Although the wind direction is identified as an important contributing factor in the failure

timing of available building envelope components, the sharp increases in debris release associated with a change in wind direction are due to the use of the modified wind pressure zones (see Figure 2.4), and in reality would most likely be represented by a smoother transition.

Figure 2.12 illustrates the time evolution of the percentage of total debris released that did and did not produce wind-borne debris impacts to a building envelope for case 1 (see Table 2.2) at each of the three POIs during the passage of Hurricane Hugo. It was evident that the percentage of debris released that did produce impacts decreased as the analysis progressed from POI #1 (see bottom of Figure 2.12) to POI #3 (see top of Figure 2.12).

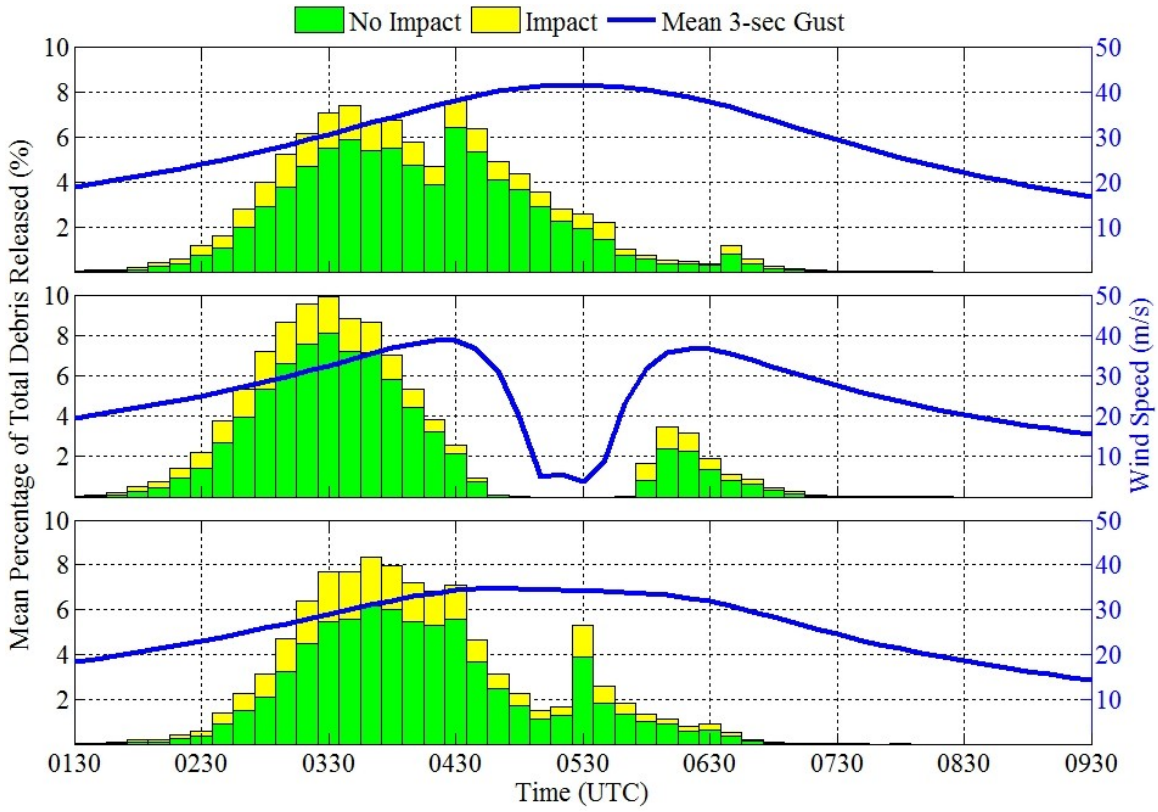

Figure 2.12: Time evolution of the percentage of total debris released that result in impact for (top) POI #3 at the NE *Rmax*, (center) POI #2 at the eye path, and (bottom) POI #1 at the SW *Rmax*.

This is attributed to the exclusion of exogenous wind-borne debris within the BEFA framework as the debris released at higher wind speeds had a tendency to fly out of the residential development before producing an impact. Based on these results, research into the influence of exogenous wind-borne debris is currently underway as it is expected to influence the damage witnessed within a residential development during exposure to hurricane wind hazards.

Figure 2.13 illustrates the time evolution of the mean building envelope surface area remaining for case 1 (see Table 2.2) during the passage of Hurricane Hugo. It should be noted that for this example, Figure 2.13 takes into account all openings that occurred in the building envelope, such as, roof and wall sheathing failure, pressure failure of the vulnerable components, and impact failure of the windows only. This example did not consider any window impact protection, and to simplify the example it was assumed that a single impact to a window constituted failure. However, window and window protection system impact performance data from research such as Masters et al. (2010) and Herbin and Barbato (2012) can be incorporated into the BEFA framework during the pre-processing phase. Doors (including garage doors) were not considered for impact failure in this example as it was assumed unlikely that a single impact would cause the same amount of damage to a door as it did to an unprotected window. With the amount of damage exhibited by many of the houses within the residential development for this example, there was a possibility of structural collapse due to loss of the building lateral capacity due to sheathing failure; however, the BEFA framework in its current state assesses the potential for damage to the building envelope without consideration of

structural integrity. Figure 2.13 further reiterates that residential developments located to the northeast of the hurricane eye path have the potential to experience greater damage than those at other locations.

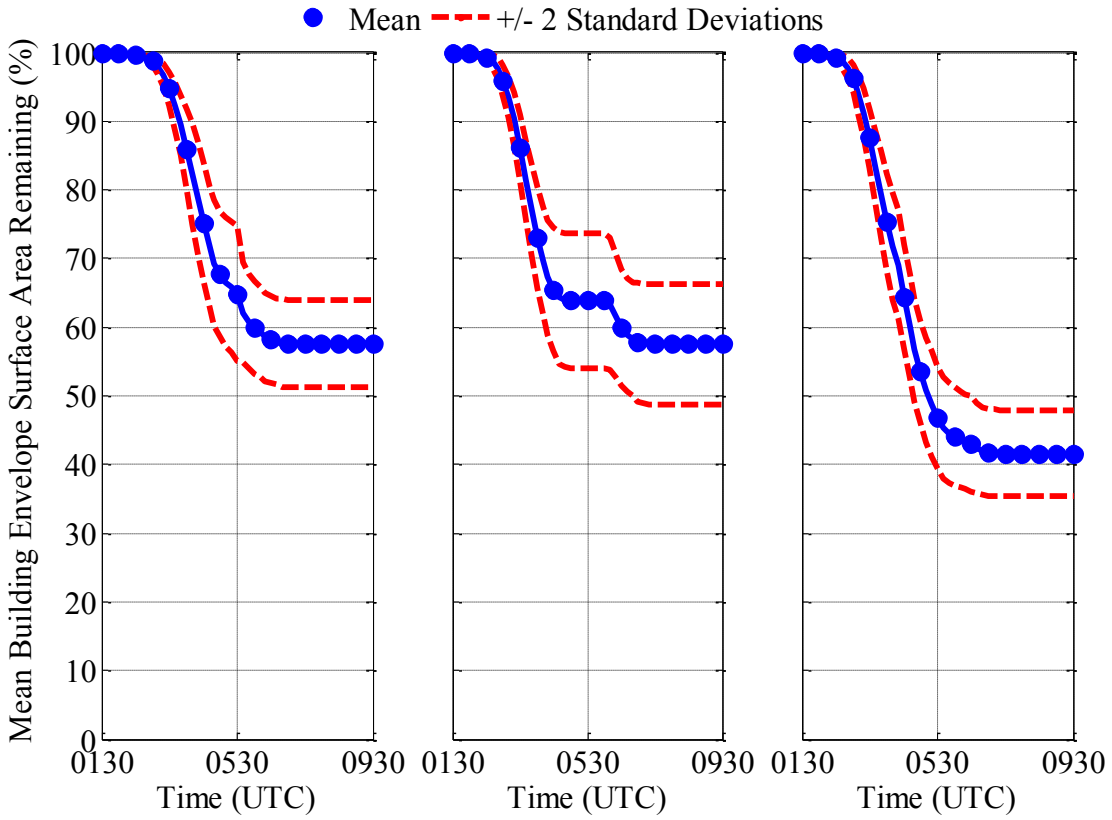

Figure 2.13: Time evolution of the mean percentage of the building envelope surface area remaining for (left) POI #1 at the SW *Rmax*, (center) POI #2 at the eye path, and (right) POI #3 at the NE *Rmax* for case 1 simulations.

Figure 2.14 illustrates the influence of various roof and wall sheathing capacities on the mean building envelope surface area remaining. These capacities are documented as four cases in Table 2.2, with the representative residential development evaluated for each case at the estimated northeast *Rmax* of Hurricane Hugo (i.e., POI #3). The results illustrated were as expected from the BEFA framework in that as the sheathing resistance

capacities increased (e.g., larger, more robust fasteners) there was a subsequent increase in the mean remaining surface area of the building. With the higher sheathing resistances, the building envelope components were able to withstand better the damaging effects of the wind pressure as the hurricane passed, which in turn decreased the amount of wind-borne debris injected into the wind field, which further reduced the amount of damage to the building envelope. Cases 2, 3, and 4 showed significant improvement in the mean performance of the building envelopes over that of case 1 with case 3 providing the greatest improvement (~115%); however, the retrofit of case 4 (~97% improvement) may be more feasible to execute in the field when mitigating existing building stock.

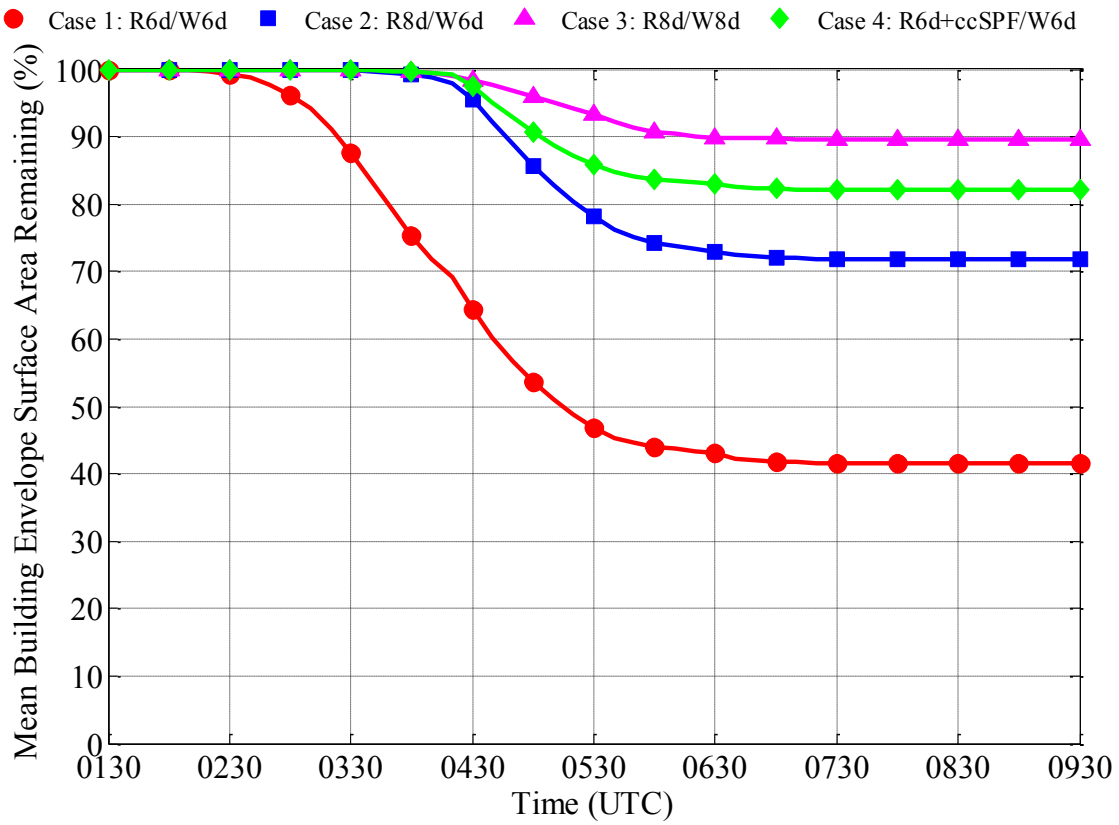

Figure 2.14: Time evolution of the mean percentage of the building envelope surface area remaining during simulations for cases 1-4 (see Table 2.2) at POI #3 at the northeast *Rmax*.

Figure 2.15 illustrates debris impact vulnerability plots for the residential development at the three POIs subjected to Hurricane Hugo. The debris impact vulnerability plots were developed by categorizing the vulnerable component normal vectors (see Figure 2.2) into eight equal-size bins (i.e., 45 degrees) in relation to the four cardinal directions (i.e., N-S-E-W) and the four intercardinal directions (i.e., NW-SW-SE-NE). The probability of at least one impact to the vulnerable components of each bin (see Table 2.3) was calculated as shown in Eqn. 2.12:

$$P_i\left[VC_I \geq 1 \mid H\right] = \frac{1}{n}\sum_{j=1}^{n}\left(\frac{A_{ij}}{B_i}\right) \qquad 2.12$$

where VC_I is the number of impacts to the vulnerable components of bin i, H is the hurricane event, A_{ij} is the number of vulnerable components impacted at least once in bin i during simulation j, B_i is the total number of vulnerable components in bin i, and n is the total number of simulations performed during the assessment.

The results presented in Figure 2.15 were expected qualitatively as the higher wind speeds observed at POI #3 produced a greater number of wind-borne debris, thus producing a greater probability of impact to the vulnerable components. The large probability of impact in the east (E) bins of POIs #1 and #3, which are 33% and 81% respectively, were due to an unsheltered garage door (i.e., the garage door was directly exposed to wind pressure and wind-borne debris). The example of the unsheltered garage door is developed further in Figure 2.16 to illustrate how the BEFA framework can be employed to assess pre- or post-construction residential developments located within hurricane-prone regions.

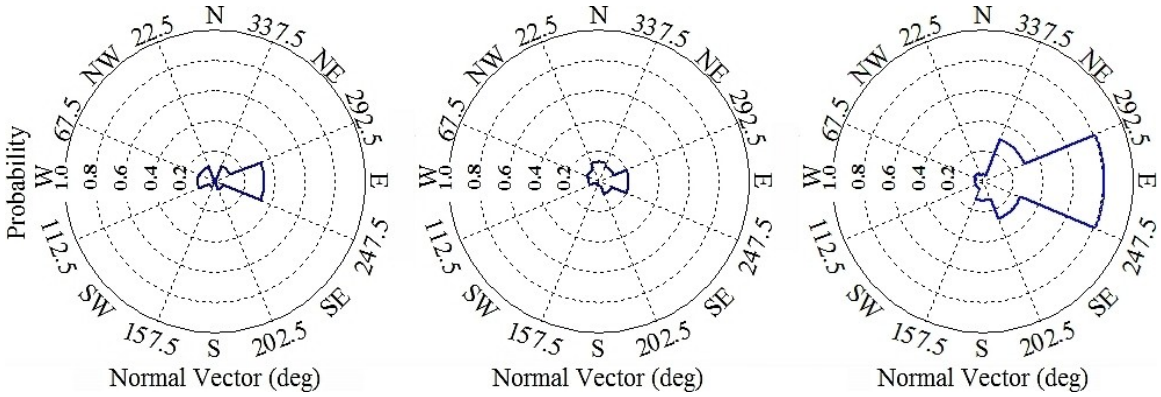

Figure 2.15: Debris impact vulnerabilities for (left) POI #1: at the estimated SW *Rmax*, (center) POI #2: at the eye path, and (right) POI#3: at the estimated NE *Rmax*.

Table 2.3: The probability of impact to the vulnerable components of the residential development.

POI	N	NW	W	SW	S	SE	E	NE
1	0.002	***0.107***	***0.113***	0.041	0.009	0.060	0.330	0.110
2	***0.128***	0.090	0.063	0.025	0.032	0.092	0.200	0.107
3	0.044	0.0632	0.050	***0.053***	***0.128***	***0.270***	***0.810***	***0.300***
Max	0.128	0.107	0.113	0.053	0.128	0.270	0.810	0.300

The maximum value in each of the eight bins (i.e., the eight principal directions) of Table 2.3 were used to develop a debris impact vulnerability envelope. Figure 2.16 (left) is the superposition of the maximum values taken from the debris impact vulnerability plots highlighted in Table 2.3. This superposition provides the debris impact vulnerability envelope for a representative SC residential development subjected to Hurricane Hugo. If it is assumed conservatively that a single impact fails the associated vulnerable component, and that impacts to areas other than vulnerable components do not proliferate damage to the building envelope, then the plots of Figure 2.16 provide the probability of failure of the building envelope due to wind-borne debris impact. Furthermore, Figure 2.16 illustrates how the BEFA framework output can be utilized by officials, developers,

architects, and designers to mitigate damage to the building envelope of homes within a residential development. In the context of this example, Figure 2.16 (right) illustrates how the protection of garage doors in some manner from wind-borne debris impact reduced the probability of damage to the building envelope, particularly in the case of the unsheltered garage door located in the east (E) bin. A pre- or post-construction residential development located within a hurricane-prone region can be modeled within the BEFA framework and subjected to a suite of historical or synthetic hurricanes. The resulting output from the BEFA framework can be analyzed to determine how parameters such as residential development or individual building orientation, component capacities, or the protection of specific vulnerable components influences the probability of damage within the residential development.

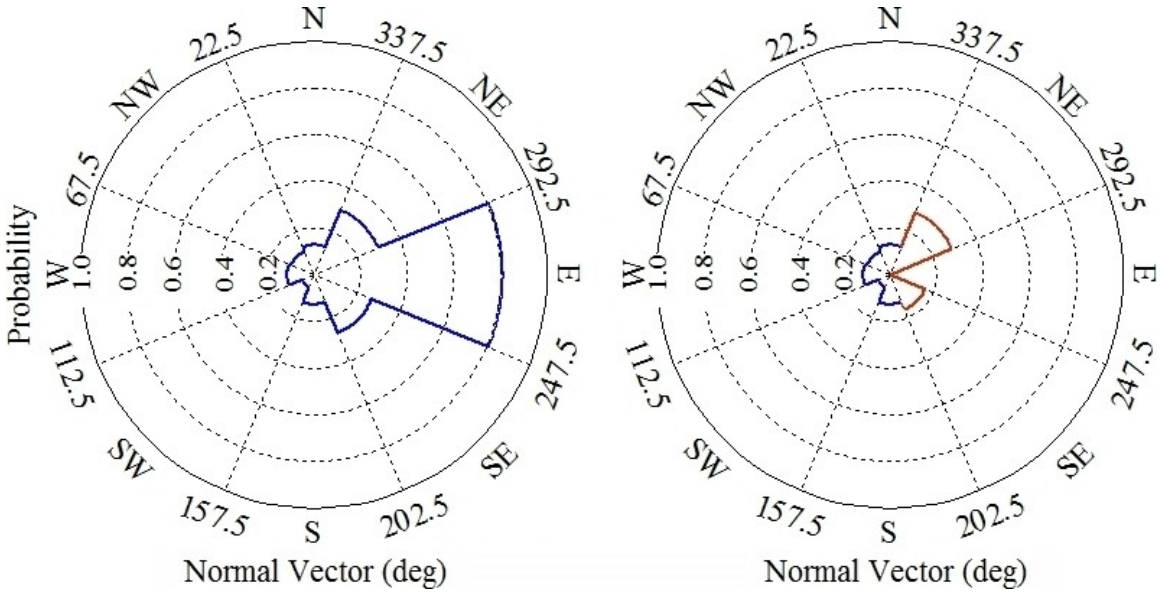

Figure 2.16: (Left) Debris impact vulnerability envelope for a representative residential SC residential development subjected to Hurricane Hugo, and (right) the same scenario except that all garage doors are protected in some manner from wind-borne debris impact.

2.4 Significance and Limitations of the BEFA Framework

Building envelope failure assessments that incorporate the influence of wind-borne debris impacts continue to play an integral part in identifying cost effective mitigation techniques for residential communities subjected to hurricane wind hazards. Hence, it becomes increasingly important to approach the problem from many different aspects to ensure a solution that is as thorough and complete as possible. The significance of the BEFA framework is that it approaches the topic of building envelope failures from a different point of view than that of research such as Herbin and Barbato (2012), which develops fragilities that capture the influence of wind-borne debris impacts on building envelope failures on an individual component level. In contrast, the flexible building stock of the BEFA framework is capable of incorporating these fragilities to investigate building envelope failures on the residential development level; thereby providing a platform for the collaboration of research in pursuit of a common goal.

Nevertheless, the assessment of building envelope failures due to hurricane wind hazards is a complex topic, and due to the limited amount of research available in some areas, several limitations exist within the BEFA framework. Consequently, the following are not considered within the framework in its current form:

- exogenous debris (i.e., debris originating outside of the residential development),
- wind-borne debris from vegetation (e.g., tree limbs, brush, etc.),
- structural collapse of buildings due to a loss of stability,
- the frangibility of building components impacted by debris (e.g., tiles), and

- water intrusion.

Another issue that needs to be addressed is the inability to verify the output of the BEFA framework due to a lack of full-scale time evolution data of building envelope failures due to hurricane exposure. Until further full-scale information becomes available, the assumptions and judgments that comprise this work are based upon current peer-reviewed research. However, comparing the framework output for various component capacities (see Table 2.2; cases 1-4) provides a basic level of verification that illustrates that the BEFA framework performs as expected in an example assessment.

3 CONSIDERATION OF EXOGENOUS WIND-BORNE DEBRIS WITHIN A MECHANICS-BASED BUILDING ENVELOPE FAILURE ASSESSMENT MODEL

3.1 Introduction

The building envelope failure assessment (BEFA) model is intended to investigate residential developments that comprise smaller, more detailed study regions that may be exposed to various surroundings (e.g., building stock, vegetation) that are not explicitly considered within the study region. Therefore, exogenous wind-borne debris generated outside of a study region that then enters the study region (see Figure 3.1) could potentially influence the results of the BEFA model. This study will determine if exogenous wind-borne debris has a statistically significant influence on the results of the BEFA model, and then develop a methodology to account for exogenous wind-borne debris within a mechanics-based building envelope failure assessment model.

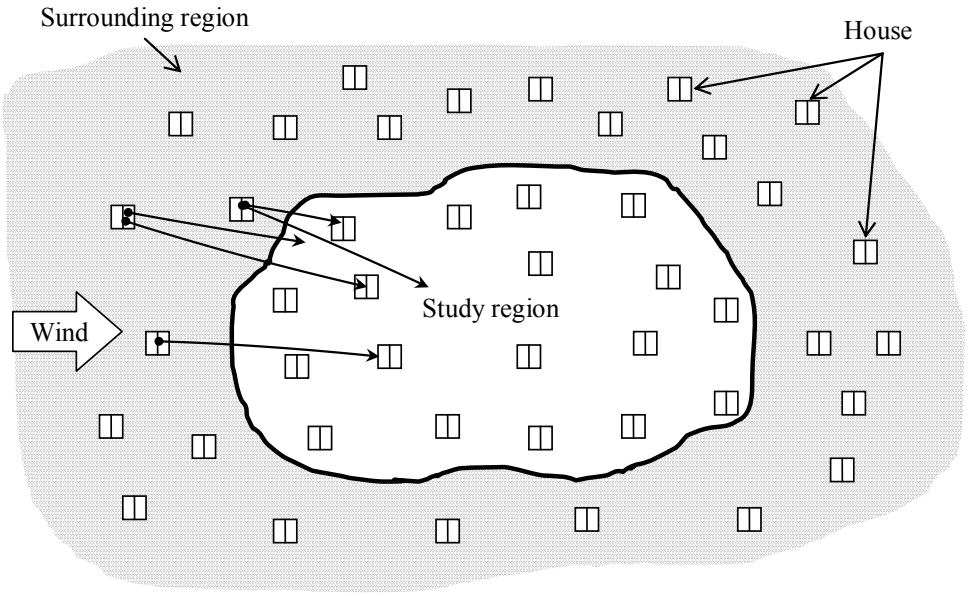

Figure 3.1: Plan view of exogenous wind-borne debris entering a study region and interacting with the building stock.

3.2 Determination of the Significance of Exogenous Wind-borne Debris

3.2.1 Modeling a Typical SC Residential Development

The study region was a 38-home residential development with house spacing, orientation, construction materials, and type of construction similar to that of a typical South Carolina (SC) residential development. Figure 3.2 provides the layout of the 38-home residential development including the surrounding debris impact surfaces (i.e., the sides of the octagon) for the eight principal directions (i.e., N-NW-W-SW-S-SE-E-NE). These impact surfaces were used to capture all relevant information pertaining to the wind-borne debris that leaves the study region during a simulation. A probabilistic three-dimensional wind-borne debris trajectory model developed by Grayson et al. (2012) is capable of providing the location, translational and rotational velocity and acceleration, in addition to the physical attributes of the wind-borne debris released during a simulation. The wind-borne debris information captured was used to determine if the influence of exogenous wind-borne debris significantly influences the results of the BEFA model and to determine best-fit statistical distributions that can be utilized to generate exogenous wind-borne debris within the BEFA model. Building component capacities utilized in the building models are the same as those presented in Chapter 2 and Grayson et al. (2013a).

3.2.2 Generation of the Historical Hurricane Hugo

The historical Hurricane Hugo was simulated from data obtained from the National Oceanic and Atmospheric Administration (NOAA) Atlantic basin hurricane database (HURDAT). The data provided by HURDAT, in conjunction with gradient-to-surface

wind speed conversion factors (Lee and Rosowsky 2007), was used to calculate the mean 10-minute surface wind speed and the eye path of Hurricane Hugo in 10-minute increments (i.e., time step (Δt) = 10 minutes). The 3-second gust wind speeds were sampled for each house within the residential development during the passage of Hurricane Hugo to simulate the variability in wind speed due to local effects created by the close proximity of the structures. Figure 3.2 illustrates the passage of Hurricane Hugo through South Carolina, and the placement of the residential development with respect to the radius-to-maximum winds (*Rmax*) of Hurricane Hugo estimated at 0530 UTC. The placement of the residential development at the northeast *Rmax* of Hurricane Hugo was chosen based on results from Grayson et al. (2013a) identifying this location as a region potentially influenced by the effects of exogenous wind-borne debris. Grayson et al. (2013a) found that the residential development at this location experienced the highest 3-second gust wind speeds but exhibited the lowest percentage of wind-borne debris impacts when compared to locations at the eye path and the southwest *Rmax* of Hurricane Hugo. This was found to be due to the majority of wind-borne debris produced from within the residential development at the northeast *Rmax* of Hurricane Hugo leaving the residential development before impact within the study region.

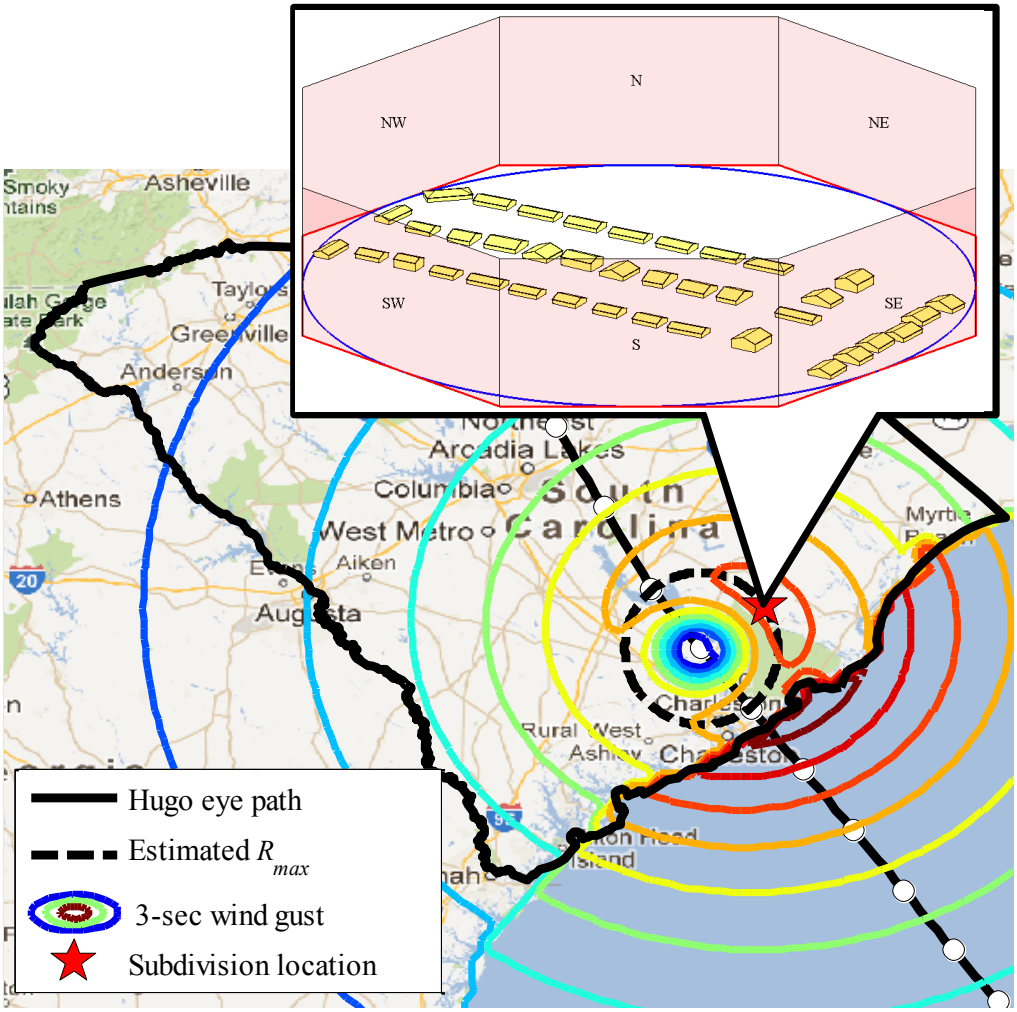

Figure 3.2: Residential development layout and placement during the passage of Hurricane Hugo. Image © 2013 TerraMetrics; © 2013 Google.

3.3 Statistical Significance of Exogenous Wind-borne Debris

There are two parameters that were of interest in this study: (1) the total wind-borne debris released (either endogenous or exogenous wind-borne debris), and (2) the total impacts that occurred within the residential development. These two parameters were further separated into two scenarios: (1) without considering exogenous wind-borne debris, and (2) considering exogenous wind-borne debris. An initial analysis of the

simulation data obtained from the BEFA model illustrates that endogenous wind-borne debris produced within the residential development was leaving the residential development before causing any impacts. The exogenous wind-borne debris captured by the impact surfaces for each of the eight principal directions were re-injected back into the residential development at each time step (see Figure 3.3). This assumes that the study region is surrounded by regions similar in building layout and stock, and that time lag due to the translational speed of the hurricane does not influence the amount of wind-borne debris produced at a particular time step.

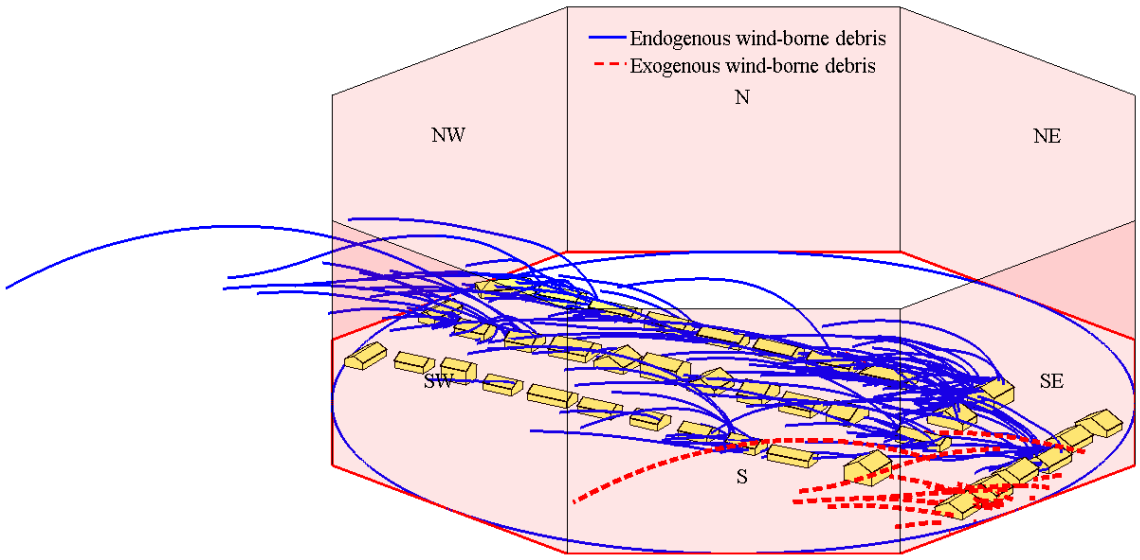

Figure 3.3: Example of wind-borne debris release including exogenous wind-borne debris at 0510 UTC during the passage of Hurricane Hugo.

A rigorous statistical analysis was performed on the captured data to determine if the study region experienced a statistically significant increase in the number of wind-borne debris present and the number of impacts produced by exogenous wind-borne debris within the study region. Figure 3.4 illustrates the influence of exogenous wind-borne

debris on the time evolution of the mean number of debris released and impacts experienced by the typical SC residential development for 100 simulations of Hurricane Hugo. The results of Figure 3.4 establish that there was an increase in both the debris released and the number of impacts experienced by a study region when considering exogenous wind-borne debris.

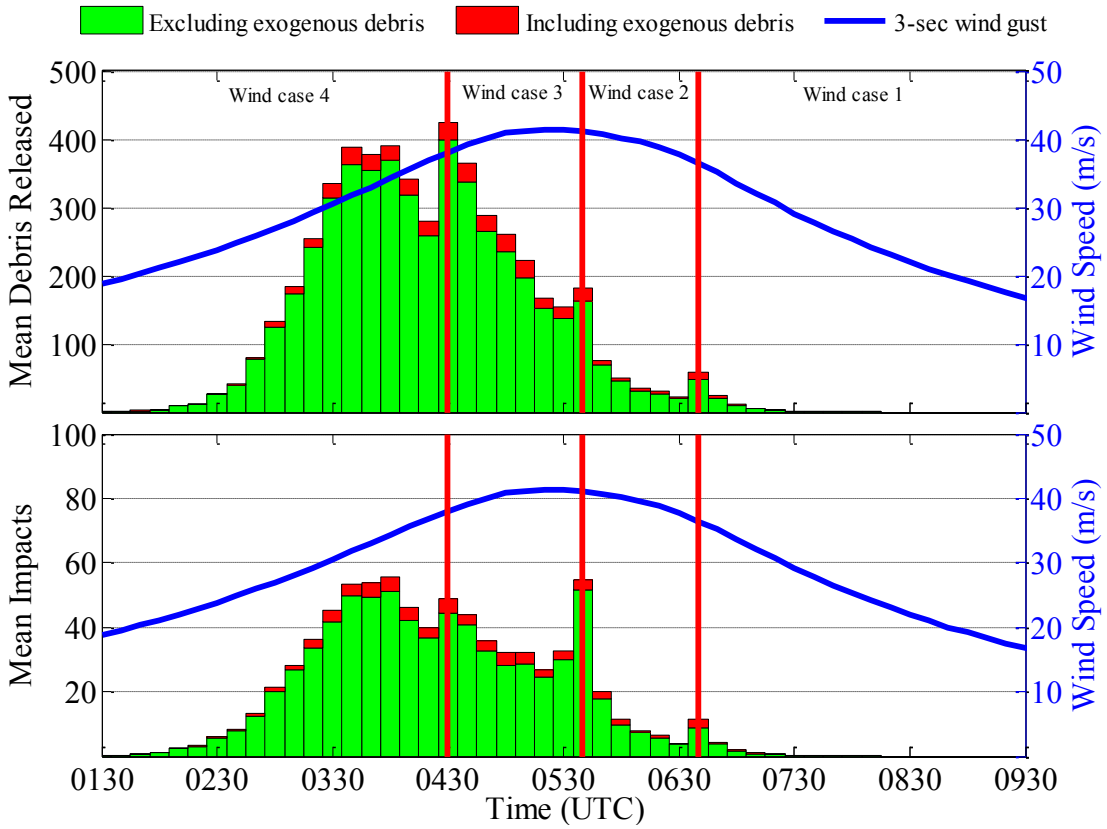

Figure 3.4: Time evolution of the mean debris released and the mean impacts to the building envelope that occurred during the passage of Hurricane Hugo with and without considering the influence of exogenous wind-borne debris. Vertical red lines delineate the wind cases (see Figure 2.3) experienced by the development.

Statistical significance for both parameters of interest (i.e., (1) the total debris released, and (2) the total impacts) was determined through inferences about the

difference in population means (e.g., $\mu_1 - \mu_2$) first without considering exogenous wind-borne debris, and then considering exogenous wind-borne debris. A research hypothesis was developed and tested using statistical methods to estimate the difference between the population means using the simulation sample statistics. Compliance of the sample data with the following requirements was established to determine which statistical test is appropriate to compare the population means:

1. random samples are independently selected from two populations,
2. both population distributions can be assumed to be normally distributed, and
3. both populations can be assumed to possess equal variance (i.e., $\sigma_1 = \sigma_2$).

It was preferable to use a simple *t*-test to determine statistical significance since only two populations were being compared in this study. However, if the populations could not be reasonably assumed to meet all of these requirements, it would be necessary to employ approximate methods. Each of the aforementioned conditions was checked in the subsequent sections to ensure that the appropriate test was performed to determine the statistical significance of the influence of exogenous wind-borne debris within the BEFA model. It is assumed that the simulations performed to capture data from a single population (i.e., the simulations performed to capture the total debris released data) and between two populations (i.e., between sets of simulations that do and do not consider exogenous wind-borne debris) were independently sampled. This assumption is due to the use of the Mersenne Twister pseudorandom number generator within MATLAB to generate the random numbers for the simulations.

3.3.1 Testing the Assumption of Normality

Testing the normality of the random samples obtained from the simulations was initially performed through graphical means for each of the two parameters of interest with a box plot and a normal probability plot (see Figure 3.5). However, these plots did not provide enough evidence to conclude that the total debris released data had been sampled from a normal distribution. Therefore, the Lilliefors test for normality was used to test both scenarios for each of the two parameters of interest to be reasonably certain that an assumption of normality was reasonable.

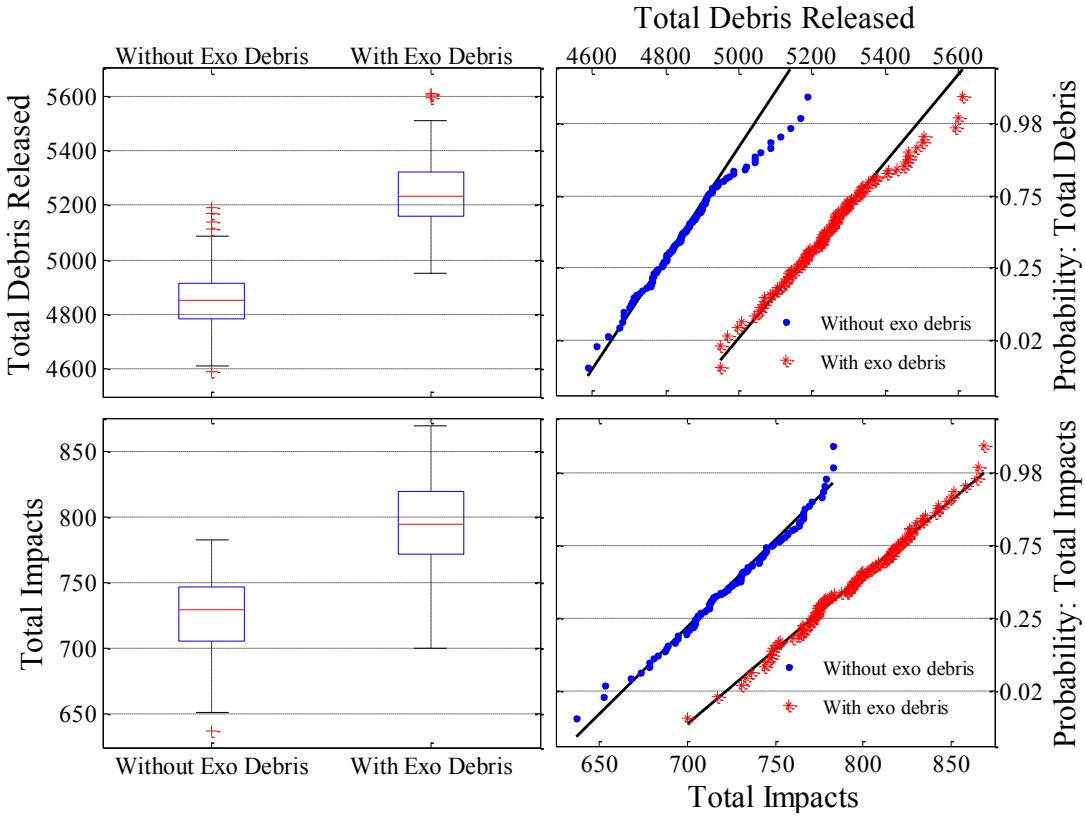

Figure 3.5: Qualitative comparisons to test the normality of the simulated data for the total number of debris released, and the total number of impacts produced during the passage of Hurricane Hugo.

The Lilliefors test for normality is an adaptation of the Kolmogorov-Smirnov (KS) goodness-of-fit test that, unlike the KS test, utilizes the sampled data to estimate the null hypothesis parameters (Abdi and Molin 2007). The null hypothesis for the Lilliefors test is that the error between the sampled data and a normal distribution (ε_x) are normally distributed as shown in Eqn. 3.1:

$$\begin{aligned} H_0 &: \varepsilon_X \sim N\left(\mu_X, \sigma_X^2\right) \\ H_a &: \varepsilon_X \neq N\left(\mu_X, \sigma_X^2\right) \end{aligned} \tag{3.1}$$

where H_0 represents the null hypothesis and H_a represents the alternative hypothesis. Eqns. 3.2 to 3.4 transform the sample data to a standard normal variable (Z_i), while Eqn. 3.5 is used to calculate the cumulative distribution function (CDF) of Z_i for the standard normal distribution:

$$\bar{y}_X = \frac{1}{n}\sum_i^n X_i \tag{3.2}$$

$$S_X{}^2 = \frac{\sum_i^n \left(X_i - \bar{y}_X\right)^2}{n-1} \tag{3.3}$$

$$Z_i = \frac{X_i - \bar{y}_X}{S_X} \tag{3.4}$$

$$N\left(Z_i\right) = \int_{-\infty}^{Z_i} \frac{1}{\sqrt{2\pi}} \exp\left\{-\frac{1}{2} Z_i^2\right\} \tag{3.5}$$

where X_i is the sampled data, $\bar{y}_X$ is the mean of the sampled data, n is the sample size (n = 100 for this study), and S_X^2 is the variance of the sampled data.

Once the data is transformed to the standard normal distribution, the Lilliefors test statistic (L_{test}) is calculated as shown in Eqn. 3.6:

$$L_{test} = \max \begin{Bmatrix} \left|S(Z_i) - N(Z_{i-1})\right|, \left|S(Z_i) - N(Z_i)\right|, \dots \\ , \left|S(Z_n) - N(Z_{n-1})\right|, \left|S(Z_n) - N(Z_n)\right| \end{Bmatrix} \quad 3.6$$

where $S(Z_i)$ is the proportion of scores smaller than Z_i (i.e., the empirical CDF of the sampled data), and the maximum absolute difference is taken between the empirical CDF and the standard normal distribution CDF. L_{test} is compared to a critical value ($L_{critical}$) and the null hypothesis is rejected if:

$$Reject\ H_0 : L_{test} \geq L_{critical} = L_{n,\alpha} \quad 3.7$$

$L_{critical}$ is dependent upon the sample size and the level of significance (α) used in the analysis and is typically taken from a table of values determined using the Monte Carlo Simulation technique for $n \leq 50$. For $n > 50$, $L_{critical}$ is calculated as shown in Eqn. 3.8 with $\alpha = 0.05$:

$$L_{critical} = \frac{0.895}{f_n} \quad 3.8$$

where 0.895 is a constant taken from a table of critical values for the Lilliefors test for normality as seen in Abdi and Molin (2007), and f_n is calculated from the sample size as shown in Eqn. 3.9.

$$f_n = \frac{83 + n}{\sqrt{n}} - 0.01 \quad 3.9$$

Figure 3.6 provides a visual illustration of the overlays of the empirical CDF and the standard normal distribution from the four cases tested for all of the simulated data. The data from all four cases met the requirements of normality since the Lilliefors test for normality failed to reject the null hypothesis of Eqn. 3.7 in all four cases.

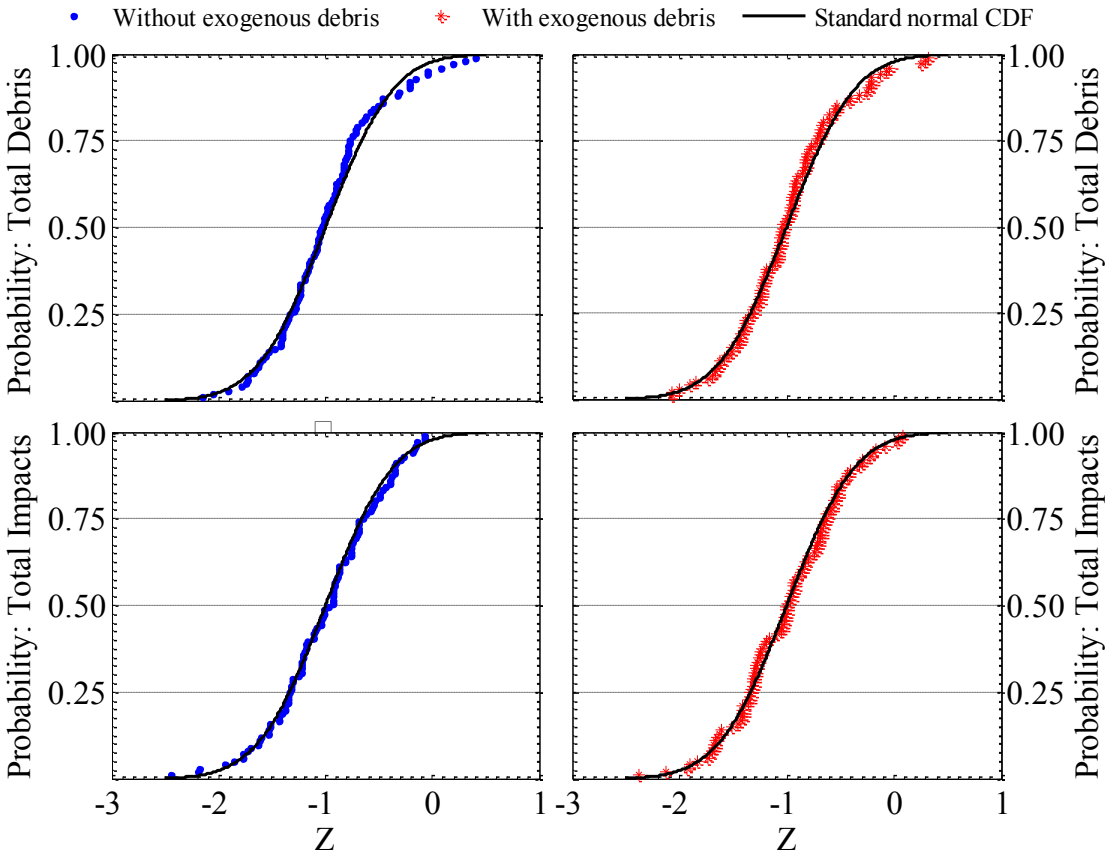

Figure 3.6: Comparison plot of the transformed empirical data used in the Lilliefors test with the standard normal CDF.

3.3.2 Testing the Assumption of Equal Variances

The final requirement that must be met was to ensure that it was reasonable to assume that the population variances were equal for both parameters of interest (i.e., the total debris released and the total impacts). This was determined using a two-tailed *F*-test to

compare the population variances estimated from the sample statistics. The research hypothesis testing the equality of the population variances was as shown in Eqn. 3.10 (Ayyub and McCuen 2002):

$$\begin{aligned} H_0 &: \sigma_1^2 - \sigma_2^2 = 0 \\ H_a &: \sigma_1^2 - \sigma_2^2 \neq 0 \end{aligned} \qquad 3.10.$$

The test statistic for the two-tailed *F*-test is calculated as the ratio of the sample variances as shown in Eqn. 3.11.

$$F_{test} = \frac{S_1^2}{S_2^2} \qquad 3.11$$

The requirements to reject the null hypothesis (H_0) for a two-tailed *F*-test are as shown in Eqn. 3.12:

$$\begin{aligned} &Reject\ H_0 : F_{test} \leq F_{critical} = F_{1-\alpha/2, df_1, df_2} \\ &Reject\ H_0 : F_{test} \geq F_{critical} = F_{\alpha/2, df_1, df_2} \end{aligned} \qquad 3.12$$

where df_1 and df_2 are the degrees-of-freedom for the two populations that are being compared. The two requirements of Eqn. 3.12 can be rearranged to provide a range of the *F*-test statistic that fails to reject the null hypothesis (H_0) as shown in Eqn. 3.13.

$$Fail\ to\ reject\ H_0 : F_{\alpha/2, df_1, df_2} < F_{test} < F_{1-\alpha/2, df_1, df_2} \qquad 3.13$$

Figure 3.7 provides graphical results from the two-tailed *F*-test of equal variances for the total debris released and the total impacts assuming a level of significance (α) = 0.05. In both cases, the *F*-test failed to reject the null hypothesis that the two population variances

for both cases are equal; therefore, it seems reasonable to assume that the data meets the requirement of equal variances.

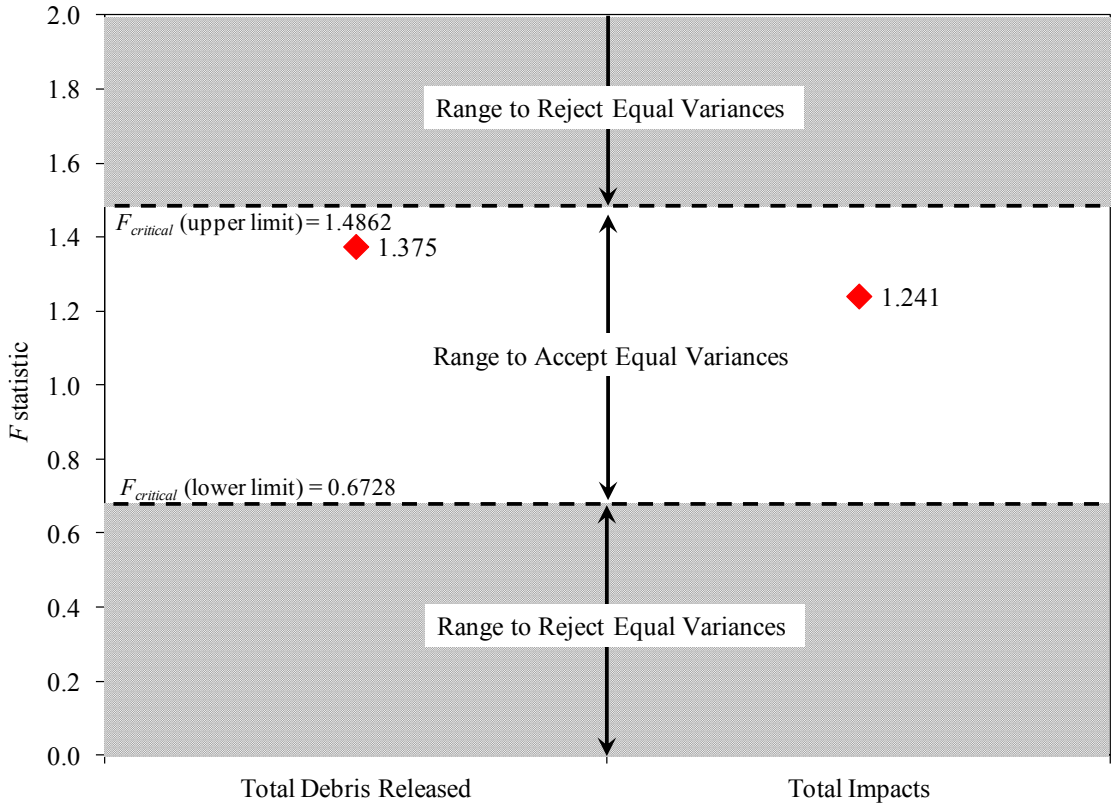

Figure 3.7: *F*-test results for the total debris released and total impacts ($\alpha = 0.05$).

3.3.3 Calculation of Statistical Significance of Exogenous Wind-borne Debris

Results have determined that the sample data intended to represent the two populations (i.e., excluding exogenous wind-borne debris and including exogenous wind-borne debris) reasonably meets the requirements of independency, normality, and equal variances. A two-tailed *t*-test was performed to determine if there is a statistically significant difference between the total debris released and the total impacts experienced when considering exogenous wind-borne debris within the simulations. The research hypothesis developed to represent the difference in total debris released and total impacts

due to the consideration of exogenous wind-borne debris is stated as the difference between the means of two populations as shown in Eqn. 3.14 (Ayyub and McCuen 2002):

$$\begin{aligned} H_0 &: \mu_1 - \mu_2 = 0 \\ H_a &: \mu_1 - \mu_2 \neq 0 \end{aligned} \tag{3.14}$$

where μ_1 and μ_2 are the population means excluding and including exogenous wind-borne debris, respectively.

The test statistic (t_{test}) illustrated in Eqn. 3.15 is calculated as the difference between the sample means minus a predetermined value (D_0) that is dependent upon the definition of the null hypothesis. In the case of this research, D_0 is equal to zero since the purpose of the test was to determine if the inclusion of exogenous wind-borne caused any type of significant difference in the population means (e.g., higher, lower, or equal).

$$t_{test} = \frac{\left(\bar{y}_1 - \bar{y}_2\right) - D_0}{S_p \sqrt{\frac{1}{n_1} + \frac{1}{n_2}}} \tag{3.15}$$

where S_p is the pooled standard deviation of the two sample standard deviations estimated for the two populations as shown in Eqn. 3.16.

$$S_p = \sqrt{\frac{\left(n_1 - 1\right)S_1^2 + \left(n_2 - 1\right)S_2^2}{n_1 + n_2 - 2}} \tag{3.16}$$

A two-tailed *t*-test was performed to determine if there was any significant difference (i.e., an increase or decrease) in the results to provide a sanity check to ensure that the simulations are providing reasonable results. A determination of a significant increase or decrease in the results is obtained from the mathematical sign of the *t*-statistic (e.g., in

this case, a positive *t*-statistic represents a decrease in the parameter tested, and a negative *t*-statistic represents an increase in the parameter tested). The criterion to reject the null hypothesis for a two-tailed *t*-test is as shown in Eqn. 3.17.

$$Reject\ H_0 : |t_{test}| \geq t_{critical} = t_{\alpha/2,df} \qquad 3.17$$

Figure 3.8 provides graphical results from the application of the two-tailed *t*-test of equal means. Comparison of the test statistic (t_{test}) to $t_{critical}$ revealed that it is reasonable to assume a significant statistical increase in the two population means for both parameters of interest as the null hypothesis was rejected in both cases (i.e. total debris generated and total impacts for cases with and without exogenous wind-borne debris).

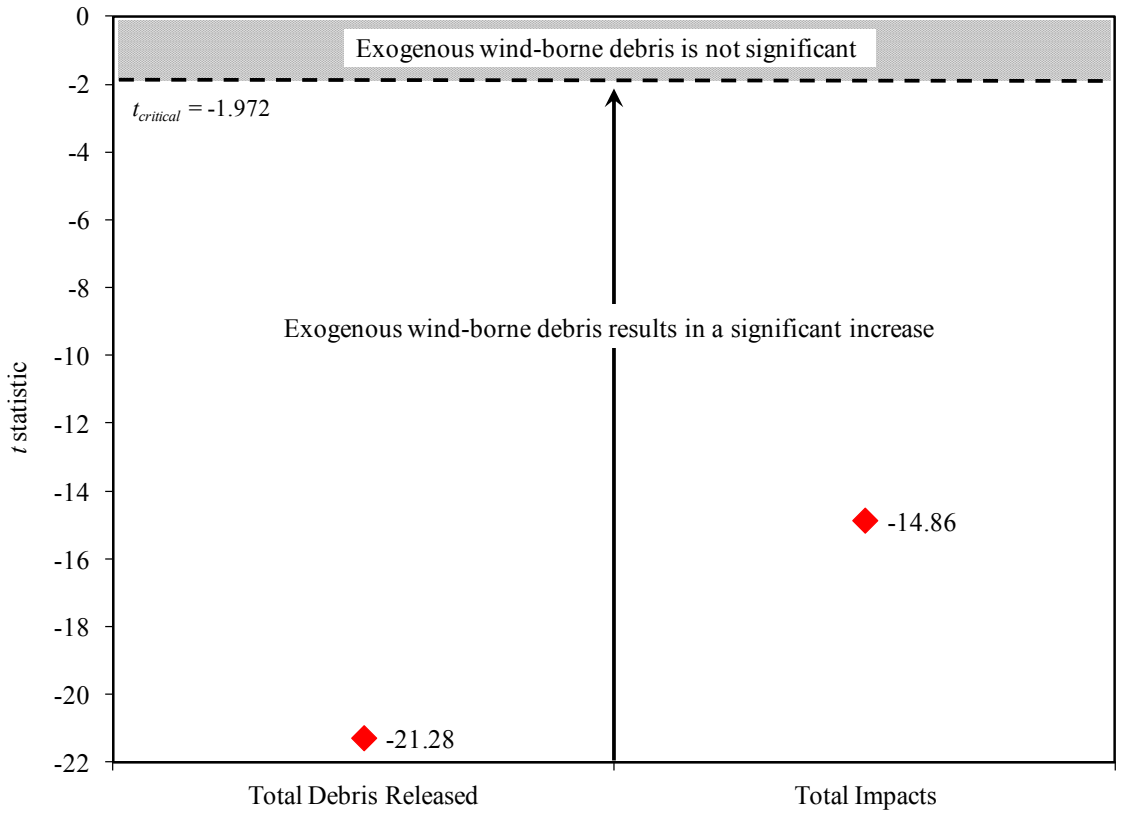

Figure 3.8: *t*-test results for the total debris released and total impacts ($\alpha = 0.05$).

3.4 Methodology to Account for Exogenous Wind-borne Debris Within the BEFA Model

The preceding sections have illustrated that exogenous wind-borne debris can cause a statistically significant, although not necessarily globally significant, increase in the output of the BEFA model. Therefore, a methodology is developed to include the influence of exogenous wind-borne debris within the BEFA model. This methodology identifies two scenarios that must be considered to account for the influence of exogenous wind-borne debris within the BEFA simulations:

1. a study region (e.g., residential development) is surrounded by similar building stock and layouts in each of the eight principal directions, and
2. a study region is surrounded by building stock, building layout, or topography (e.g., wooded area versus populated area) that are deemed to contain enough significant differences as to influence the amount and type of exogenous debris entering the study region.

3.4.1 Scenario 1: Study Region with Similar Surroundings

The first scenario (see Figure 3.9) is addressed through a one-step process that captured the wind-borne debris exiting the study region and re-injects the exiting wind-borne debris back into the study region. For example, if the debris released within a residential development exits the study region to the northwest of the residential development, then the debris would be re-injected back into the study region from the southeast. Since the study region in this scenario is similar to its surroundings, the re-injected exogenous wind-borne debris retains the traits of the endogenous debris from

when it initially left the study region. This is the same scenario assumed in the preceding sections of this study to determine the significance of exogenous wind-borne debris.

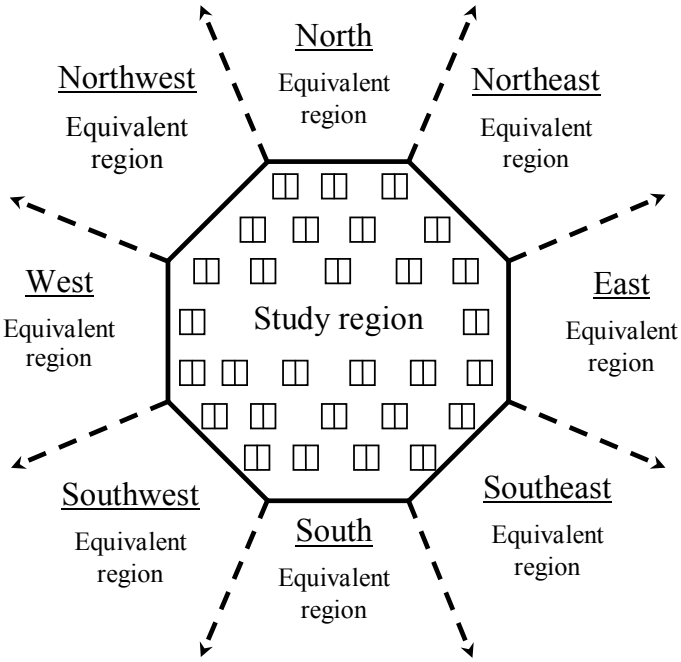

Figure 3.9. Plan view of study region illustrating scenario 1.

3.4.2 Scenario 2: Study Region with Different Surroundings

The second scenario (see Figure 3.10) requires a two-step process to account for identified differences in building stock, building layout, and/or topography in one or more of the eight principal directions. The first step of the second scenario consists of assessing the surrounding areas with the mechanics-based building envelope failure assessment model for the hurricane event of interest. The results from this assessment utilize the method of the first scenario to capture the relevant wind-borne debris parameters (e.g., debris path, velocity, location, physical attributes, and the rate that the debris exit the study region) for each of the surrounding areas that differ from the primary

study region. Once the surrounding areas have been evaluated, the second step in the process imports the identified statistical distributions and relevant exogenous wind-borne debris information into the hurricane damage assessment model to generate the appropriate type and amount of wind-borne debris entering the study region from the surrounding areas. Scenario 2 has the potential to become very computationally demanding since information will have to be collected for each of the different surrounding areas. However, simulations for typical residential areas, for example, basic layouts for residential developments where the majority of homes have asphalt shingle roofs as opposed to clay tile roofs, can be performed in advance and the results retained to create a database of information that can be utilized at a later date.

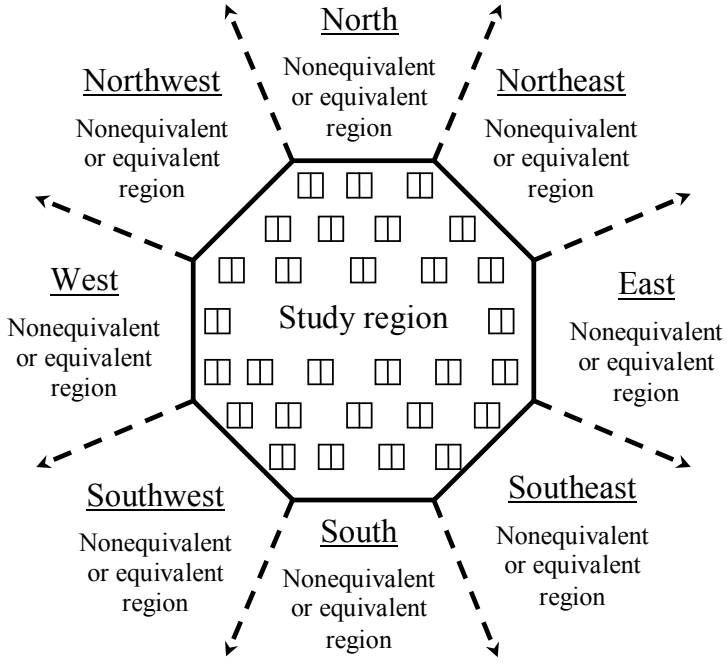

Figure 3.10: Plan view of study region illustrating scenario 2.

3.5 Development of an Exogenous Wind-borne Debris Generator

It is necessary to develop an exogenous wind-borne debris generator to include the appropriate type and amount of wind-borne debris at each time step of the simulation for scenario 2. Figures 3.11 and 3.12 illustrate the time evolution of the plate (e.g., roof and wall sheathing, and roof covering) and rod (e.g., roof fascia and truss members) debris rates for each of the eight principal directions for 100 simulations of the residential development exposed to Hurricane Hugo. The variations in the debris released that left the study region closely followed the peaks observed at various time steps during the time evolutions presented by Grayson et al. (2013a).

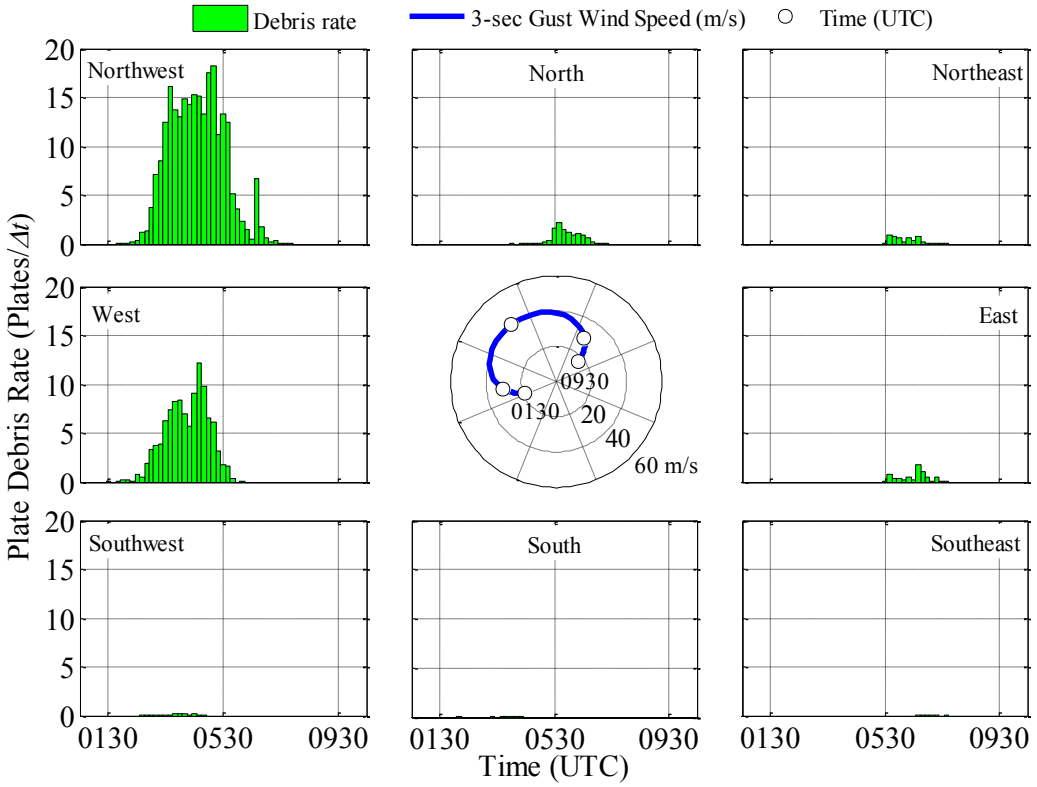

Figure 3.11: The time evolution of the plate debris captured by the impact surfaces that surround the residential development in this study.

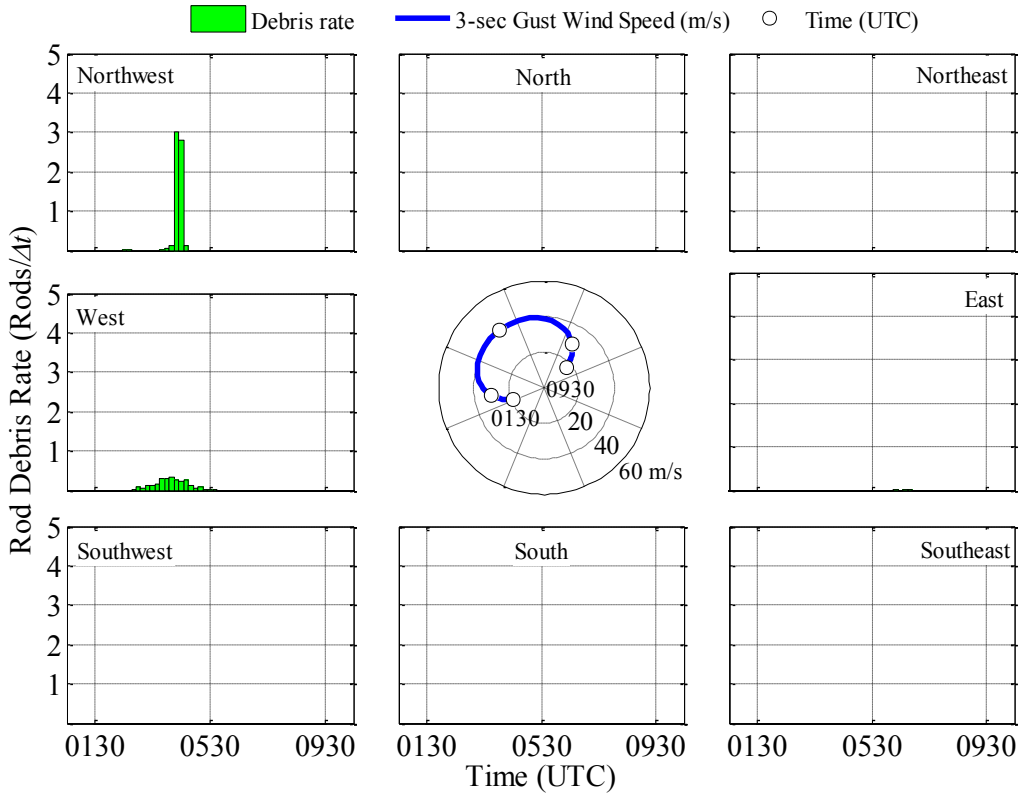

Figure 3.12: The time evolution of the rod debris captured by the impact surfaces that surround the residential development in this study.

It was determined by Grayson et al. (2013a) that this phenomenon was due to a change in wind direction that subjects the homes of the residential development to a different set of wind pressure zones, thereby altering the amount of debris released into the windfield during that particular time step. As the wind speed increases in velocity and the wind pressure applied to the homes changes with a change in wind direction, there can be a significant increase in wind-borne debris released during the initial time step after the change in wind direction. Therefore, a best-fit statistical distribution was selected by fitting the data at each time step and selecting the distribution that generated

debris that most closely matched the captured debris data taken from the simulations for the duration of the hurricane.

3.5.1 Best-fit Statistical Distribution to Model Exogenous Wind-borne debris

Analysis of exogenous wind-borne debris rates for plates and rods at each time step during the passage of Hurricane Hugo identified several potential best-fit distributions that could be utilized as the basis for an exogenous wind-borne debris generator. Exogenous wind-borne debris values can theoretically range from zero to any positive integer value, which would imply that a discrete distribution might be the choice for an exogenous wind-borne debris generator, however, both discrete and continuous distributions were considered as potential best-fit statistical distribution.

An initial assessment of the domain of the sample data coupled with a graphical comparison of the captured (empirical) data identified six potential cumulative distribution functions (CDF) and cumulative mass functions (CMF). The six potential distributions investigated were the (1) lognormal, (2) exponential, (3) type I extreme value largest (Gumbel), (4) two-parameter type III extreme value smallest (Weibull), (5) Poisson, and (6) negative binomial distributions. Figure 3.13 provides an example using the plate debris rates captured from the northwest impact surface to illustrate the graphical comparison that was performed at each time step during the passage of Hurricane Hugo.

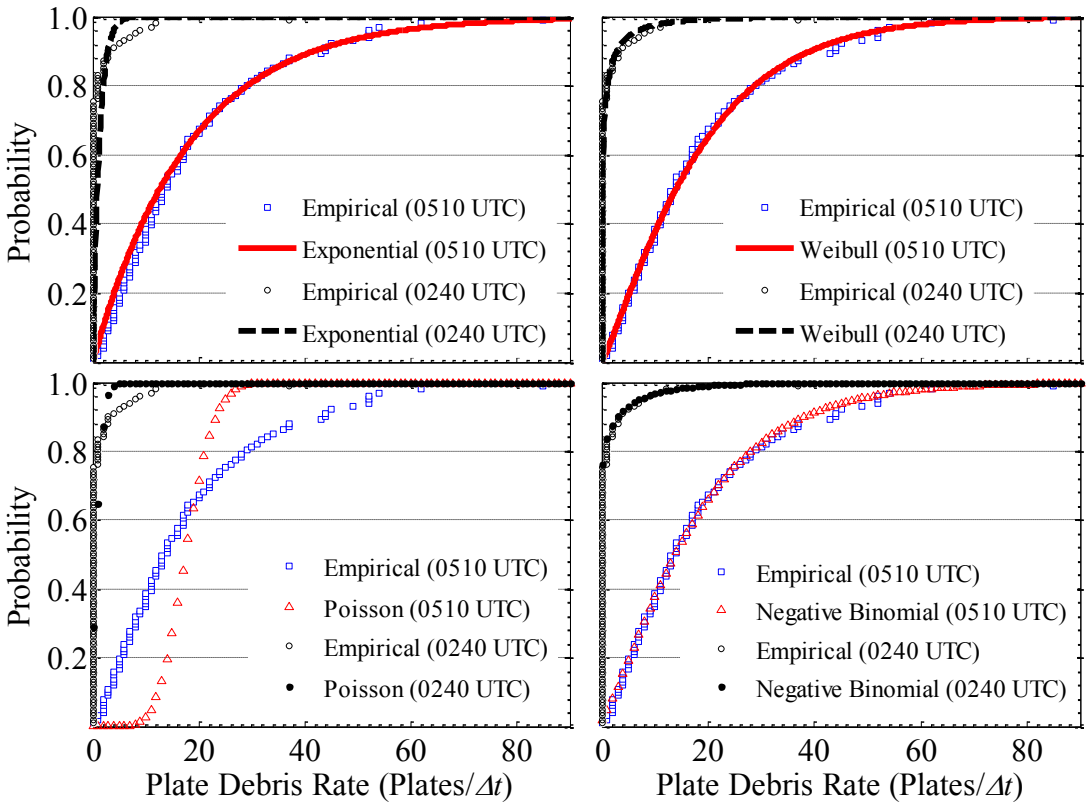

Figure 3.13: Graphical comparisons for both discrete and continuous distributions to the plate debris rate leaving the study region from the northwest.

3.5.2 Continuous Distributions Investigated as Best-fit Distributions

The following section provides the CDFs that were investigated as a best-fit statistical distribution to the captured exogenous wind-borne data. The maximum likelihood estimate (MLE) method was used to estimate the parameters of the distributions except in the case of the type III smallest extreme value (Weibull) distribution. Due to the necessity to include zero in the domain of the distribution, the method of least squares was used to determine the parameters of the Weibull distribution that best fit the data in this study.

The lognormal distribution is useful for modeling data in which only positive values (i.e., x > 0) satisfy the domain of the event of interest. The CDF of the lognormal distribution is defined as shown in Eqn. 3.18:

$$P_X(x) = \int_{-\infty}^{Z_{ln}} \frac{1}{\sqrt{2\pi}} exp\left(-\frac{Z_{ln}^2}{2}\right) dz \qquad 3.18$$

where Z_{ln}, defined in Eqn. 3.19, is a transformation variable developed from the relationship of the lognormal distribution with the normal distribution that simplifies the integration of the lognormal probability distribution function.

$$Z_{ln} = \frac{ln\, X - \mu_{ln}}{\sigma_{ln}} \qquad 3.19$$

where μ_{ln} and σ_{ln} are the parameters of the lognormal distribution.

The exponential distribution is a single-parameter distribution with a CDF defined as shown in Eqn. 3.20:

$$F_X(x) = 1 - exp(-\lambda x) \qquad 3.20$$

where λ is the return period of the event of interest.

The type I largest extreme value distribution, also known as the Gumbel distribution, is useful for modeling the upper tail values of the parent distribution. The CDF of the Gumbel distribution is defined as shown in Eqn. 3.21:

$$F_X(x) = exp\left\{-exp\left[-\frac{(x-u)}{\beta}\right]\right\} \qquad 3.21$$

where u is the location parameter and β is the shape parameter of the Gumbel distribution.

The two-parameter type III smallest extreme value distribution, also known as the Weibull distribution, is another limiting distribution similar to the exponential distribution that is useful for modeling data that contains only positive values including zero (i.e., $x \geq 0$). The CDF of the two-parameter Weibull distribution is defined as shown in Eqn. 3.22:

$$F_X(x) = 1 - exp\left[-\left(\frac{x}{v}\right)^k\right] \tag{3.22}$$

where v is the scale parameter and k is the shape parameter of the two-parameter Weibull distribution provided that $v > 0$ and $k > 0$. The two-parameter Weibull distribution parameters are related to the first and second moments of the sample data as illustrated in Eqns. 3.23 and 3.24:

$$\mu_X(v,k) = v\left[\Gamma\left(1+\frac{1}{k}\right)\right] \tag{3.23}$$

$$\sigma_X^2(v,k) = v^2\left[\Gamma\left(1+\frac{2}{k}\right) - \Gamma^2\left(1+\frac{1}{k}\right)\right] \tag{3.24}$$

where $\Gamma(.)$ is the gamma distribution. The MLE method maximizes the logarithm of the likelihood function for the Weibull distribution to estimate the parameters, which is not applicable if zero is a possibility within the data. The method of least squares was used to estimate the parameters of the two-parameter Weibull distribution by minimizing the error (ε_{Fit}) between the mean and standard deviation of the captured data and the mean

and standard deviation obtained from the estimated first and second moments as illustrated in Eqns. 3.25 to 3.27:

$$\varepsilon_{Fit} = \sqrt{\varepsilon_{\mu}^2 + \varepsilon_{\sigma}^2} \tag{3.25}$$

where

$$\varepsilon_{\mu} = \mu_{Data} - \mu_X(v,k), \text{ and} \tag{3.26}$$

$$\varepsilon_{\sigma} = \sigma_{Data} - \sqrt{\sigma_X^2(v,k)}. \tag{3.27}$$

3.5.3 Discrete Distributions Investigated as Best-fit Distributions

The following section provides the CMFs that were investigated as best-fit statistical distributions for use as an exogenous wind-borne debris generator. The MLE method was used to estimate the parameters of the distribution for both the Poisson and the negative binomial distributions.

The Poisson distribution is a single-parameter discrete distribution that is useful for modeling data that occur over a continuous interval (i.e., time or space), such as natural hazards (e.g., hurricanes, tornadoes, and earthquakes) (Ayuub and McCuen 2002). The CMF for the Poisson distribution is defined as shown in Eqn. 3.28:

$$F_X(x) = exp\left(-\lambda_p\right) \sum_{i=0}^{floor(x)} \frac{{\lambda_p}^i}{i!} \tag{3.28}$$

where λ_p is the average rate of occurrence of the event. The Poisson distribution is sensitive to the dispersion of the data since it is a single-parameter distribution that

cannot adjust for variations in the variance of the sample data unlike the exponential distribution. This inflexibility can create significant problems, especially when fitting data that is overdispersed as shown in Figure 3.13.

The negative binomial distribution is a two-parameter discrete distribution that is a general form of the geometric distribution which can be useful for modeling count data that exhibit overdispersion (i.e., the sample variance is larger than the sample mean). The CMF for the negative binomial distribution is defined as shown in Eqn. 3.29:

$$F_X(x) = \sum_{i=0}^{floor(x)} \binom{r+i-1}{i} p^r (1-p)^i \tag{3.29}$$

where r is the number of successes and p is the probability of success in a single trial.

3.5.4 Goodness-of-fit Tests Used to Determine the Best-fit Statistical Distributions

Goodness-of-fit tests were performed at each time step to select the two distributions that were used ultimately to generate exogenous wind-borne debris for comparison to the exogenous wind-borne debris captured by the impact surfaces surrounding the residential development. Discrete distributions were tested using the Chi-square test for goodness-of-fit in which the chi-square test statistic, defined in Eqn. 3.30, is calculated based on the observed and expected frequencies of the sample data (Ayuub and McCuen 2002).

$$\chi^2 = \sum_{i=1}^{k} \frac{O_i - E_i}{E_i} \tag{3.30}$$

The research hypothesis for the Chi-square test in this case is as shown in Eqn. 3.31:

$$H_0 : X \sim f_X(x)$$
$$H_a : X \neq f_X(x) \tag{3.31}$$

where $F_x(x)$ is the assumed probability mass or density function that is being compared to the test data. Eqn. 3.32 provides the Chi-square test criteria to reject the null hypothesis:

$$Reject\ H_0 : \chi^2 > \chi^2_{critical} = \chi^2_{\alpha,df}\ . \tag{3.32}$$

Continuous distributions were tested using the Kolmogorov-Smirnov (KS) goodness-of-fit test. The research hypothesis for the KS test is equivalent to the hypothesis test defined for the chi-square test in Eqn. 3.31, and Eqn. 3.33 defines the empirical CDF of the test data:

$$F_s(x) = \begin{cases} 0 & for\ x < x_1 \\ \dfrac{i}{n} & for\ x_i \le x < x_{i+1} \\ 1 & for\ x \ge x_n \end{cases}. \tag{3.33}$$

The KS test statistic is calculated in a similar fashion to the Lilliefors test statistic by determining the maximum absolute error between the empirical CDF and the CDF of the suspected distribution as shown in Eqn. 3.34 (Ayuub and McCuen 2002):

$$KS_{test} = \max \begin{Bmatrix} \left|F_x(x_i) - F_s(x_{i-1})\right|, \left|F_x(x_i) - F_s(x_i)\right|, \ldots \\ , \left|F_x(x_n) - F_s(x_{n-1})\right|, \left|F_x(x_n) - F_s(x_n)\right| \end{Bmatrix}. \tag{3.34}$$

Eqn. 3.35 provides the KS test criteria used to reject the null hypothesis:

$$Reject\ H_0 : KS_{test} \ge KS_{critical} = KS_{n,\alpha}\ . \tag{3.35}$$

The critical *KS* value ($KS_{critical}$) is a function of the sample size and the level of significance (α) assumed in the analysis. For $n > 35$ and assuming a level of significance (α) of 0.05, the critical *KS* value is calculated as shown in Eqn. 3.36 (Ayuub and McCuen 2002):

$$KS_{critical} = \frac{1.36}{\sqrt{n}} \tag{3.36}$$

where 1.36 is a constant taken from a table of critical values found in Ayuub and McCuen (2002) and *n* is the sample size.

3.5.5 Selection of the Best-fit Distribution for Exogenous Wind-borne Debris

The goodness-of-fit tests identified the two-parameter Weibull distribution and a negative binomial/Poisson distribution combination as the best potential candidates to be used as an exogenous wind-borne debris generator. A negative binomial/Poisson combination is needed due to the invalidity of the negative binomial for data that is underdispersed (i.e., the mean of the data is greater than the variance of the data). Data that is underdispersed is modeled reasonably well with the Poisson distribution since it is a single-parameter distribution that is incapable of adjusting to variability in the data. The negative binomial/Poisson combination, and the two-parameter Weibull distribution were used to generate exogenous wind-borne debris for comparison to the data collected from the debris impact surfaces for the plate and rod debris rates in Figures 3.11 and 3.12.

Figures 3.14 and 3.15 provide a comparison of the generated exogenous wind-borne debris rates (i.e., the debris rates generated using the statistical distributions) and the

captured exogenous wind-borne debris rates (i.e., the debris rates captured on the impact surfaces from the simulations) obtained from the northwest impact surface during the passage of Hurricane Hugo. The rates of the generated debris from the two-parameter Weibull distribution and the negative binomial/Poisson combination fit the captured debris rates reasonably well in both cases.

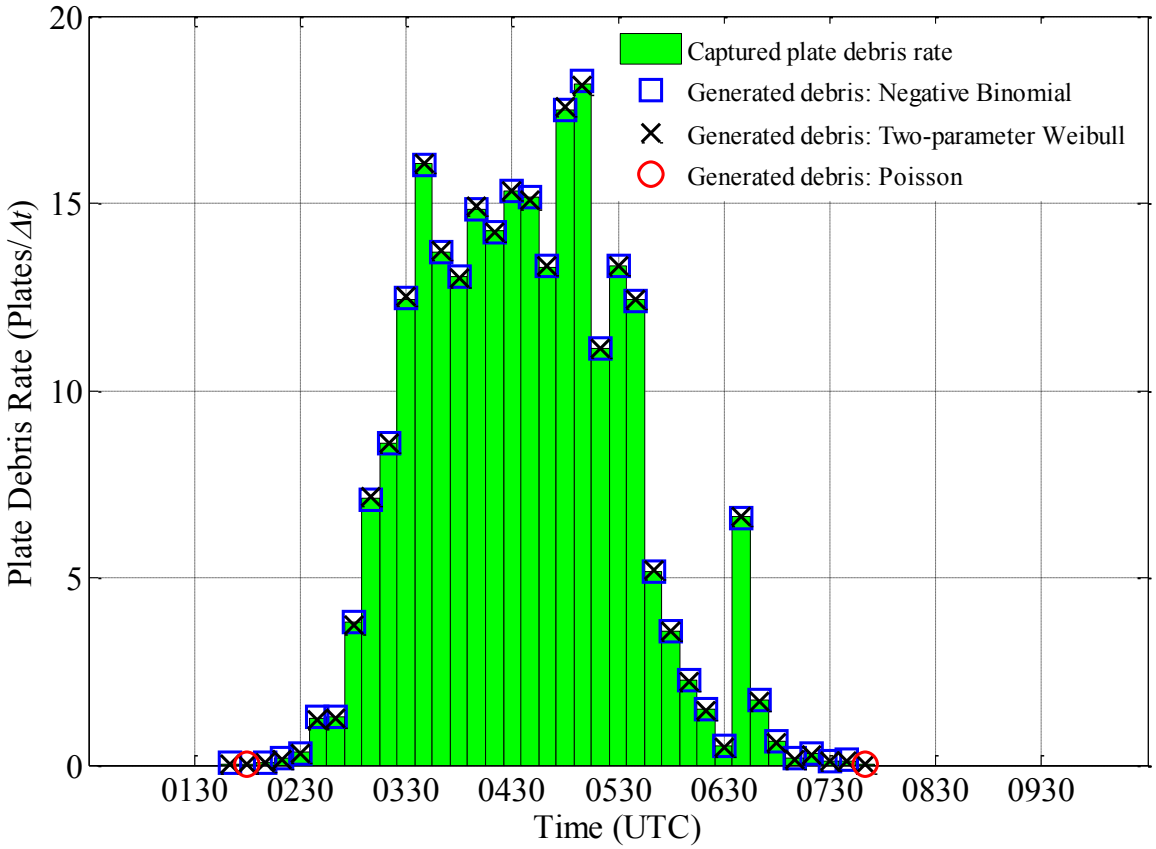

Figure 3.14: Comparison of the generated and captured exogenous wind-borne plate debris rates obtained from the northwest impact surface. Note that the Poisson distribution was only used to generate debris for the instances when the negative binomial is not valid.

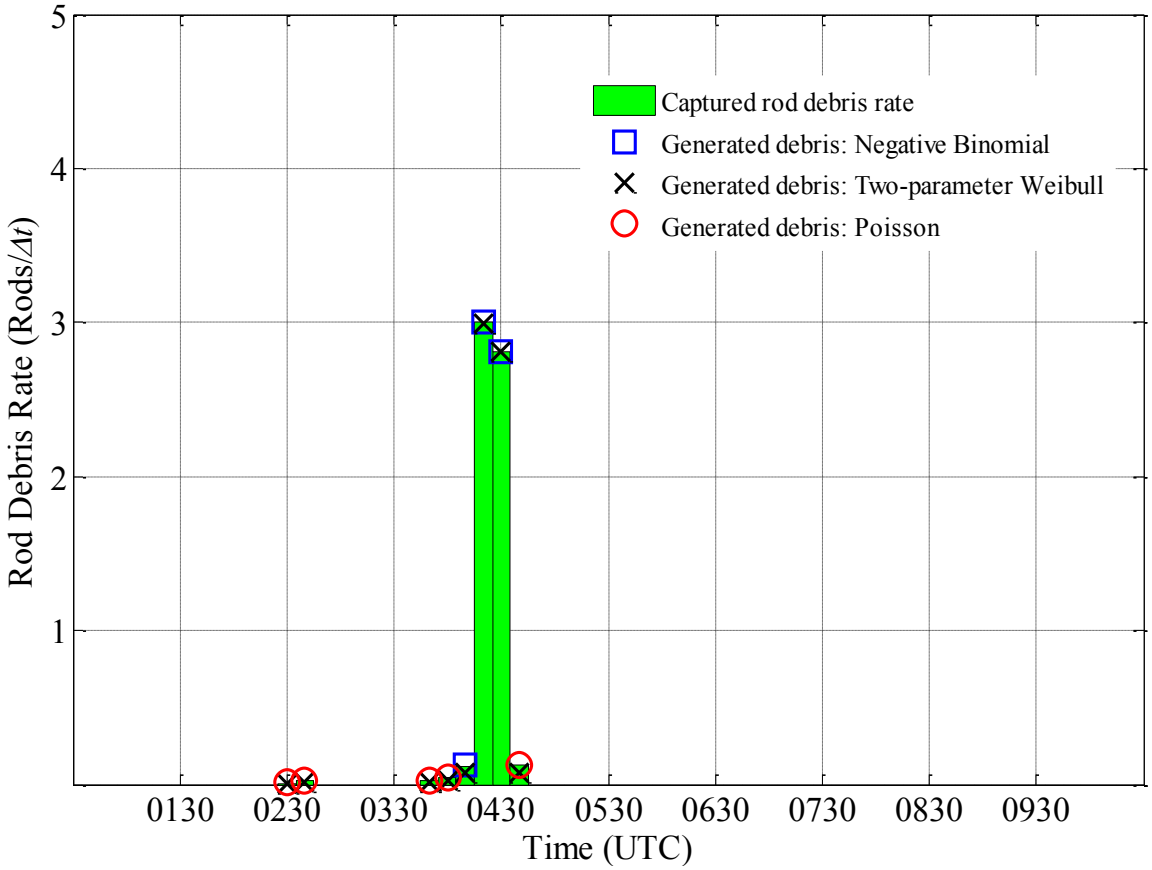

Figure 3.15: Comparison of the generated and captured exogenous wind-borne rod debris rates obtained from the northwest impact surface. Note that the Poisson distribution was only used to generate debris for the instances when the negative binomial is not valid.

Figures 3.16 and 3.17 illustrate the total error (ε_T) between the generated and captured exogenous wind-borne debris rates obtained from the northwest impact surface during the passage of Hurricane Hugo. The total error was calculated from the square root of the sum of the squared errors (SRSS) as shown in Eqn. 3.37:

$$\varepsilon_T = \sqrt{\varepsilon_1^2 + \varepsilon_2^2} \qquad 3.37$$

where, ε_1 and ε_2 are the difference between the arithmetic mean of the captured data and the generated data, and the standard deviation of the captured data and the generated data, respectively.

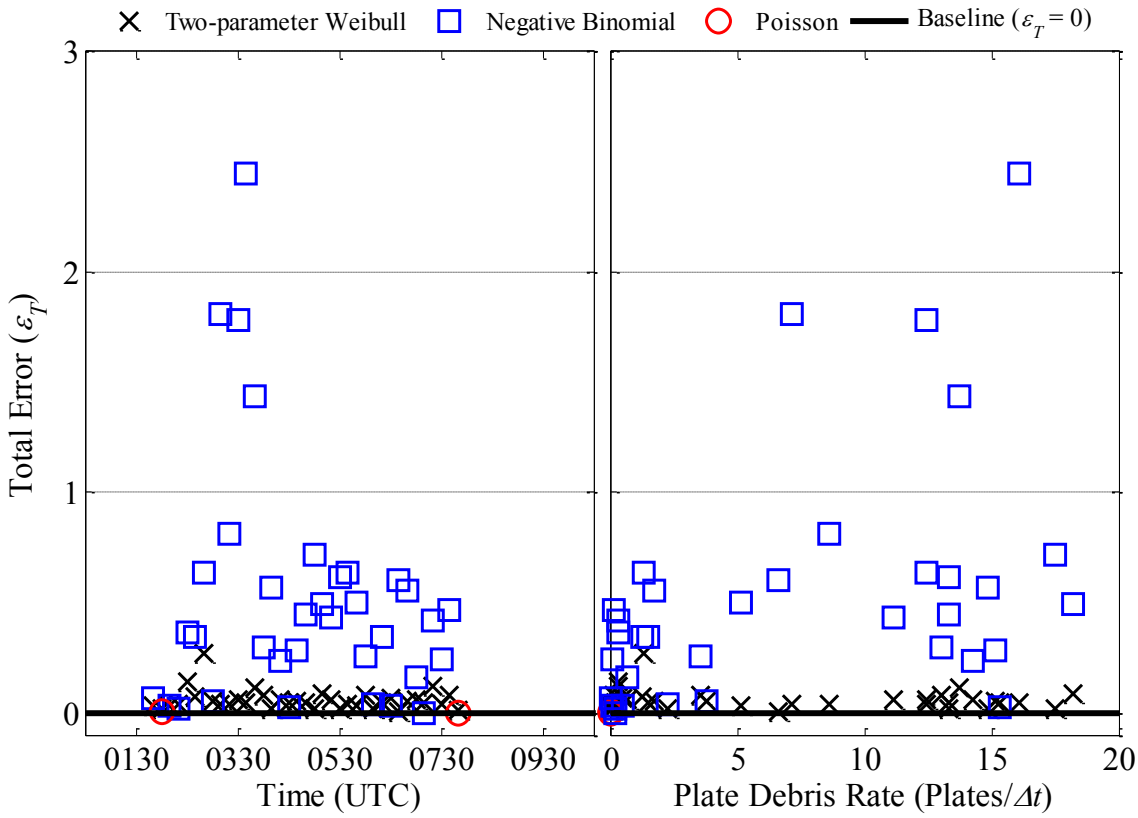

Figure 3.16: Total error as a function of time and mean debris rate for the comparison of the generated and captured exogenous wind-borne plate debris rates.

While both the two-parameter Weibull distribution and the negative binomial/Poisson combination fit the data reasonably well for both rod and plate debris, the negative binomial and the Poisson distributions, as discrete distributions, are the theoretically more appropriate distributions to generate the number of exogenous wind-borne debris needed at each time step. Combining the error of the data statistics in this manner caused the loss of the influence of the individual data statistics on the total error. However,

minimizing the overall influence of the data statistics was deemed more important at this stage of the investigation than closely matching the individual data statistics (i.e., the arithmetic mean and standard deviation). Comparison of the results of this analysis to previous analyses of the generated exogenous wind-borne plate rates (i.e., Grayson et al. 2013b; Grayson et al. 2013c) illustrates that it is the variability of the data that appears to be causing the increased total error for the negative binomial/Poisson combination.

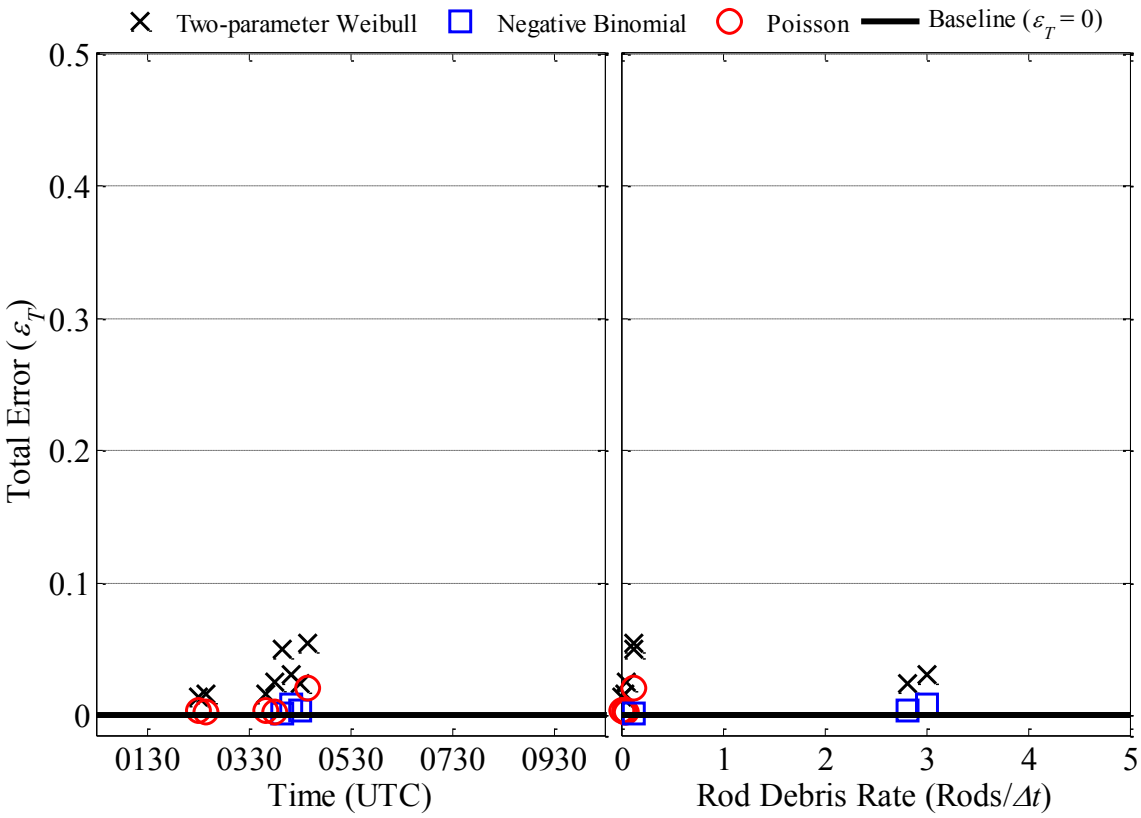

Figure 3.17: Total error as a function of time and mean debris rate for the comparison of the generated and captured exogenous wind-borne rod debris rates.

The final results of Figures 3.16 and 3.17 illustrate that the two-parameter Weibull distribution is the more consistent distribution when generating exogenous wind-borne plate debris, and that the negative binomial/Poisson combination is better suited for the

generation of rod debris. However, closer inspection of the scale of the total error revealed that it is relatively small in both cases. Due to the results of the goodness-of-fit tests and the small differences in the total error of the data statistics, it seems reasonable to conclude that both distributions (i.e., the two-parameter Weibull, and the negative binomial/Poisson combination) would adequately generate the appropriate exogenous wind-borne debris rates.

4 QUANTIFICATION OF BUILDING ENVELOPE DAMAGE WITHIN A MECHANICS-BASED BUILDING ENVELOPE FAILURE ASSESSMENT MODEL

4.1 Quantification of Building Envelope Damage in the BEFA Model

It is necessary to establish a metric to quantify the amount of damage incurred by the individual building envelopes within a residential development. This is accomplished by adapting the damage state descriptions for residential housing defined within the HAZUS-MH model (Vickery et al. 2006b) to delineate between specific damage zones. Table 4.1 lists the damage state descriptors provided by Vickery et al. (2006b) and the failure types that correspond with each damage state. Quantification of these damage descriptors consist of failures of specific building envelope components that are presented as a number or percentage of failed envelope components and a number of wind-borne debris impacts.

Table 4.1: Damage state descriptions defined within HAZUS (Vickery et al. 2006b)

	Failure type			
Damage	Roof covering	Windows/doors	Sheathing	Impact
Very minor	≤ 2%	0	0	0
Minor	> 2% and ≤ 15%	1 window or door	0	< 5
Moderate	> 15% and ≤ 50%	> 1 and ≤ max(20%, 3)	1 to 3 panels	5-10
Severe	> 50%	> max(20%, 3) and ≤ 50%	3 and ≤ 25%	10-20
Destruction	> 50%	> 50%	> 25%	> 20

4.1.1 Determination of Building Envelope Damage Zone Boundaries

The building envelope failure assessment (BEFA) model tracks which building envelope components have failed either due to direct wind pressure or wind-borne debris impact; therefore, it is relatively straightforward to determine a percentage of the building

envelope that had been penetrated by window, door, and sheathing failures, and the percentage of roof covering that was missing from the roof sheathing. The damage zones are assumed to be comparable to the damage states defined by Vickery et al. (2006b) in Table 4.1, however, these damage state values must be converted to a common measure as a percentage of building envelope damage. Roof covering is already given as a percentage and does not need to be further converted. However, window and door failures and sheathing failures are given as a mixture of failed components or percentages; therefore, an average area of each failed component was determined from the residential development represented within the BEFA model from Chapter 2. These average failed component areas were used to determine the percentage of building envelope represented by each component as shown in Table 4.2.

There is little research that has sought to quantify the number of impacts required for complete destruction of the building envelope of a structure. Therefore, at this point it is assumed that the total number of impacts that would cause complete destruction of a building is seventy-five impacts in order to convert the number of impacts to a percentage of building envelope damage. Seventy-five impacts was chosen to provide building envelope damage percentages that are comparable to the other failure types within each damage state taken from Vickery et al. (2006b) as shown in Table 4.2.

The BEFA model is capable of measuring each of these failure types, but it was necessary to determine how these failure types contribute to an overall building envelope damage value. Therefore, the four failure types defined in Tables 4.1 and 4.2 were grouped into three failure modes (see Table 4.3) and ranked based on their damage

potential to the building envelope. Figure 4.1 illustrates the definition of each of the building envelope failure modes from Table 4.3.

Table 4.2: Failure type damage values (ψ)

	Failure type			
Damage	Roof covering	Windows/doors	Sheathing	Impact
Very minor	0.02	0	0	0
Minor	0.15	0.05	0	0.07
Moderate	0.50	0.20	0.06	0.13
Severe	> 0.50	0.50	0.25	0.27
Destruction	> 0.50	> 0.50	> 0.25	> 0.27

Table 4.3: Ranking the building envelope damage potential of the failure types

Failure type	Failure mode	Rank
Sheathing/window/door failure	Building envelope penetration	3
Impact from wind-borne debris	Potential for building envelope penetration	2
Roof covering loss	No building envelope penetration	1

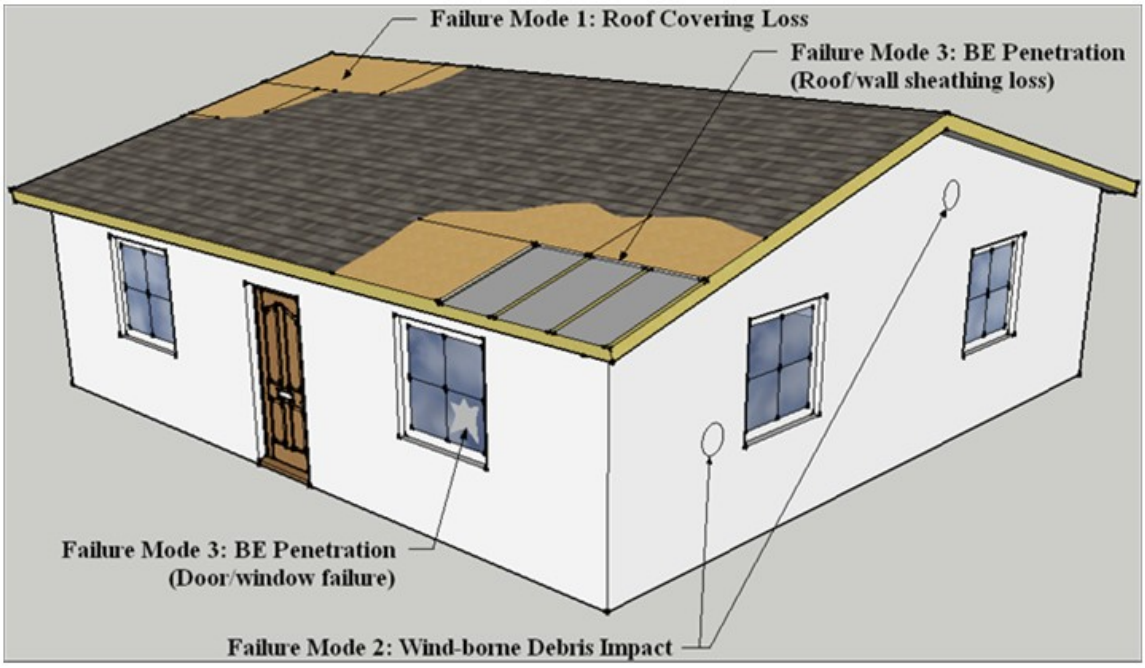

Figure 4.1: Definition of the building envelope failure modes.

Determination of the contribution from each of the two failure types in failure mode 3 (i.e., sheathing failure, and window and door failure) consisted of weighting the damage based on the percentage of the building envelope that they occupy on average as shown in Eqn. 4.1.

$$\psi_{3_i} = \lambda_{vc}\psi_{vc_i} + \lambda_{sh}\psi_{sh_i} \qquad 4.1$$

where, λ_{vc} and λ_{sh} are the fraction of the building envelope occupied by the vulnerable components (i.e., windows and doors) and sheathing, respectively, and ψ_{vc_i} and ψ_{sh_i} are the damage values for the vulnerable components and sheathing for damage state boundary *i* (see Table 4.2), respectively. Using the residential development modeled in this study as an example, the vulnerable components occupied approximately ten percent (i.e., $\lambda_{vc} = 0.10$) and the sheathing occupied the remaining ninety percent (i.e., $\lambda_{sh} = 0.90$) of the building envelope surface area. Table 4.4 provides the failure mode damage values used to delineate between the damage zones that correspond with the damage states identified by Vickery et al. (2006b) in Table 4.1.

Table 4.4: Failure mode damage values (ψ).

	Failure mode		
Damage state	1	2	3
Very minor	0.02	0	0
Minor	0.15	0.07	0.005
Moderate	0.50	0.13	0.074
Severe	> 0.50	0.27	0.275
Destruction	> 0.50	> 0.27	> 0.275

4.1.2 Calculation of building envelope damage

Assuming that the three failure modes defined in Figure 4.1 are the only failures modes possible for a building envelope, Figure 4.2 illustrates the general logical relationship between the failure modes for an individual house within the residential development. Figure 4.2 provides a reasonable assumption for the failure modes as none of the three failure modes are conditional on the other three for an individual home (e.g., wind-borne debris impacts can occur to a home within the residential development without any roof covering, sheathing, or window/door failures occurring to that particular home).

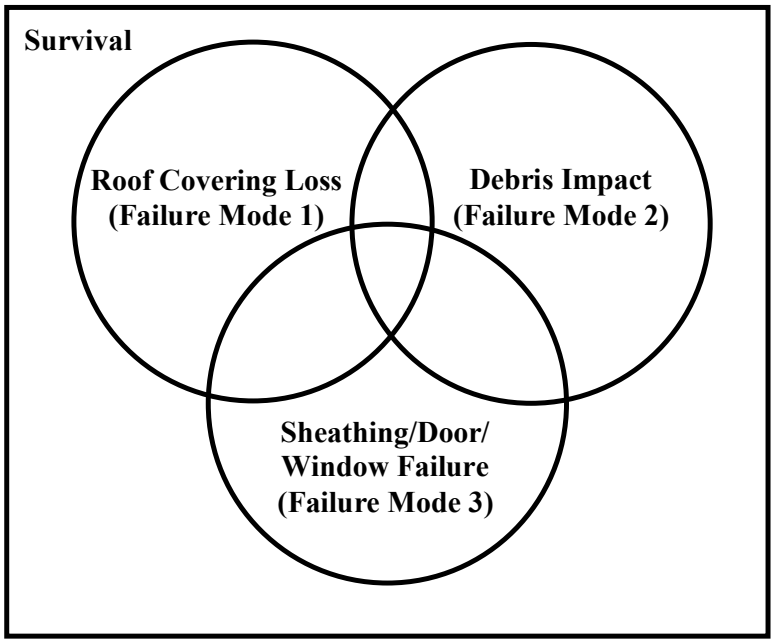

Figure 4.2: Venn diagram illustrating the general logical relationship between the failure modes for an individual home within a residential development.

Vickery et al. (2006b) assumes that a building is classified in a particular damage state if it exceeds the criteria of any one of the failure types for the corresponding damage state (see Table 4.1). Utilization of the axioms of probability coupled with the general

logical relationships illustrated in Figure 4.2 permits the building envelope damage caused by the three failure modes to be calculated as the union of three events:

$$BED_{n,t} = FM_{1,n,t} \cup FM_{2,n,t} \cup FM_{3,n,t}, \quad 4.2$$

where $BED_{n,t}$ is the building envelope damage for house *n* at time step *t*, and $FM_{j,n,t}$ is the damage determined by the BEFA model for failure mode *j* at time step *t*. However, resilience is best thought of in terms of the building envelope survival, which is the complement of the building envelope damage. De Morgan's law states that the complement of the union of events can be calculated as the intersection of the complement of the individual events:

$$\overline{E_1 \cup E_2 \cup \ldots} \qquad \ldots \quad 4.3$$

where E represents a generic event (Ayyub and McCuen 2002). Substituting the three failure mode damages for the generic events provides:

$$\overline{FM_1 \cup FM_2 \cup FM_3} = \overline{FM_1} \cap \overline{FM_2} \cap \overline{FM_3} \quad 4.4$$

Therefore, the building envelope survival becomes:

$$BES_{n,t} = \prod_{j=1}^{k=3} \left(1 - FM_{j,n,t}\right) \quad 4.5$$

where $BES_{n,t}$ is the building envelope survival for house *n* at time step *t*. The failure mode rankings (see Table 4.3) are used to determine the contribution of each failure mode to the overall building envelope damage value. Damage to the building envelope is treated as a fraction of the entire building envelope; therefore, each failure mode had a

corresponding damage factor (φ) that essentially weights the failure mode damage relative to their potential for penetration of the building envelope. The failure mode damage factors (see Table 4.5) are calculated by Eqn. 4.6.

$$\varphi_j = \frac{\text{Rank of failure mode } j \text{ (from Table 4.3)}}{\text{Number of failure modes (i.e., } k = 3)} \tag{4.6}$$

Table 4.5: Calculation of the failure mode damage factors

Failure mode	Rank	Damage factor (φ)
Building envelope penetration	3	1.00
Potential building envelope penetration	2	0.67
No building envelope penetration	1	0.33

The damage contributed to a building envelope by each failure mode becomes:

$$FM_{j,n,t} = \varphi_j \psi_{j,n,t} \tag{4.7}$$

where φ_j is the damage factor for failure mode j (see Table 4.5), and $\psi_{j,n,t}$ is the damage value for failure mode j provided by the BEFA model for each house n at each time step t. Substituting the results of Eqn. 4.7 into Eqn. 4.5 the building envelope survival for each house n at each time step becomes:

$$BES_{n,t} = \prod_{j=1}^{k=3} \left(1 - \varphi_j \psi_{j,n,t}\right). \tag{4.8}$$

The time evolution of the building envelope survival for the residential development is the arithmetic mean of the results from Eqn. 4.8:

$$BES_t = \frac{1}{N} \sum_{n=1}^{N} BES_{n,t} \,. \tag{4.9}$$

4.1.3 Calculation of building envelope damage zone boundaries

The damage zone boundaries used to delineate between the various damage states identified by Vickery et al. (2006b) were calculated in the same manner as the building envelope survival in Eqn. 4.8 with the only change being that the failure mode damage values provided in Table 4.4 were used in place of the BEFA model output:

$$BES_i = \prod_{j=1}^{k=3}\left(1-\varphi_j \psi_{j,i}\right) \tag{4.10}$$

where BES_i is the value of damage zone boundary corresponding to damage state *i* from Table 4.1, and $\psi_{j,i}$ is the failure mode values corresponding to damage state *i* in Table 4.4. Figure 4.3 provides an illustration of the damage zone boundaries.

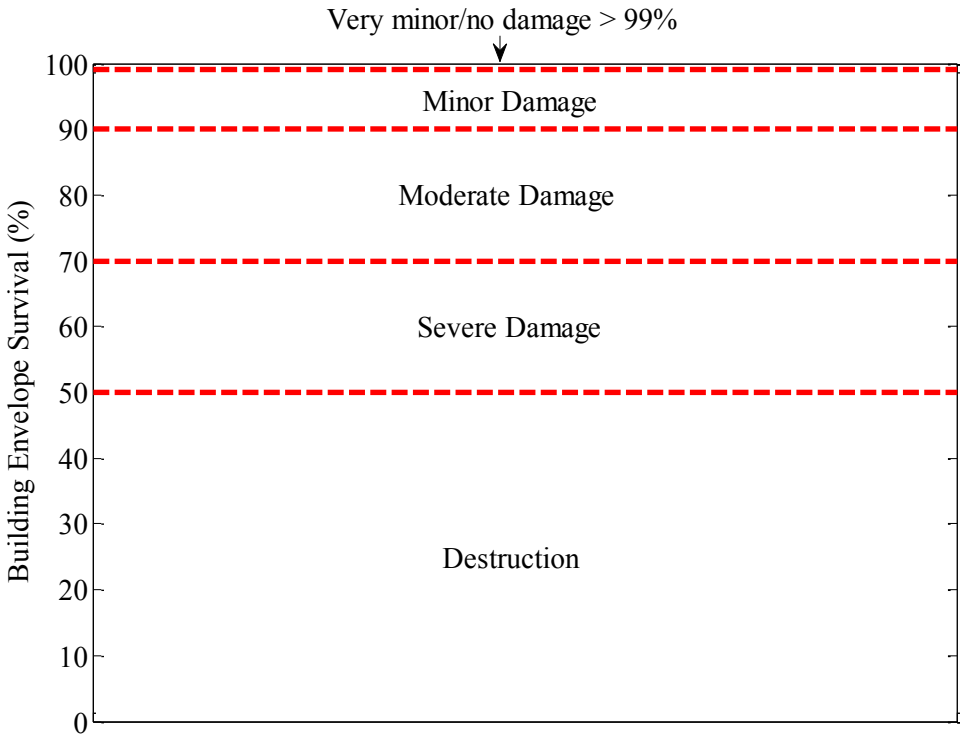

Figure 4.3: Illustration of the calculated damage zone boundaries.

4.2 Building Envelope Damage Contributed by Wind-borne Debris Impact

It is assumed that the number of wind-borne debris impacts contributing to each damage state identified by Vickery et al. (2006b) in Table 4.1 are significant wind-borne debris impacts. The issue then became determining what constitutes a significant wind-borne debris impact. There is little research that quantifies how wind-borne debris impact damage contributes to the cumulative damage of the building envelope, and it is unreasonable to assume that all wind-borne debris impacts to the building envelope of a home within a residential development contribute equally to damage. A more reasonable assumption is that wind-borne debris impacts inflict various amounts of damage to a building envelope dependent upon the kinetic energy or momentum possessed by the wind-borne debris at impact. Therefore, an innovative method was developed to account for the cumulative damage incurred by the building envelope due to wind-borne debris impact.

4.2.1 Methodology to Quantify Wind-borne Debris Impact Damage

Research studies have shown that the kinetic energy possessed by wind-borne debris provides a better correlation to the damage experienced by typical building envelope components (Herbin and Barbato 2012). Therefore, previous research, including building codes and standards, were utilized to determine how the kinetic energy threshold of commonly used building materials could be related to the damage of a building envelope. In order to determine a reasonable kinetic energy threshold to represent the materials of

the building envelope, failure criteria was established to define what was to be considered a significant wind-borne debris impact to the building envelope in this study.

Texas Tech University (TTU) has performed extensive wind-borne debris impact studies since the 1970's with the majority of impact tests performed at TTU focusing on missiles prevalent in regions prone to tornadic winds (Texas Tech 2006). As part of the studies at TTU, McDonald (1990) provides classifications for two types of failure seen during impact testing: (1) penetration, which describes a failure in which damage occurs without breach of the back plane of the test specimen, and (2) perforation, which describes a failure in which the missile passes through the thickness of the test specimen. This study assumes that any penetration, and not perforation, of the building envelope components will constitute damage to the building envelope. Additional impact studies pertaining to common light-frame wood construction building materials have been performed by Clemson University (Reinhold et al. 2000, 2002), and Florida A&M University-Florida State University in conjunction with the University of Florida (Scheer 2005; Yazdani et al. 2004, 2006). However, there are many differences in the materials tested and even the pass/fail criteria, which made it difficult to identify a suitable kinetic energy threshold for the building envelope. The most practical option at this point was to utilize current building code testing requirements to determine a suitable building envelope kinetic energy threshold.

The Florida Building Code (FBC 2010) requires that all parts or systems of the exterior building envelope located within high-velocity hurricane zones meet the large missile impact test criteria, and states that a part or system is considered to comply with

the impact test criteria if the specimen rejects the impact without penetration. The large missile impact test consists of subjecting a test specimen to impact with a piece of timber weighing 4.1 kg (9 lb.) and having nominal dimensions of 51 x 102 mm (2 x 4 in.) on end at a speed of 15.2 m/s (50 ft/s) (FBC 2010). It seems reasonable to assume that an impact kinetic energy threshold calculated from the energy imparted by the large missile stipulated by the FBC (2010) would provide a reasonable, conservative impact kinetic energy threshold for the entire building envelope until further cumulative building envelope damage research could be performed. The calculation of the impact kinetic energy threshold (*KET*) used to determine a significant impact in the BEFA model is as shown in Eqn. 4.11.

$$KET = \frac{1}{2}mv^2 = \frac{1}{2}(4.1kg)(15.2m/s)^2 \approx 475 \text{ N-m} \qquad 4.11$$

It is assumed in this study that all wind-borne debris impacts contribute to the cumulative building envelope damage; however, some impacts contribute more damage than others dependent on their relation to the impact kinetic energy threshold (see Eqn. 4.11). Since Vickery et al. (2006b) classifies the damage to the building envelope in number of impacts, an impact kinetic energy ratio is calculated to determine how much a particular impact contributed to the building envelope damage. The impact kinetic energy ratio is used to determine an adjusted number of impacts that a home experienced during the passage of the hurricane event as shown in Eqn. 4.12:

$$Adjusted\ Number\ of\ \ Im pacts_{i,n,t} = \frac{KE_{i,n,t}}{KET} \qquad 4.12$$

where the *Adjusted Number of Impacts* is the equivalent number of significant impacts contributing to the damage of the building envelope based on the kinetic energy of impact i that occurs to house n during time step t, and $KE_{i,n,t}$, is the kinetic energy of impact i that occurs to house n during time step t. The impact kinetic energy ratio essentially provides how many times greater an impact is in terms of the assumed significant impact threshold. Therefore, the *Adjusted Number of Impacts* is essentially the equivalent number of significant impacts contributed by a single impact based on the impact kinetic energy that it possessed.

5 THE INFLUENCE OF HURRICANE WIND HAZARD MITIGATION RETROFITS ON RESIDENTIAL DEVELOPMENT PERFORMANCE

5.1 Introduction

Community resilience is heavily dependent on the socioeconomic response of the community before, during, and after a hurricane wind hazard event. However, Gaynor and Simiu (2007) conclude that the performance of the built environment is a significant contributor to the overall resiliency of the community. Addressing community resilience from a structural engineering standpoint must focus on limiting the damage sustained by a residential development subjected to a hurricane wind hazard event in order to prevent a hazard event from becoming a disaster event. The goal of this study is to determine how mitigating the "initial shock" created by hurricane wind events experienced by a residential development influences the response (i.e., the survival) of the community building stock. This is accomplished by simulating five scenarios that vary the percentage of the number of homes retrofitted within a Building Envelope Failure Assessment (BEFA) model developed by Grayson et al. (2013a). The variation of the percentage of homes retrofitted is representative of a common situation in which newer homes within a residential development are built after the adoption of a stricter building code. Existing homes in this situation are typically grandfathered in to the current building code, which can produce areas of vulnerability within the residential development.

5.2 Methodology

This study did not attempt to incorporate the incentive for a homeowner to institute a specific retrofit or combination of retrofits. Therefore, an "all or nothing" approach was taken in applying the retrofits to each home (i.e., a homeowner either institutes all of the retrofits or none of the retrofits). Four retrofits were considered in this study as follows:

1. roof sheathing attached with 6d fasteners using a 6"/12" nailing schedule is supplemented with closed-cell spray foam along the rafter on the underside of the roof sheathing,
2. standard three-tab asphalt shingles are replaced with Class H wind-resistant shingles,
3. all personnel/garage doors are upgraded for increased pressure capacity, and
4. impact protection systems (i.e., shutters) are added to all windows.

Tables 5.1 and 5.2 provide the unretrofitted and retrofitted building component capacities, respectively, implemented within the BEFA model. The majority of the building component capacities were obtained from the HAZUS-MH program (Vickery et al. 2006b) and the Florida Public Hurricane Loss Projection Model (FPHLPM) (Gurley et al. 2005); however, research that is more current was utilized when available. It should be noted that the roof and wall sheathing values were updated from those values utilized in Chapter 2 to provide results that are more consistent with post-hurricane damage assessments. Additionally, it is noted that the roof covering pressure capacity is relatively large compared to the other component capacities for both the unretrofitted and retrofitted cases, which has the potential to influence the results of this study. However, the large

coefficient of variation (COV) illustrates the significant level of uncertainty associated with these values and would benefit from more research in this area.

Table 5.1: Unretrofitted building component capacities

Component	Resistance	COV	Distribution	Reference
Roof sheathing	2610 Pa	0.11	Lognormal	Vickery et al. (2006b)
Wall sheathing	2610 Pa	0.11	Lognormal	Vickery et al. (2006b)
Roof covering	3350 Pa	0.40	Normal	Gurley et al. (2005)
Personnel door	2390 Pa	0.20	Normal	Vickery et al. (2006b)
Garage door	957 Pa	0.20	Normal	Vickery et al. (2006b)
Small window	5000 Pa	0.20	Normal	Gurley et al. (2005)
Medium window	3330 Pa	0.20	Normal	Gurley et al. (2005)
Tall window	2500 Pa	0.20	Normal	Gurley et al. (2005)
Picture window	1780 Pa	0.20	Normal	Gurley et al. (2005)
Glass (impact)	68 N-m	Deterministic		Vickery et al. (2006b)

Table 5.2: Retrofitted building component capacities

Component	Resistance	COV	Distribution	Reference
Roof sheathing	9090 Pa	0.11	Lognormal	Datin et al. (2011)
Wall sheathing	2610 Pa	0.11	Lognormal	Vickery et al. (2006b)
Roof covering	6220 Pa	0.40	Normal	Appendix A
Personnel door	4780 Pa	0.20	Normal	Vickery et al. (2006b)
Garage door	2490 Pa	0.20	Normal	Vickery et al. (2006b)
Small window	5000 Pa	0.20	Normal	Gurley et al. (2005)
Medium window	3330 Pa	0.20	Normal	Gurley et al. (2005)
Tall window	2500 Pa	0.20	Normal	Gurley et al. (2005)
Picture window	1780 Pa	0.20	Normal	Gurley et al. (2005)
Shutters (impact)	475 N-m	Deterministic		Vickery et al. (2006b)

Table 5.3 provides the number of homes retrofitted for each scenario investigated in this study. The homes selected for retrofit from the residential development in scenarios 2 to 4 were randomly selected without replacement from a uniform distribution for each subsequent simulation to remove the influence that the location of the retrofitted homes within the residential development had on the final results.

Table 5.3: Scenarios for the percentage of homes retrofitted in this study

Scenario	Percentage of homes retrofitted (%)	Number of homes retrofitted
1	0	0
2	25	10
3	50	19
4	75	29
5	100	38

5.2.1 Accounting for the Variability of the Hurricane Wind Hazard

The BEFA model includes a Hurricane Simulation Module that is capable of simulating historical or synthetic hurricane events. For this study, it was desired to use a synthetic 700-year mean recurrence interval (MRI) hurricane wind event to represent a design-level wind event that is consistent with the ASCE 7 design standard for Risk Category II (i.e., residential structures) (ASCE 2010). Liu (2014) has developed a synthetic hurricane database and a hurricane selection method that was employed to select the desired synthetic hurricane events for the specific location investigated in this study.

The MRI of a location is site specific and represents the point risk of that location which can be used in the design and/or analysis of individual buildings (Vickery et al. 2009). Due to the smaller, more detailed region (i.e., residential development level) investigated in this study, a point risk approach was utilized as opposed to an area risk approach (Liu 2014).

Liu (2014) calculates the MRI at a specific location with Eqn. 5.1:

$$MRI\left(v_i > V\right) = \frac{1}{\lambda P\left(v_i > V\right)} = \frac{Y}{n} \qquad 5.1$$

where $P(v_i > V)$ is the probability that the wind speed for event *i* exceeds the threshold wind speed (V), λ is the mean annual occurrence rate of the hurricane events, n is the number of events with wind speed v_i, and Y is the total number of simulation years. Since the MRI is site specific, only hurricane events that were tracked to within 250 km of the location were selected to reduce the computational requirements of the selection process. The maximum wind speeds for each of the selected synthetic hurricane events at the location are ranked and Eqn. 5.1 was solved for n to determine the hurricane event number selected from the ranked hurricane events to provide the desired MRI hurricane event at that specific location.

The probabilistic nature of hurricane hazard events made it important to capture the variability of the events to ensure that the results obtained in this study considered the various hurricane parameters that are subject to change from event to event. Liu (2014) generated the 500,000-year synthetic hurricane database that was utilized in this study and provides some insight into the size of the database subset required to obtain reasonable results in the selection of multiple MRI events. Therefore, ten 700-year MRI synthetic hurricane events were selected from ten 50,000-year subsets of the original 500,000-year database. Figure 5.1 provides the overlay of the hurricane tracks with respect to the location of the 38-home residential development near Moncks Corner, SC. Figures 5.2 and 5.3 illustrate the 3-second gust wind speed profiles and time evolution of the wind direction during the passage of the hurricane events, respectively. Figure 5.4 overlays the information from Figures 5.2 and 5.3 to illustrate the coverage provided by the selected synthetic hurricane wind events.

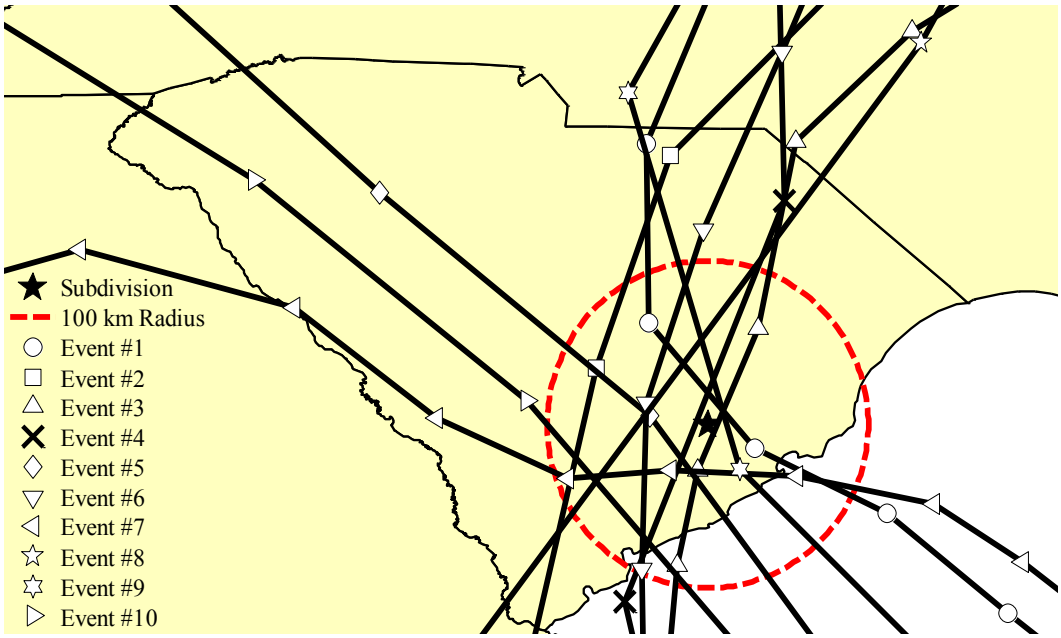

Figure 5.1: The ten selected 700-year MRI synthetic hurricane events with reference to the location of a 38-home residential development near Moncks Corner, SC.

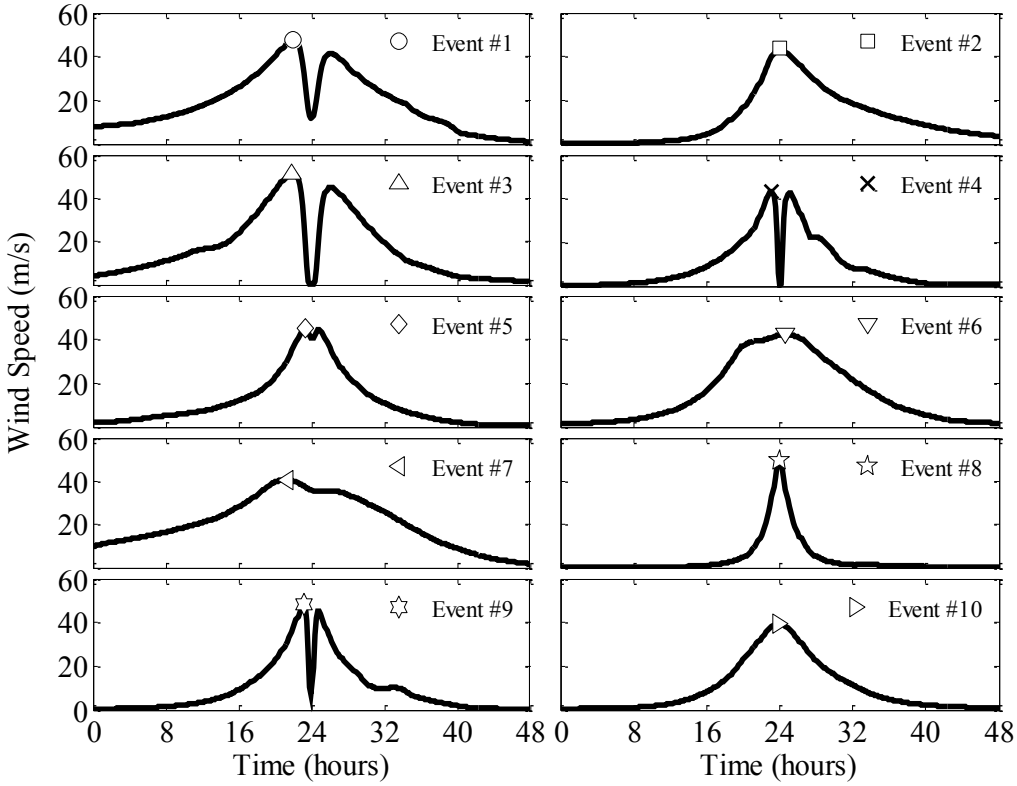

Figure 5.2: 3-second gust wind speed profiles for the ten 700-year MRI events.

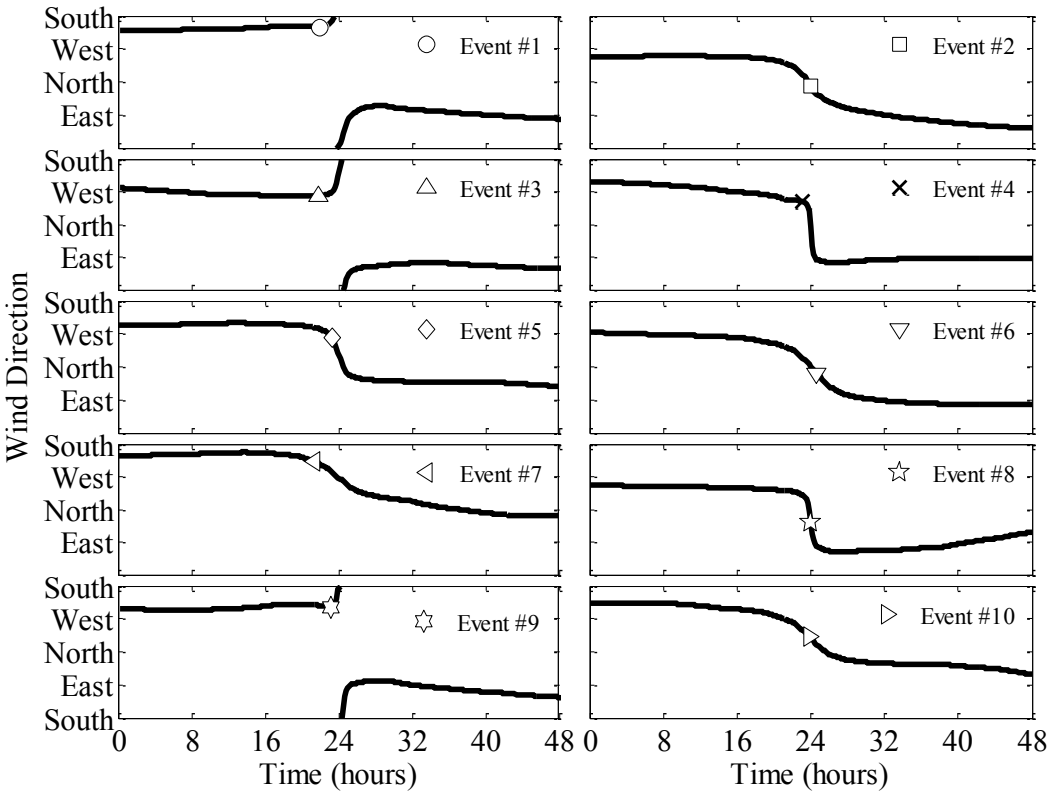

Figure 5.3: Time evolution of the wind direction for the ten 700-year MRI events. The markers denote the occurrence of the peak wind speed.

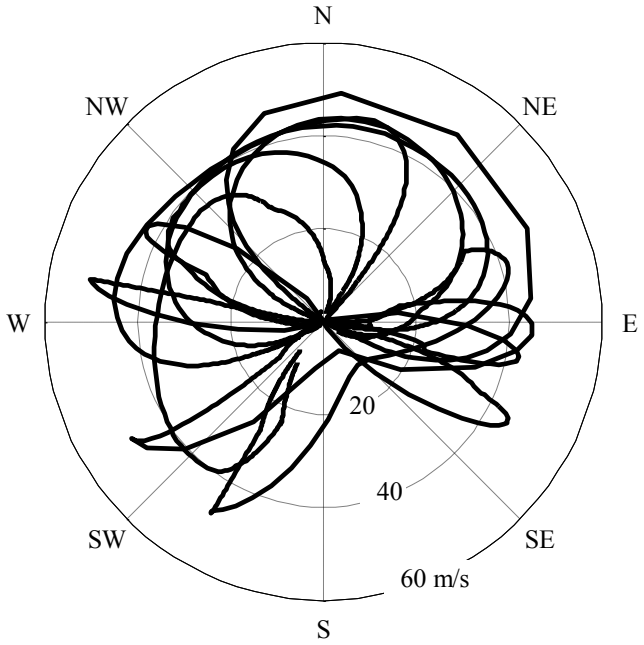

Figure 5.4: Wind coverage provided by the ten 700-year MRI hurricane events.

Based on the qualitative results of Figures 5.1 to 5.4, it seems reasonable to assume that the selected hurricane events adequately capture the event-to-event uncertainty that is likely to be experienced by a residential development at this location.

5.2.2 Determination of the Number of Simulations Required for the Study

A convergence study was conducted using the ten 700-year MRI events selected to ensure that an appropriate number of simulations were performed to capture the variability of each retrofit scenario. Initially, 50 simulations were performed for each of the ten 700-year MRI events. Since this study was concerned with the mean response of the residential development to the ten hurricane wind events, the simulations were aggregated to form a pool of 500 simulations for each of the five retrofit percentage scenarios. Simulations were randomly selected using a uniform distribution and the coefficient of variation (COV) for the final residential development building survival was calculated for an increasing number of simulations (e.g., 5, 10, 25 … 500 simulations). Figure 5.5 illustrates the results of the convergence study performed for all five of the retrofit scenarios tested, which confirms that performing at least 350 simulations for each scenario tested was sufficient for reproducible results. Therefore, all 500 simulations were utilized in this study since the data was readily available. In the event that convergence was not observed for all five of the scenarios, another 500 simulations would have been performed and the process repeated until convergence was obtained for all five scenarios.

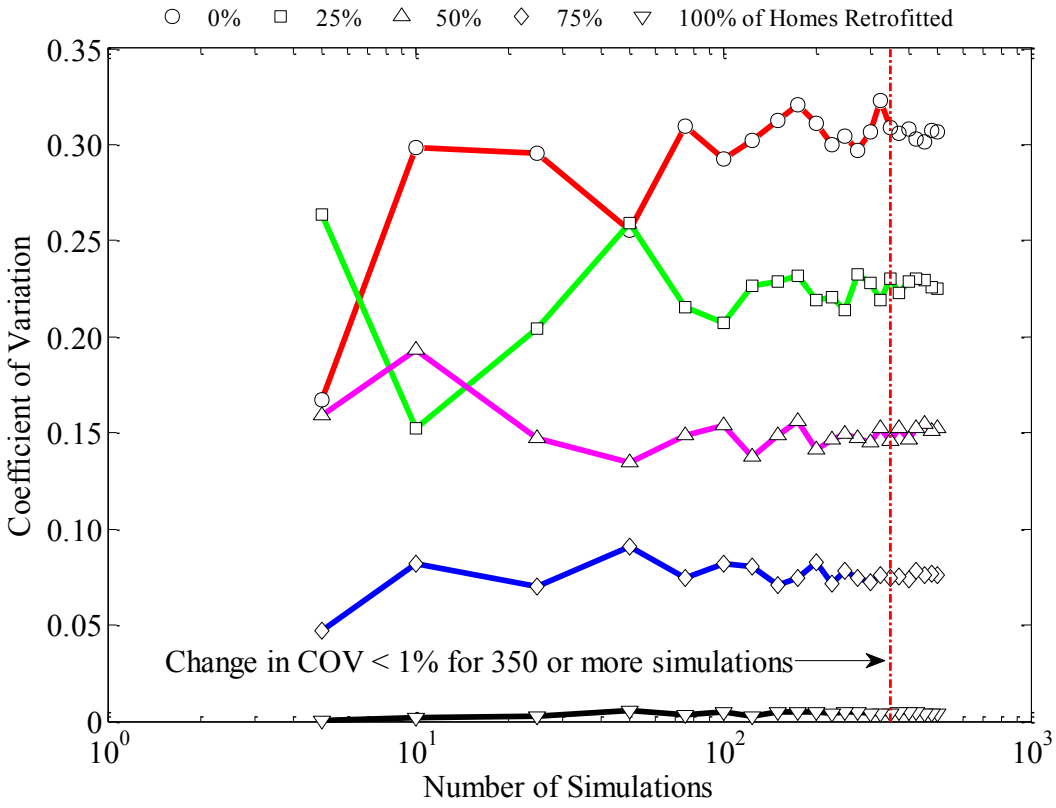

Figure 5.5: Results of the convergence study to identify the appropriate number of simulations required to capture the variability of the hurricane events.

5.3 Results and Discussion

The results of this study illustrate how the residential building stock of a community performed when subjected to a 700-year MRI hurricane event at various percentages of retrofit as described in Table 5.3. The discussion begins with the presentation of the overall performance of the residential building stock and then proceeds to analyze the contributions of each of the ten synthetic hurricane events, the individual failure modes, and finally the retrofitted versus unretrofitted homes.

5.3.1 Response of the Residential Development to a 700-year MRI Hurricane Event

Figure 5.6 illustrates the time evolution of the overall building envelope survival of the residential development to a 700-year MRI hurricane wind event. The time evolution of the overall building envelope survival was calculated using Eqns. 4.8 and 4.9 (see Chapter 4). Figure 5.7 illustrates the contribution of each of the three failure modes to the final building envelope survival (i.e., the data points at hour 32 from Figure 5.6). The final building envelope survival increased linearly with a linear increase in the percentage of homes retrofitted within the residential development. This was not initially expected, as it was assumed that the wind-borne debris released in the residential development at lower retrofit percentages would have a nonlinear influence on the results.

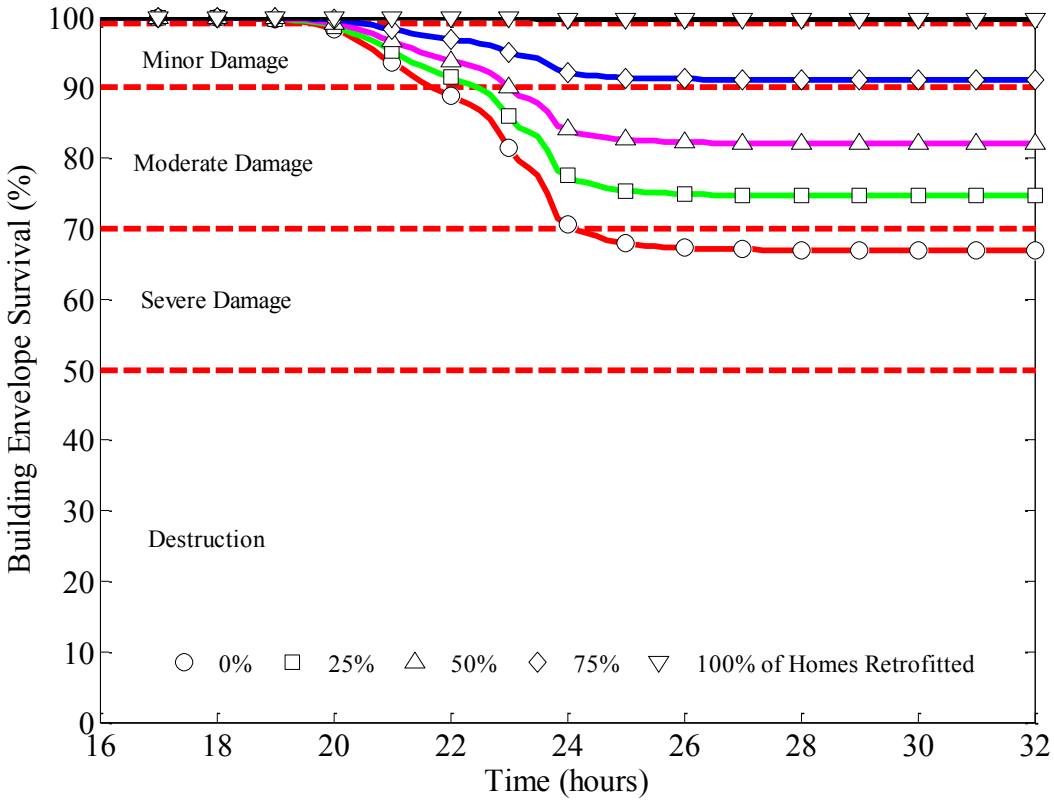

Figure 5.6: Evolution of the building envelope survival for the five retrofit scenarios.

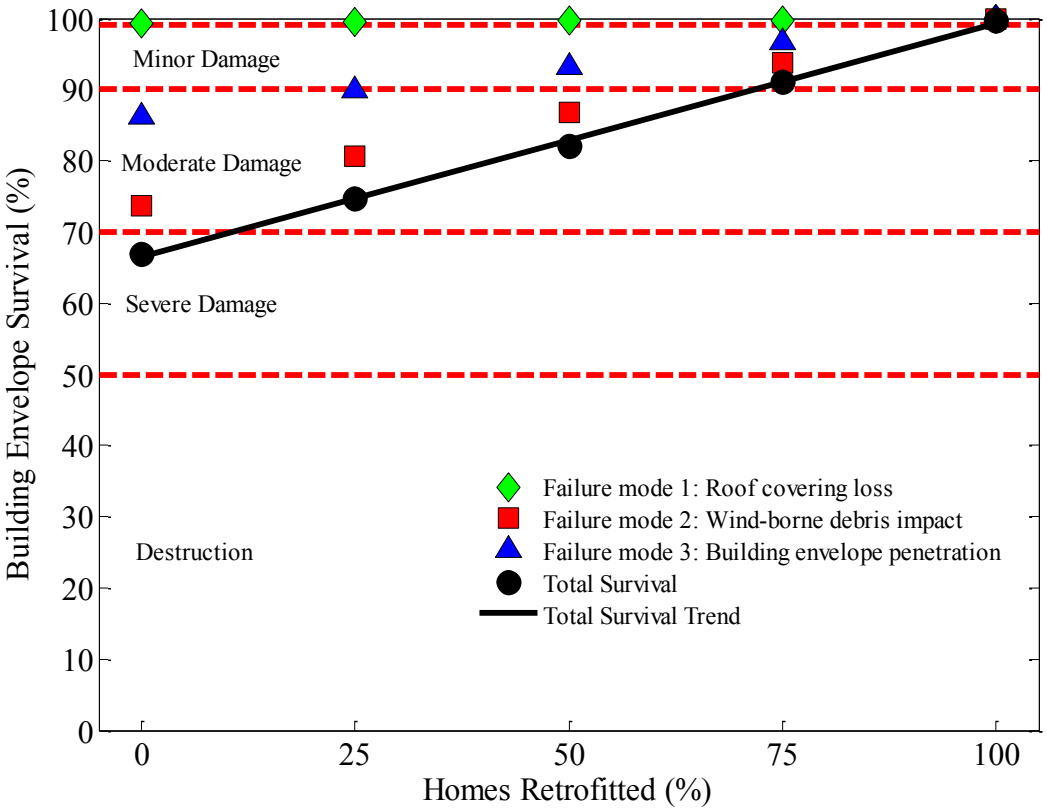

Figure 5.7: Final building envelope survival failure mode contributions.

Information provided in Figure 5.7 is utilized to assign values to the general logical relationships between the three failure modes presented in Chapter 4 (see Figure 4.2). The failure mode damage values that provide the general logical relationships of Figure 4.2 are the complement of the survival values for each of the failure modes illustrated in Figure 5.7. The complement survival (i.e., damage) values for each of the failure modes determine their contribution to the total building envelope survival as calculated with Eqns. 4.5 to 4.9. Table 5.4 provides the failure mode logical relationship values (i.e., Venn diagram values) and final building envelope survival for the five retrofit scenarios. It is important to note that the contribution of each failure mode is not one-to-one; rather, each failure mode contributes to the total damage based on their potential for penetration

of the building envelope ranking (see Table 4.3). This is one reason for the low contribution of failure mode 1 (i.e., roof covering loss). Another reason is the high-pressure capacity of the roof covering obtained from Gurley et al. (2005) that was used for the unretrofitted homes. Additionally, it is assumed that the "all or nothing" approach to the application of retrofits to the homes added to the low contribution of failure mode 1. The BEFA model only considers roof-covering loss that left roof sheathing exposed in the damage calculations at the end of each time step, which means that roof covering that is lost from an area that also experienced a roof sheathing failure contributed as failure mode 3 and not failure mode 1. The unretrofitted homes possessed both the lower capacity roof sheathing and roof covering. Therefore, the greater loss of roof sheathing on the unretrofitted homes contributed as failure mode 3. Conversely, retrofitted homes typically experienced no loss of roof sheathing and little to no loss of roof covering, which again did not significantly contribute to failure mode 1. Future studies will consider various implementations of retrofit to an individual home, such as a homeowner that retrofits the roof sheathing but neglects to upgrade the roof covering, which should increase the contribution of failure mode 1 considerably.

Table 5.4: Failure mode logical relationship values for the residential development.

	Failure mode damage			
Scenario	1	2	3	Survival
1	0.007	0.238	0.139	0.670
2	0.005	0.181	0.101	0.747
3	0.004	0.126	0.069	0.821
4	0.002	0.061	0.033	0.911
5	0.001	0.002	0.001	0.997

5.3.2 Contribution of the Ten Hurricane Events to the Building Envelope Damage

Figure 5.8 illustrates the time evolution of the building envelope survival for each of the ten 700-year MRI hurricane events for 0% and 100% of the homes retrofitted within the residential development. The variability in performance observed in the residential development with 0% of the homes retrofitted is significant with one hurricane event causing only minor damage, two more causing destruction, and the remaining seven hurricane events causing from moderate to severe damage. The residential development with 100% of the homes retrofitted exhibited a key trait of a resilient residential development building stock, namely, the ability to perform relatively well regardless of the event encountered.

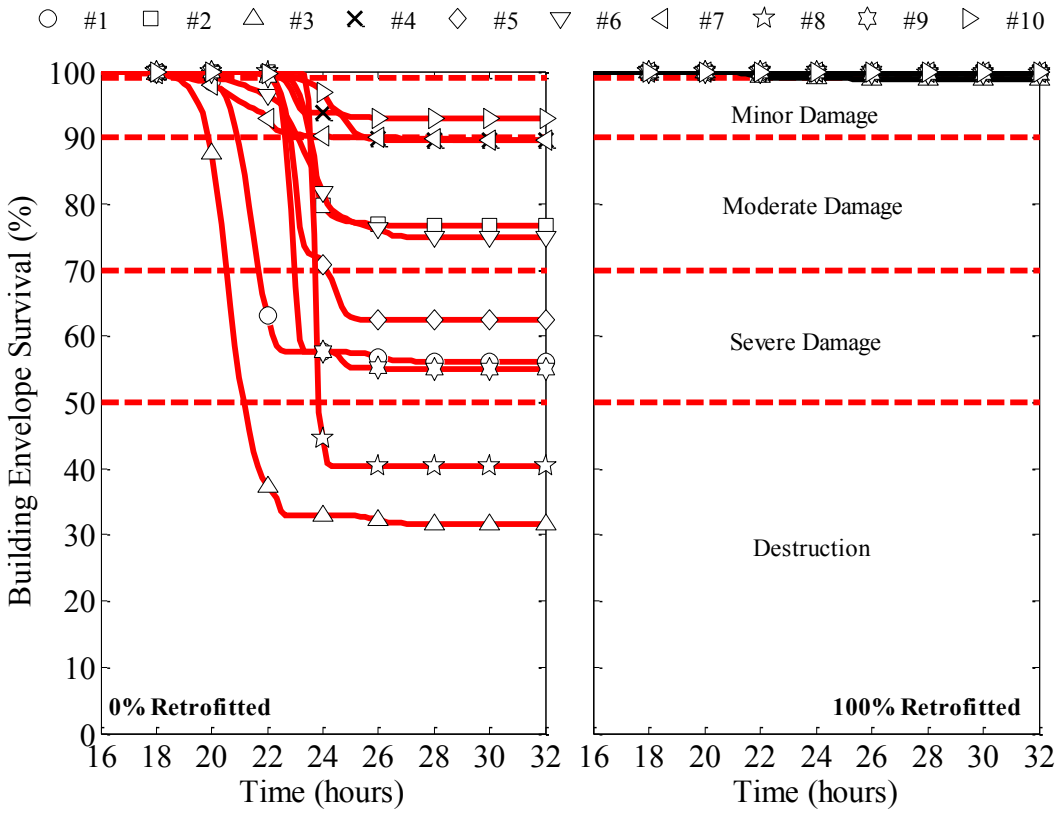

Figure 5.8: Building envelope survival from the ten 700-year MRI hurricane events.

Figure 5.9 expands upon Figure 5.8 to illustrate the variability in the final building envelope survival for all five retrofit scenarios. Although the residential development appears to exhibit a linear increase in survival with a linear increase in the percentage of homes retrofitted, it has been documented in post-hurricane damage assessments that wind-borne debris can cause a chain reaction effect (Holmes 2010). This chain reaction effect is initiated by wind-borne debris damage to a home that increases the internal pressurization of the damaged building, which in turn releases even more wind-borne debris into the wind field with the potential for damaging further downstream homes. It would seem that this chain reaction effect would manifest itself as a nonlinear increase in the building envelope survival as the wind-borne debris created by an unretrofitted home, along with any additional wind-borne debris created by the chain reaction effect, is removed due to retrofit.

The linear trend in Figure 5.9 suggests that the building survival is simply a function of the number of homes retrofitted without any contribution from additional wind-borne debris created during the hurricane event. However, investigation of the extreme survival cases (i.e., hurricane events #3 and #10) in Figure 5.10 reveals that the chain reaction effect from wind-borne debris may indeed be present in the underlying trend of the building envelope survival for hurricane event #3. The results of Figure 5.10 suggest that the minor damage occurring during hurricane event #10 did not produce enough wind-borne debris to establish a noticeable chain reaction effect. However, the severe damage of hurricane event #3, particularly with less than 50% of the homes retrofitted, produced a significant amount of wind-borne debris, which suggests that the nonlinear increase in

building envelope survival in this case was due to wind-borne debris damage (i.e., a chain reaction effect).

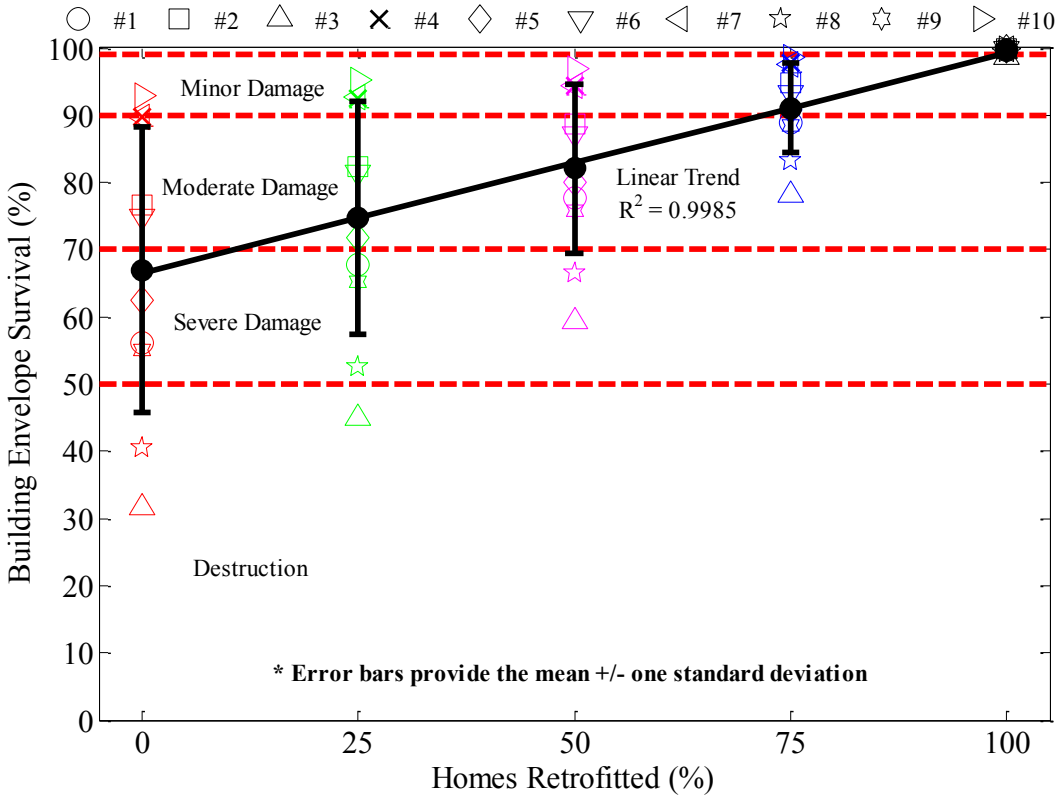

Figure 5.9: Contribution of the ten 700-year MRI hurricane events to the final building envelope survival.

An inspection of Figures 5.1 to 5.3 reveals that both hurricane events are comparable in terms of wind direction experienced by the residential development during the translational approach of the hurricanes as they reached their respective peak wind speeds. Although there were variations between the two events in regards to the hurricane track parameters (e.g., translational speed, angle of approach, etc.), it appears that wind speed is the biggest indicator of residential development damage in this case. This is interesting in that hurricane events #3 and #10 are both 700-year MRI events based on

peak wind speed, yet there is a considerable variation in the peak wind speeds between the two events (~ 12 m/s), and by extension the damage, experienced by the residential development when subjected to these two events. This variation in the peak wind speeds between these two 700-year MRI events is attributed to the bin size utilized to the select the hurricane events from the synthetic hurricane database. The utilization of a larger bin size, for example 100,000 years as opposed to the 50,000 years used in this study, should decrease the event-to-event wind speed variations. The variations in wind speed causing an increase in damage between the two events further supports the assumption that it is the wind-borne debris released during hurricane event #3 that is responsible for the nonlinearity in the final building envelope survival values.

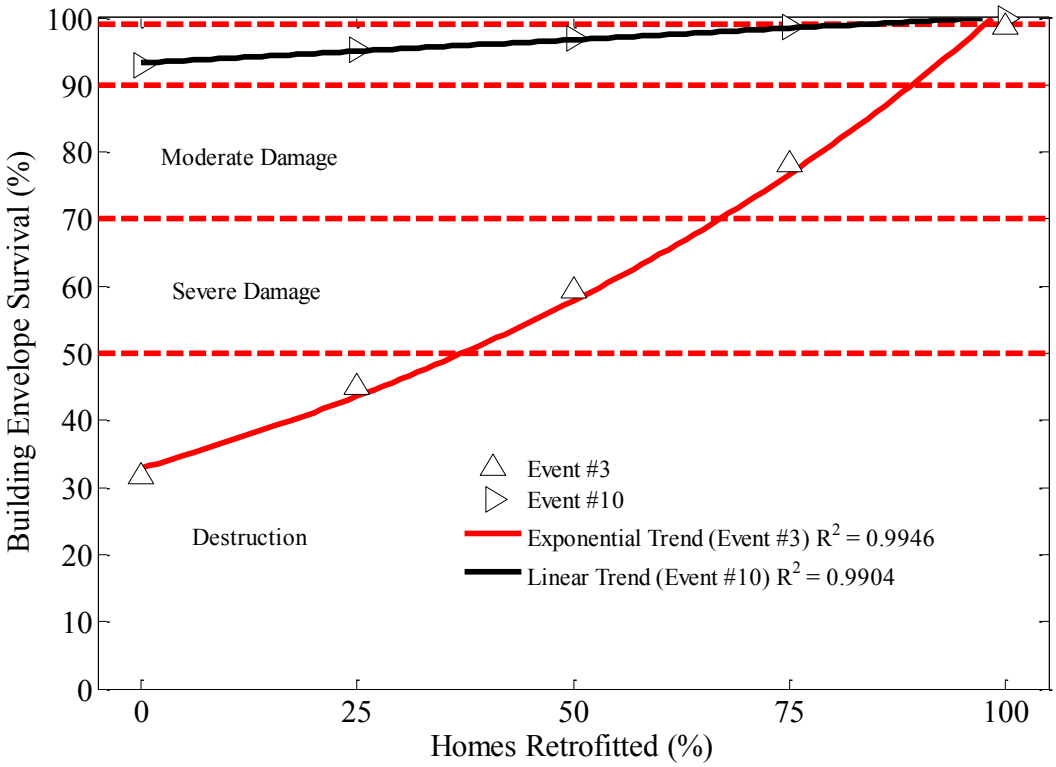

Figure 5.10: Final building envelope survival data trends for the two hurricane events that cause the least and most damage to the building envelopes.

5.3.3 Retrofitted Home Versus Unretrofitted Home Performance

Figure 5.11 breaks down the contribution of the retrofitted and unretrofitted homes to the time evolution of the overall building envelope survival to a 700-year MRI hurricane wind event. Even though there is a definite benefit to the unretrofitted homes as more of the homes within the residential development are retrofitted, there is a considerable difference between the performances of the retrofitted homes versus the unretrofitted homes.

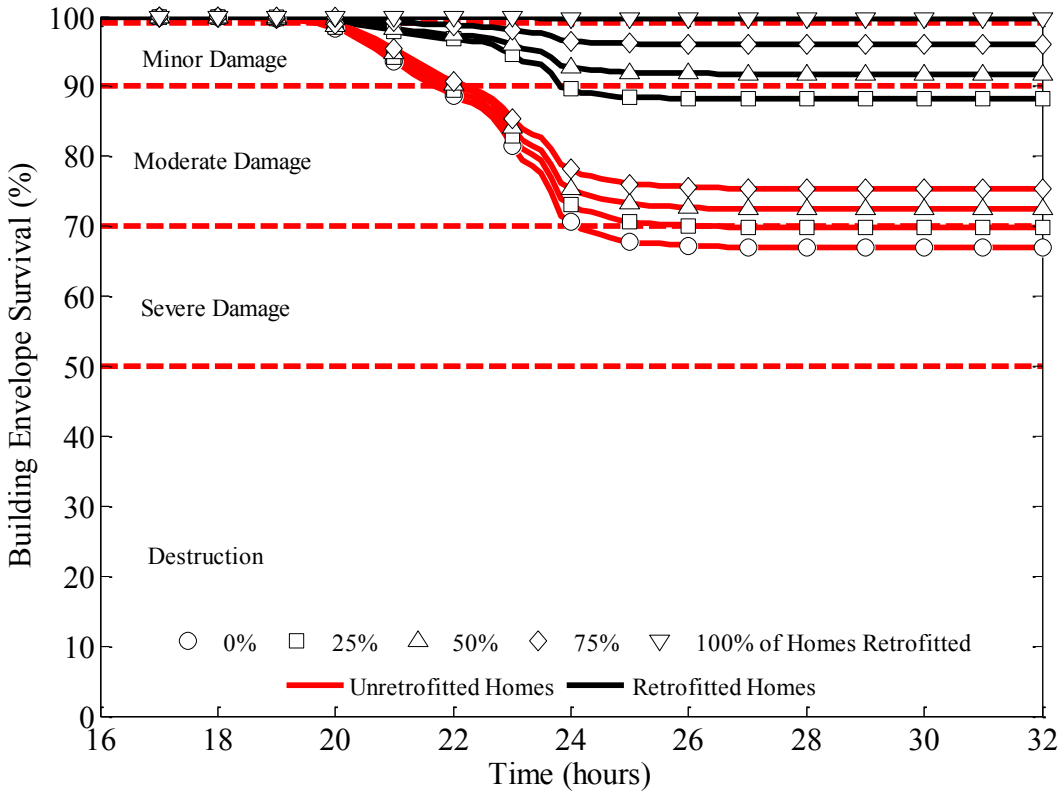

Figure 5.11: Time evolution of the building envelope survival for each of the five retrofit scenarios for the retrofitted and unretrofitted homes.

Figure 5.12 further breaks down the performance of the retrofitted versus the unretrofitted homes into the individual contributions of each failure mode. The

contributions of failure modes one and three (i.e., roof covering loss and sheathing/window/door failures, respectively) remain relatively constant for the retrofitted and unretrofitted homes regardless of the percentage of homes retrofitted in the residential development. The significant variable for both the retrofitted and unretrofitted homes is the damage contributed by failure mode 2 (i.e., wind-borne debris impacts). Any increase in the contribution of failure mode 2 due to window failures from wind-borne debris impacts is small when compared to the overall damage caused by the aggregate 700-year MRI hurricane wind events, which further reiterates the findings of Figure 5.10. Additionally, the information provided in Figure 5.12 was utilized to assign values to the general logical relationships between the failure modes presented in Chapter 4 (see Figure 4.2). This process is exactly the same as presented for Figure 5.7 and Table 5.4 with the only difference being that the individual failure mode contributions are separated between the retrofitted and unretrofitted homes (see Tables 5.5 and 5.6) of the residential development.

The results of Tables 5.5 and 5.6 confirm that the damage inflicted from failure modes 1 and 3 were for the most part constant for both the retrofitted and unretrofitted homes regardless of the percentage of the residential development that was retrofitted. This left failure mode 2 (i.e., wind-borne debris impacts) as the dominant variable with the increased wind-borne debris generated by the unretrofitted homes directly affecting the retrofitted homes. It is interesting to note the higher failure mode 2 damages for the unretrofitted homes (see Table 5.6) over that of the retrofitted homes (see Table 5.5). This is attributed to a higher number of self-impacts experienced by the unretrofitted

homes and the reduction in damage to the retrofitted homes due to the window impact protection.

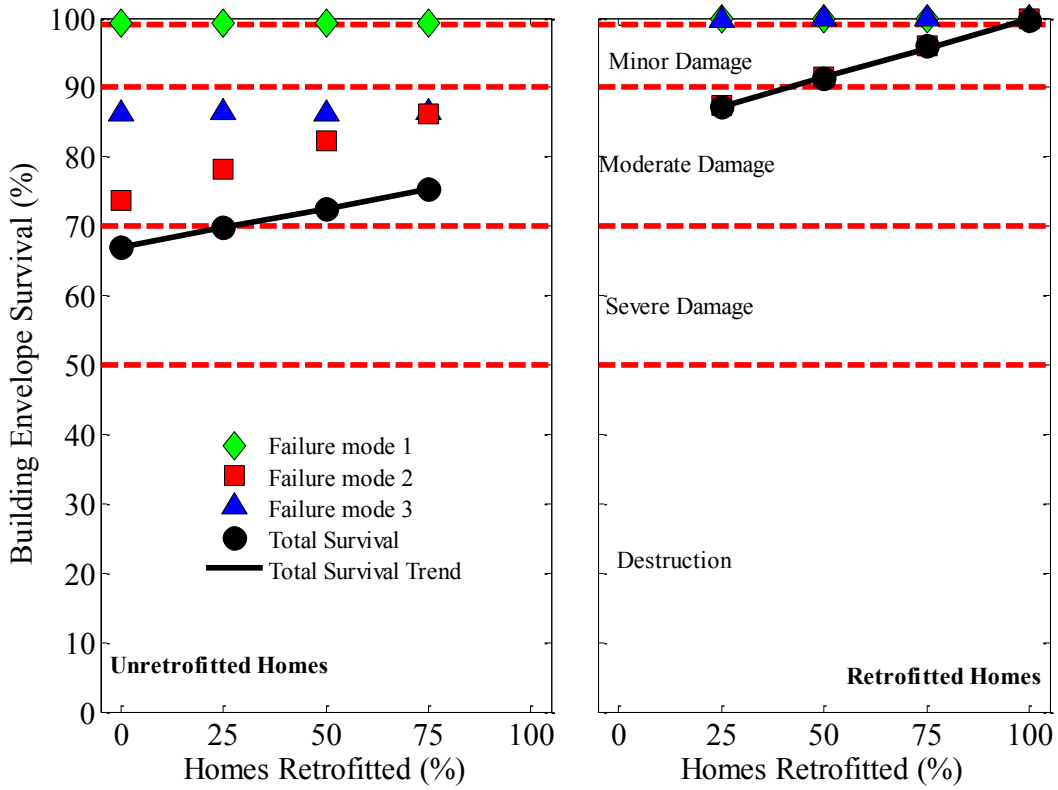

Figure 5.12: Individual damage contributions of each of the three failure modes to the final mean building envelope survival for the retrofitted and unretrofitted homes.

Table 5.5: Failure mode logical relationship values for the retrofitted homes of the residential development.

Scenario	Failure mode damage			Survival
	1	2	3	
1	-	-	-	-
2	0.001	0.l16	0.002	0.882
3	0.001	0.080	0.002	0.918
4	0.001	0.038	0.001	0.960
5	0.001	0.002	0.001	0.997

Table 5.6: Failure mode logical relationship values for the unretrofitted homes of the residential development.

Scenario	Failure mode damage			Survival
	1	2	3	
1	0.007	0.238	0.139	0.670
2	0.007	0.204	0.136	0.698
3	0.007	0.171	0.137	0.724
4	0.007	0.135	0.137	0.754
5	-	-	-	-

Figure 5.13 confirms that there was an approximately 12% increase in the building envelope survival for the unretrofitted homes with at least 75% of the homes in the residential development retrofitted. This benefit to the unretrofitted homes is attributed to the reduction in wind-borne debris available to cause damage as more of the homes were retrofitted. However, the building envelope performance of the retrofitted homes with only 25% of the homes retrofitted showed an approximately 20% increase over the unretrofitted homes with 75% of the homes retrofitted and an approximately 32% increase over the unretrofitted residential development. Therefore, while there was a benefit to unretrofitted homes surrounded by retrofitted homes, the building envelope survival of a home greatly increases if a home has been properly prepared. The overall performance of the residential development with all of the homes retrofitted showed an approximately 49% increase in final building envelope survival over the unretrofitted residential. This is a substantial increase that will be investigated further in future studies to determine which of the employed retrofits provide the best performance for the cost and how incentives influence the performance of residential developments subjected to hurricane wind hazards.

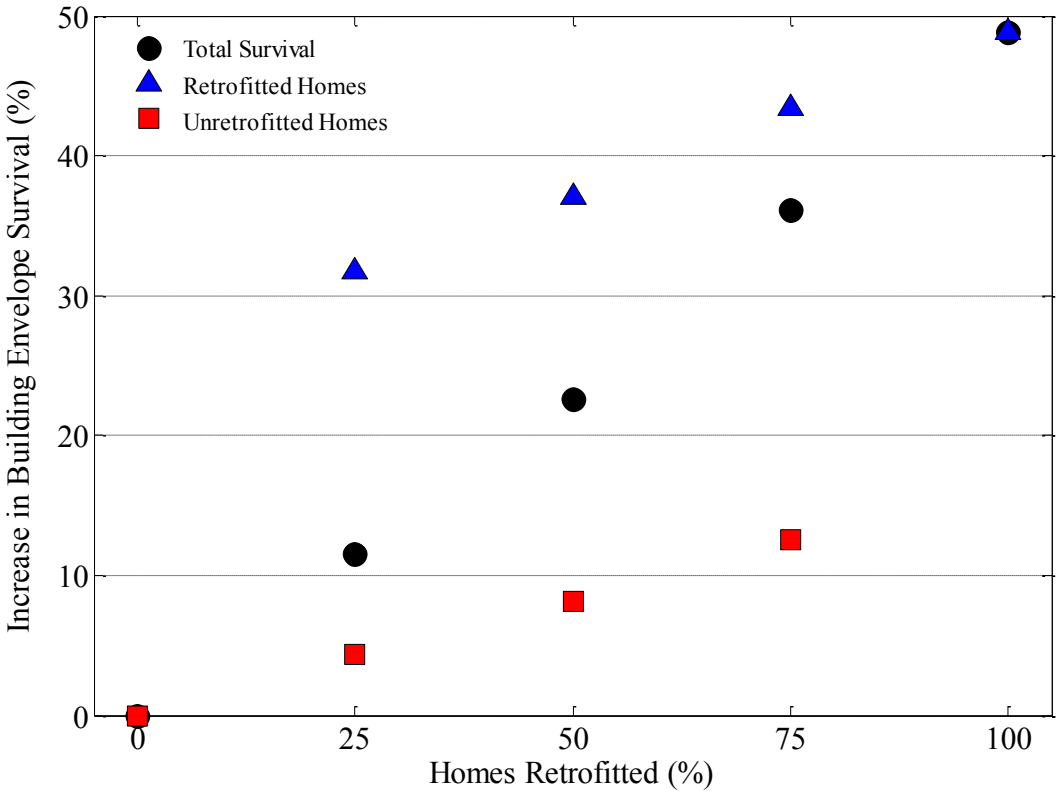

Figure 5.13: Increase in the final building envelope survival over the unretrofitted residential development scenario.

5.3.4 Variability of Damage to the Residential Development

A key aspect of community resilience is the ability to perform consistently to a broad range of hazards events. Although this study focused on the response of the residential development to a 700-year MRI hurricane wind event based on the 3-second gust wind speed, there was considerable variation in other hurricane parameters, such as the translational speed and wind direction of the hurricane, that vary the intensity of the hurricane event experienced by the residential development. Figure 5.14 illustrates the final damage response for 0% and 100% of the homes retrofitted based on the wind speed demand. It is important to note the significant reduction in not only damage, but also

reduction of the variability in performance of the retrofitted residential development when subjected to the same hazard demand. Grayson et al. (2013a) notes the influence that wind direction can have on the failure of building envelope components; therefore, Figure 5.15 illustrates the same concept as Figure 5.14 but with the wind direction as the hazard demand. As with the wind speed demand, there was a significant reduction in the damage and the variability in performance of the residential development. While a reduction in the variability of performance is not a direct metric of community resiliency, it is certainly a crucial piece of information in determining how much recovery might be expected when a residential development is subjected to a hurricane wind hazard event.

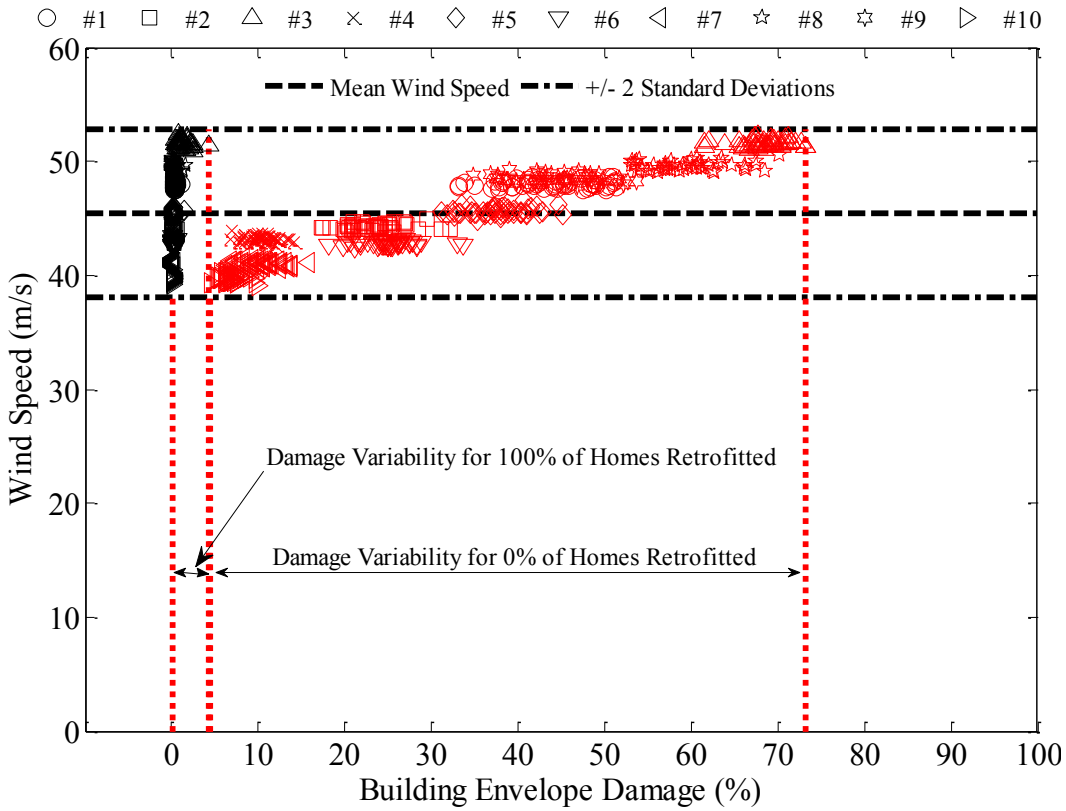

Figure 5.14: Damage variability of the residential development exposed to the ten 700-year MRI hurricane wind events based on wind speed demand.

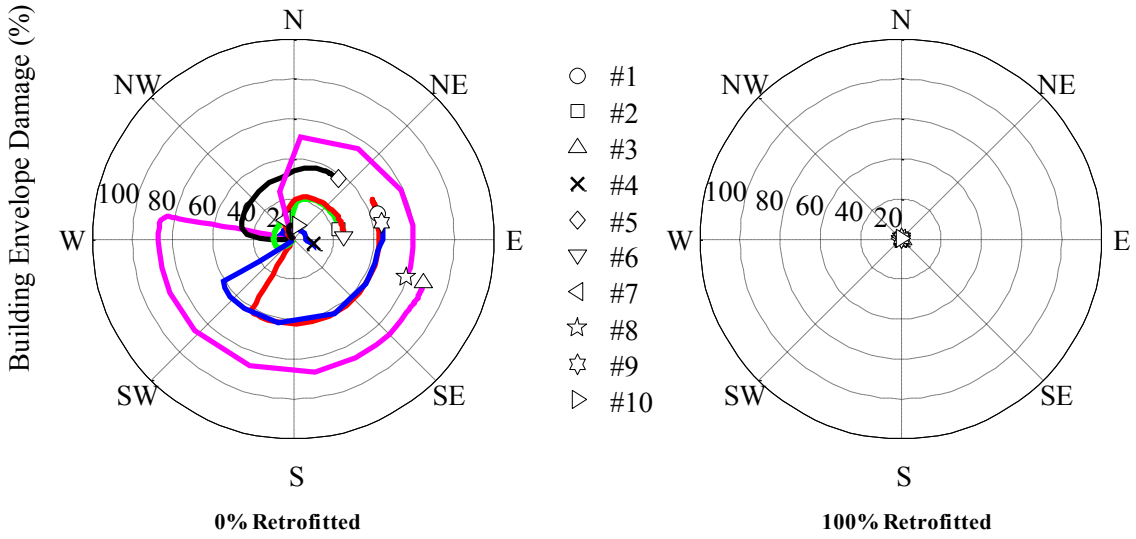

Figure 5.15: Damage variability of the residential development exposed to the ten 700-year MRI hurricane wind events based on wind direction demand. The markers denote the location of the maximum building envelope damage value during the time evolution of the passage of the hurricane.

5.3.5 Damage Probabilities of the Residential Development

Damage probabilities are important in determining the likelihood that a residential development will exceed a certain level of damage when subjected to a particular hurricane wind event. Figure 5.16 sorts and ranks the final building envelope survival for all 500 simulations to produce the empirical cumulative distribution functions (CDF) for each of the five retrofit scenarios. Figure 5.17 utilizes the data from Figure 5.16 to provide the probability that a residential development will receive a certain level of damage when subjected to a 700-year MRI hurricane event. Figure 5.18 aggregates this data to develop damage curves that provide the probability of the residential development exceeding a particular level of damage when subjected to a 700-year MRI hurricane event. It is interesting to note how the damage curves change as a result of the

contribution of the retrofitted homes. The probability of the residential development receiving greater than minor damage can be estimated with a third-order polynomial trend, which works well to illustrate that the unretrofitted homes and the retrofitted homes control the reduction in overall damage to the residential development for less than and greater than 50% of the homes retrofitted, respectively. The probability of the residential development receiving greater than moderate can be estimated with a second-order polynomial trend as the contribution of the retrofitted homes is reduced due to very few of the retrofitted homes sustaining greater than moderate damage. The probability of the residential development attaining destruction can be approximated by a linear trend, as the unretrofitted homes become the only contributor to damage at that point.

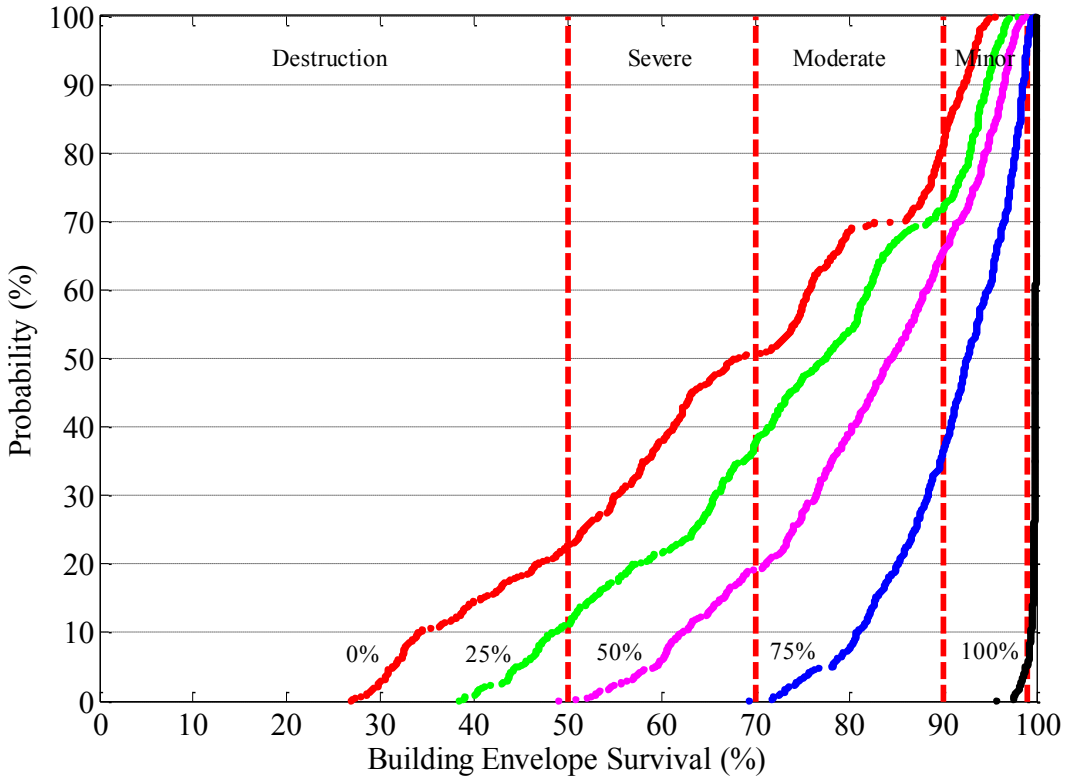

Figure 5.16: Empirical cumulative distribution functions for the final mean building envelope survival for each of the five retrofit scenarios.

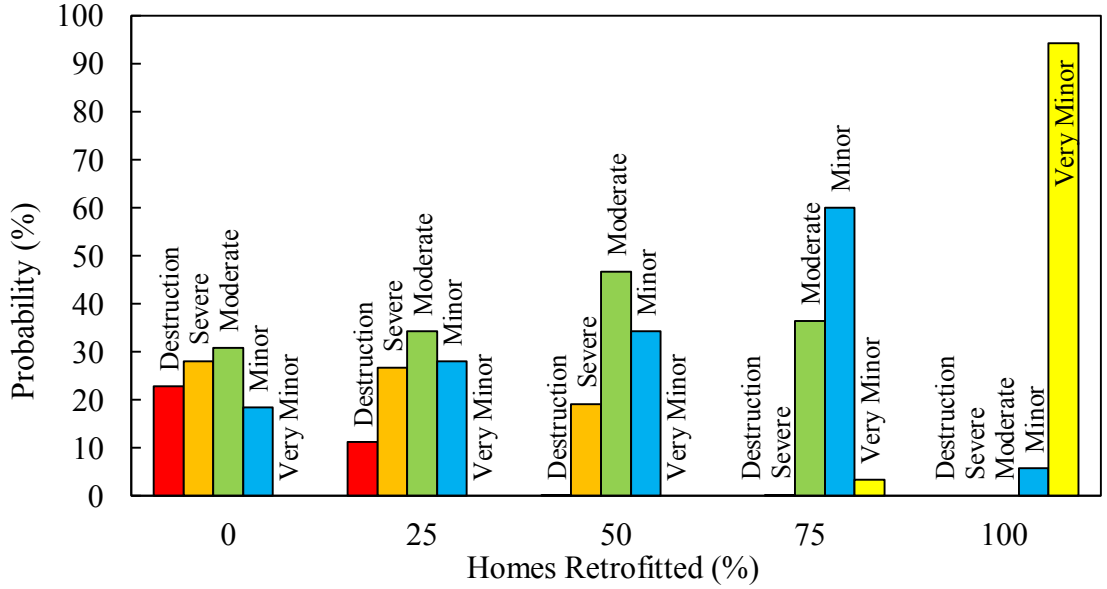

Figure 5.17: Residential development damage probabilities for each damage zone based on the percentage of homes retrofitted within the residential development.

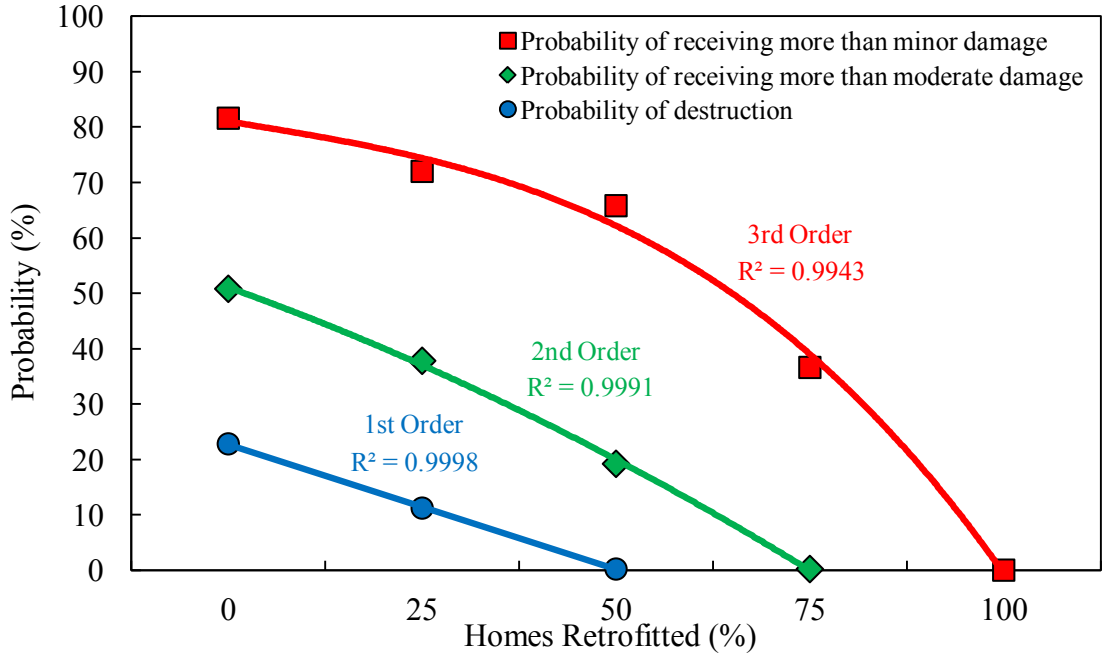

Figure 5.18: Probability of the residential development exceeding a particular damage level based on the percentage of homes retrofitted within the residential development.

6 CONCLUSIONS AND RECOMMENDATIONS

6.1 Conclusions

Due to the numerous socioeconomic factors that influence the recovery of a community after experiencing a hazard event, it is beneficial for the structural engineer to think of community resiliency in terms of mitigating or preventing damage to developments from degenerating to disaster levels. The current paradigm of "build-disaster-rebuild" is no longer a viable plan, and the determination of the influence of residential development-wide disaster mitigation retrofits have the capability of providing insurance companies with the information necessary to better set insurance premiums within hurricane-prone regions and provide homeowners with the incentive for individual members to work together towards a more disaster–resilient community.

A framework for the assessment of building envelope failures of residential communities subjected to hurricane wind hazards is presented in this study. The proposed framework develops an integrated building envelope model that is based on current peer-reviewed research of individual component capacities, and differs from other current loss models in its flexibility to investigate any number of "what if" scenarios within a residential development on a more intricate level. Key modules include a wind-borne debris generation module and an impact-tracking module that will interact with a hurricane simulation module capable of simulating a suite of synthetic hurricanes and historical hurricanes. The proposed framework is driven by a mechanics-based 3D probabilistic debris trajectory model that is capable of providing the debris trajectory information required for assessing impacts to any component of a building envelope. The

incorporation of a 3D probabilistic debris trajectory model capable of tracking wind-borne debris from source to impact is a significant distinction from other frameworks that utilize empirical fragility curves developed from observed post-hurricane assessments, insurance claim data, or basic probabilistic analyses of wind-borne debris.

A representative SC residential development was modeled within the proposed framework and subjected to the historical Hurricane Hugo. Results from this example illustrate the critical role that fasteners perform in maintaining the integrity of the building envelope, and it has led to the development of a debris impact vulnerability envelope for assessing the probability of impact and/or damage (failure) of the vulnerable components (i.e., windows and doors) of the building envelope. The probabilities provided by these plots are site specific and can be utilized by government officials, developers, architects, and designers as a pre-construction planning tool for residential developments, or by homeowners post-construction to identify which vulnerable areas of the building envelope would benefit the most from protection in the event of limited resources to devote to mitigation.

This research explicitly addresses the influence of exogenous wind-borne debris within a mechanics-based building envelope failure assessment (BEFA) model. Results from this study confirm that exogenous wind-borne debris can have an influence on a mechanics-based building envelope failure assessment model that focuses on smaller, more detailed regions of interest. A methodology to include exogenous wind-borne debris in a mechanics-based building envelope failure assessment model is developed, and the two-parameter type III smallest extreme value (Weibull) distribution and negative

binomial/Poisson distribution combination identified as reasonable distributions to generate exogenous wind-borne debris within the building envelope failure assessment model. Additionally, a novel method is developed to account for the cumulative damage incurred by the building envelope due to wind-borne debris impact.

Residential development performance is studied by varying the percentage of the number of homes retrofitted to determine how mitigating the "initial shock" created by a hurricane wind events influences the response of the residential development building stock. An "all or nothing" approach is taken to applying the retrofits to each home that address upgrades to the roof covering, roof sheathing, personnel and garage doors, and the installation of window impact protection. The variability of the hurricane wind hazard is considered by selecting ten synthetic 700-year mean recurrence interval events that represent a design-level wind event that is consistent with the ASCE 7 design standard for Risk Category II. Results illustrate that a fully retrofitted residential development increases the mean survival of the building envelopes by approximately 49% above the performance of the unretrofitted residential development. A significant contributor to the increase in survival as a greater percentage of the residential development is retrofitted is mainly attributed to the reduction of damaging wind-borne debris. It is also evident that having at least 50% of the homes retrofitted, at least within this particular residential development, represents the point where the majority of the retrofitted homes, on average, experiences no more than minor damage.

6.2 Recommendations for Future Research

This work is only the initial step required to investigate the resilience of a community to hurricane wind hazards. There is a significant amount of research that must be performed in the future to continue to refine the response of low-rise residential wood construction to natural hazards and to incorporate the recovery response of the community before, during, and after a hazard event. The following recommendations are separated into two categories that address experimental and analytical research needed to continue building resilient residential communities to natural hazards.

6.2.1 Experimental Research

Further experimental research is necessary to incorporate the system response of low-rise residential to natural hazards. This research will address not only hurricane wind hazards, but will expand the current research to incorporate multiple hazards. Recommendations for future experimental research will complement the aforementioned analytical recommendations and include, but are not limited to:

- the development of low-cost structural health monitoring methods to determine the "health" of the building envelope after hazard events, and how the building envelope performs when exposed to hazard events that are close in proximity temporally and spatially,
- the investigation of building envelope component failure mechanisms when subjected to extreme wind hazard events to better account for the trajectories

of wind-borne debris within mechanics-based three-dimensional probabilistic wind-borne debris trajectory models,

- the investigation of the contribution of cumulative wind-borne debris impacts to the overall damage of a building envelope,
- the identification of a suitable impact kinetic energy threshold or thresholds to represent the building envelope within a mechanics-based building envelope failure assessment model,
- initiate multi-disciplinary collaboration that identifies the key socioeconomic parameters of community recovery, and implement experimental studies to obtain the necessary information to develop community recovery algorithms to multiple hazard events, and
- the development of an innovative building envelope failure and wind-borne debris tracking system that can provide the information necessary to verify the results of current hurricane damage assessment models.

6.2.2 Analytical Research

Further analytical research is necessary to expand the building envelope failure assessment model to incorporate damage due to multiple hazards and to incorporate the socioeconomic response of the community, both of which are needed to perform resilience assessments over the life cycle of a community. Future analytical research needs include, but are not limited to:

- a cost-benefit analysis of current hurricane wind mitigation techniques that provide a homeowner with the best value for the money spent,

- the incorporation of real-time building component loading scenarios (e.g., cyclic loading) to better represent real-life building envelope failure mechanisms,
- the determination of the size of the study region at which point exogenous wind-borne debris no longer has a statistically significant influence on the results of a mechanics-based building envelope failure assessment model,
- the investigation of parameters (e.g., building stock, vegetation, etc.) that define the regions surrounding a residential development to determine if exogenous wind-borne debris should accounted for in an analysis,
- the investigation of wind-borne debris produced by vegetation,
- the development of additional modules that can expand the building envelope failure assessment model to include multiple hazards, such as earthquakes and tornadoes, and
- the development of community recovery algorithms that incorporate the socioeconomic aspects of recovery to multiple hazards.

APPENDICES

A TRUNCATION OF THE GAUSSIAN DISTRIBUTION

Gurley et al. (2005) uses a truncated Gaussian (i.e., normal) distribution to represent the capacities of typical building materials within the Florida Public Hurricane Loss Projection Model (FPHLPM). The FPHLPM justified the selection of the Gaussian distribution over other distributions by reasoning that the numerous variables (e.g., size, type, construction quality, etc.) associated with building component capacities, when sampled over a large number of iterates, approximates a Gaussian distribution pursuant to the central limit theorem. However, the Gaussian distribution must be truncated to prevent the possibility of sampling impossible or unreasonable component capacities if used in this manner.

A truncated Gaussian distribution within an interval $[a,b]$ must still adhere to the axioms of probability, namely, the area under the probability density function must equal one. Therefore, the distribution must be modified to account for the lost area under the tails. Olive (1998) demonstrates that a normally distributed random variable, $X \sim N(\mu,\sigma^2)$, truncated within the interval $[a=\mu-k\sigma, b=\mu+k\sigma]$ will be a normally distributed variable, $Y \sim TN(\mu,\sigma^2,a,b)$, with the mean and variance of the original Gaussian distribution equal to:

$$E(Y)=E(X)=\mu \tag{A.1}$$

$$\sigma_Y^2=\sigma_X^2\left[1-\frac{2k\varphi(k)}{2\Phi(k)-1}\right] \tag{A.2}$$

where k is the number of standard deviations away from the mean, $\varphi(.)$ is the standard normal PDF, and $\Phi(.)$ is the standard normal CDF. Gurley et al. (2005) sets the interval of truncation at +/- two standard deviations. Therefore, the multiplier to adjust the variance of the truncated distribution becomes:

$$\sigma_Y^2 = \sigma_X^2\left[1-\frac{2k\varphi(2)}{2\Phi(2)-1}\right] \approx 0.774\sigma_X^2. \qquad \text{A.3}$$

Figure A.1 illustrates a comparison of the correct and incorrect truncation of a normally distributed random variable with mean equal to 100 and standard deviation equal to 40. It is evident that for the area under the PDF curve to remain equal to one that the truncated distribution had to adjust accordingly.

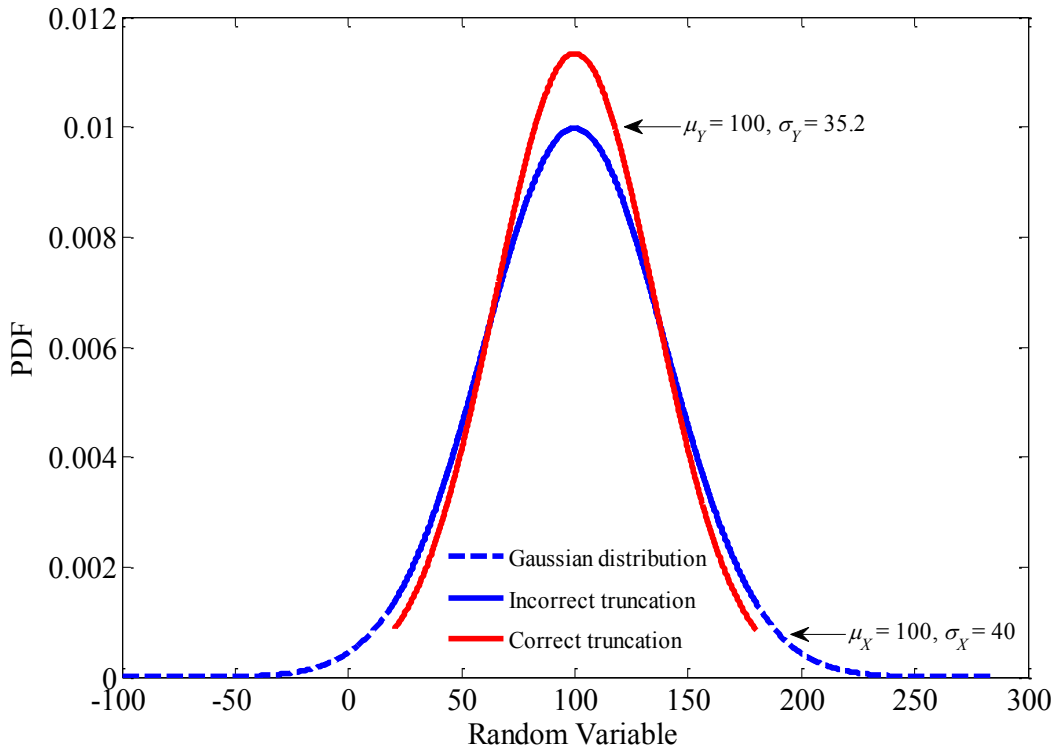

Figure A.1: Correct and incorrect truncation of a Gaussian distribution.

Figure A.2 provides verification that the truncated Gaussian distribution performs as expected with the probability of attaining any values greater than +/- two standard deviations is equal to zero.

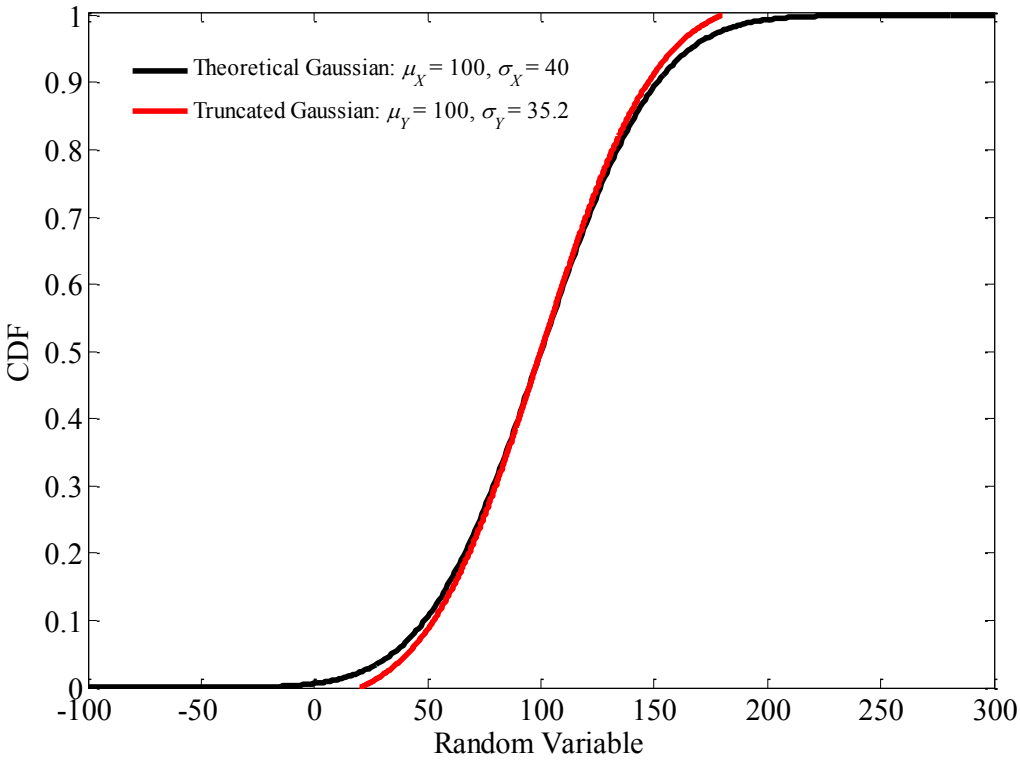

Figure A.2: Verification of Gaussian distribution truncated within an interval.

B UPLIFT CAPACITY OF CLASS H ROOF COVERING

In order to assess the retrofitted residential development, it is necessary to determine an appropriate uplift pressure capacity for Class H shingles. The American Society of Testing and Materials (ASTM) categorizes the highest level of wind resistance for asphalt shingles as Class H, which is a shingle that has been tested and passed at basic wind speeds up to and including 67 m/s (150 mph) (ASTM 2011). However, there is little research that assigns an actual uplift capacity to Class H shingles. Therefore, for the purposes of this research, the method utilized within the FPHLPM (Gurley et al. 2005) to calculate the roof covering uplift capacity of common residential roof coverings in Florida (i.e., mean failure pressure = 3.35 kPa; COV = 0.4) was utilized to arrive at a reasonable uplift capacity for Class H shingles.

Gurley et al. (2005) calculated the uplift pressure capacity of common residential roof coverings in Florida from the average of two values based on two separate assumptions. The first assumption operates on the premise that the majority of roof coverings currently utilize manufacturing processes and techniques that were similar to those used in the 1970s. It was further assumed that many of these coverings were subject to the Southern Building Code Congress international (SBCCI) requirement that these materials be able to withstand a positive or negative external pressure equal to 1.20 kPa. Assuming that at least 90% of the current roof coverings on the market would meet or exceed this requirement, a mean failure strength was calculated by using the standard Gaussian distribution to back–calculate the mean failure pressure:

$$\bar{x} = \frac{x}{z \bullet} \qquad \text{B.1}$$

where $\bar{x}$ is the mean failure pressure, z is a value from the standard normal distribution with the same likelihood as x, and COV is the coefficient of variation. Assuming x is equal to 1.20 kPa, z is equal to -1.28 for 90% probability, and the COV is equal to 0.4 due to material and construction variations provides a mean failure pressure of 2.44 kPa.

The second assumption made by Gurley et al. (2005) determined the capacity of the roof covering by using the 49 m/s (110 mph) design wind speed required by Dade County to calculate a mean failure capacity. For this approach, Gurley et al. (2005) calculated a design wind pressure utilizing Eqns. B.2 and B.3 from ASCE 7 (1998):

$$q_h = 0.00256 K_h K_{zt} K_d V^2 I \qquad \text{B.2}$$

and,

$$p = \left| GC_p - GC_{pi} \right| \qquad \text{B.3}$$

where q_h is the velocity pressure at mean roof height, K_h a the terrain exposure coefficient, K_{zt} is a topographic effect factor, K_d is a directionality factor, V is the design wind speed in miles per hour, I is an importance factor for the building, and GC_p and GC_{pi} are the external and internal pressure coefficients, respectively.

Assuming an enclosed building in open terrain (Exposure C) and that 90% of the current coverings meet or exceed the 110 mph (≈ 49 m/s) requirements set forth by the Dade County provision, Gurley et al. (2005) arrived at a mean failure pressure equal to 4.98 Pa. It was rationalized that the 2.44 kPa value from the first assumption was too low,

and the 4.98 kPa value from the second assumption was too high based on damage reports and engineering judgment. Therefore, Gurley et al. (2005) reasoned that the best value to represent the roof covering for a majority of the homes was an average value of approximately 3.35 kPa with a COV of 0.4.

It is assumed that the mean uplift capacity of Class H shingles can be determined using the second assumption method employed by Gurley et al. (2005). Therefore, the 49 m/s (110 mph) design wind speed of the Dade County requirements replaced with the 67 m/s (150 mph) design wind speed of the Class H shingles in Eqn. B.2. Assuming that Class H shingles have a COV equal to 0.4 to account for material and construction quality, the mean failure pressure capacity is back calculated as 9.24 kPa. It is further assumed that this design value is too high as reasoned by Gurley et al. (2005) for the 110 mph (≈49 m/s) rated roof covering. There is not a viable assumption for a minimum mean failure pressure capacity for Class H shingles as was the case in Gurley et al. (2005). Therefore, the average mean failure pressure capacity is calculated by setting the ratio of the average mean failure pressure capacity to the high mean value pressure capacity calculated by Gurley et al. (2005) equal to the ratio of the average mean failure pressure capacity and the high mean value pressure capacity for Class H shingles as shown in Eqn. B.4.

$$\frac{\overline{x}_{\text{Class H - Average}}}{\overline{x}_{\text{Class H - High}}} = \frac{\overline{x}_{\text{Gurley et al. (2005) - Average}}}{\overline{x}_{\text{Gurley et al. (2005) - High}}} \qquad \text{B.4}$$

Solving for the average mean failure pressure capacity of the Class H shingles in Eqn. B.4 and substituting the previously calculated values into Eqn. B.5 provides an average mean failure pressure capacity equal to 6.22 kPa for Class H shingles.

$$\bar{x}_{\text{Class H - Average}} = \left(\frac{\bar{x}_{\text{Gurley et al. (2005) - Average}}}{\bar{x}_{\text{Gurley et al. (2005) - High}}} \right) \bar{x}_{\text{Class H - High}} = \left(\frac{3.35 \text{ kPa}}{4.98 \text{ kPa}} \right) 9.24 \text{ kPa} = 6.22 \text{ kPa} \qquad \text{B.5}$$

C RESPONSE OF THE BEFA MODEL TO THE WIND-BORNE DEBRIS DAMAGE ASSUMPTIONS

Three assumptions were made to quantify the contribution of wind-borne debris impact to the cumulative damage incurred by a building envelope during a hurricane wind hazard event, namely:

1. seventy-five cumulative impacts causes complete destruction of a home,
2. the impact kinetic energy threshold of the building envelope is 475 N-m, and
3. there is no upper limit to the impact kinetic energy threshold.

Although there is little research that directly quantifies the contribution of wind-borne debris impact to the overall cumulative damage to a building envelope, the most relevant research available has been incorporated to justify these assumptions (see Chapter 4). However, it is important to determine if the BEFA model results are sensitive to these assumptions, so that future research can focus on refining these assumptions as needed. A basic sensitivity analysis was performed to illustrate how the performance of the residential development responds to deviations in the values attained for each of the aforementioned assumptions. The data used for this sensitivity study was obtained from the study performed investigating the influence of hurricane wind hazard mitigation retrofits on residential development performance (see Chapter 5). The black markers in Figure C.1 to Figure C.4 represent the assumed methods and parameter values justified and used within the BEFA model for this study.

Figure C.1 provides an illustration showing the differences between counting all impacts as a significant impact (i.e., each impact contributes one impact) and the

proposed methodology presented in Chapter 4 that adjusts the number of significant impacts based on the impact kinetic energy ratio. The contribution of the significant impacts based on the impact kinetic energy ratio (i.e., impact kinetic energy/impact kinetic energy threshold) is less than counting each impact as a significant impact up to approximately hour 20 during the passage of the hurricane event. This is due to the low windspeeds present during this time producing very low impact kinetic energies that do not inflict much damage to the residential development. However, the significant number of impacts based on the impact kinetic energy ratio quickly increases as the wind speed and the mass of the failed building envelope components increases.

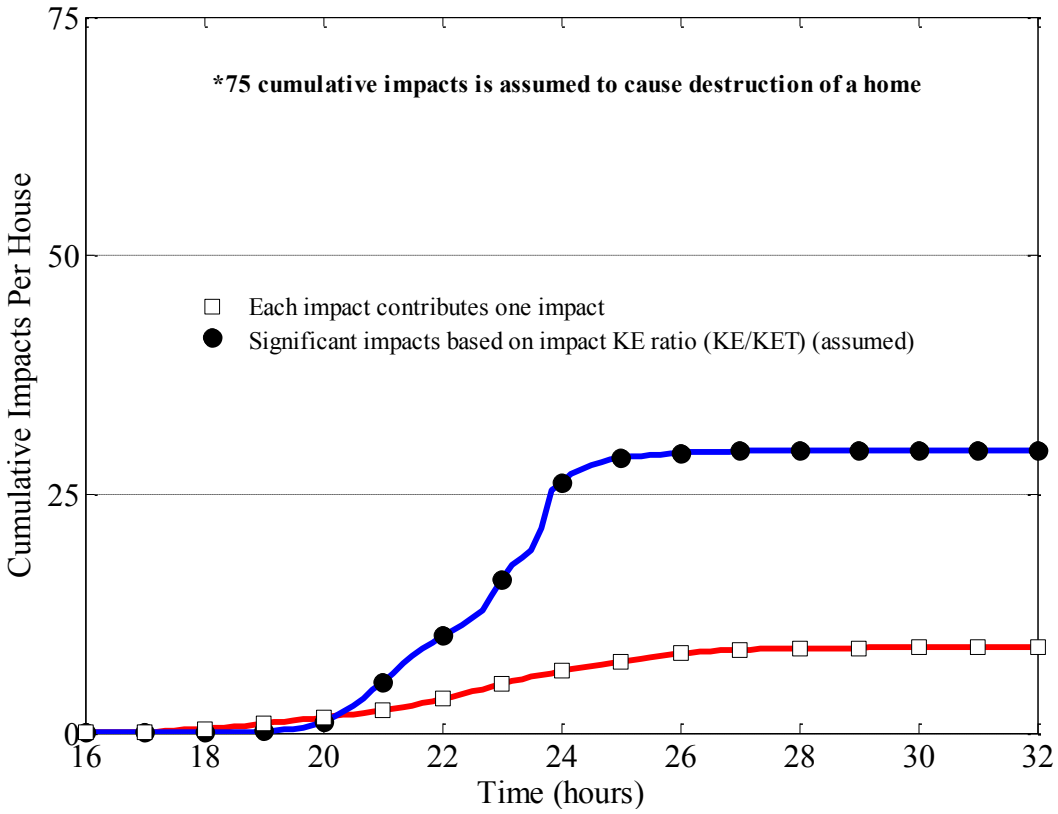

Figure C.1: The influence of using the impact kinetic energy threshold of the building envelope to determine the number of significant impacts.

Figure C.2 illustrates the sensitivity of the BEFA model output to the total number of impacts assumed for a home to reach the destruction threshold (i.e., assumption #1) that is used to calculate the damage values for the impacts in Table 4.2. There is a nonlinear increase in the final building envelope survival with a linear increase in the total number of impacts assumed. This is as expected since the impact ratio used directly determines the damage values (ψ) for failure mode 3 (i.e., wind-borne debris impacts) shown in Eqns. 4.7 and 4.8. The final building envelope survival will continue to increase as the total number of impacts assumed to cause destruction of the home increases. This trend will continue until the contribution from wind-borne debris impacts is essentially zero.

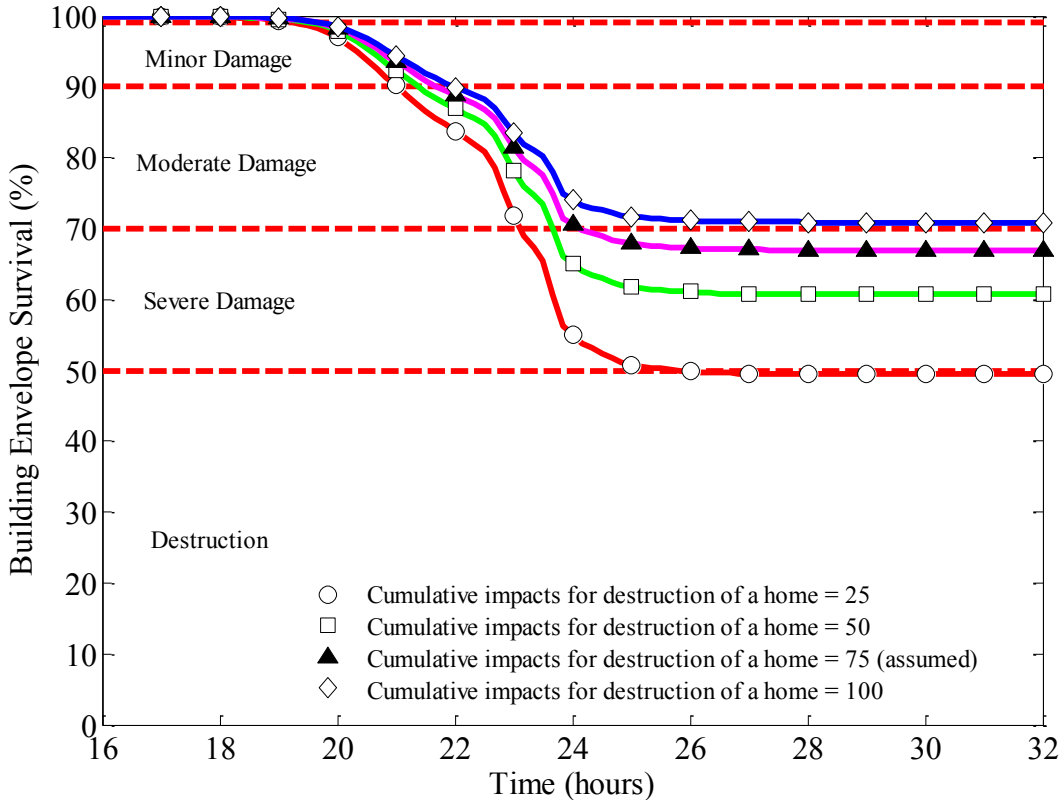

Figure C.2: Sensitivity of the BEFA model output to the total number of impacts assumed to cause complete destruction of a single home.

Once this occurs, all damage to the building envelopes can be attributed to building envelope penetrations due to vulnerable component (i.e., windows and doors) and sheathing failures, and roof covering loss. It is evident that the BEFA model output is highly sensitive to this assumption with the final residential development damage ranging from moderate damage to destruction. Unfortunately, the assumed total number of impacts required for destruction of a building envelope has the least amount of research available for justification, and will require a dedicated research effort in the future.

Figure C.3 illustrates the sensitivity of the BEFA model output to the assumed impact kinetic energy threshold (i.e., assumption #2). The final building envelope survival increases non-linearly similar to the total number of impacts in assumption #1, but with less sensitivity. As with the total number of impacts assumption, the impact kinetic energy threshold will benefit from a concerted research effort to identify a value or values that either validate or refute the assumptions made herein. Calculating the adjusted number of significant impacts based on the impact kinetic energy ratio (see Eqn. 4.12) can result in a home experiencing a considerable amount of damage to the building envelope if it is not limited in some manner. Although it is recognized that there should be some limit on the adjusted number of significant impacts, more research is needed to determine how and where this limit should be set.

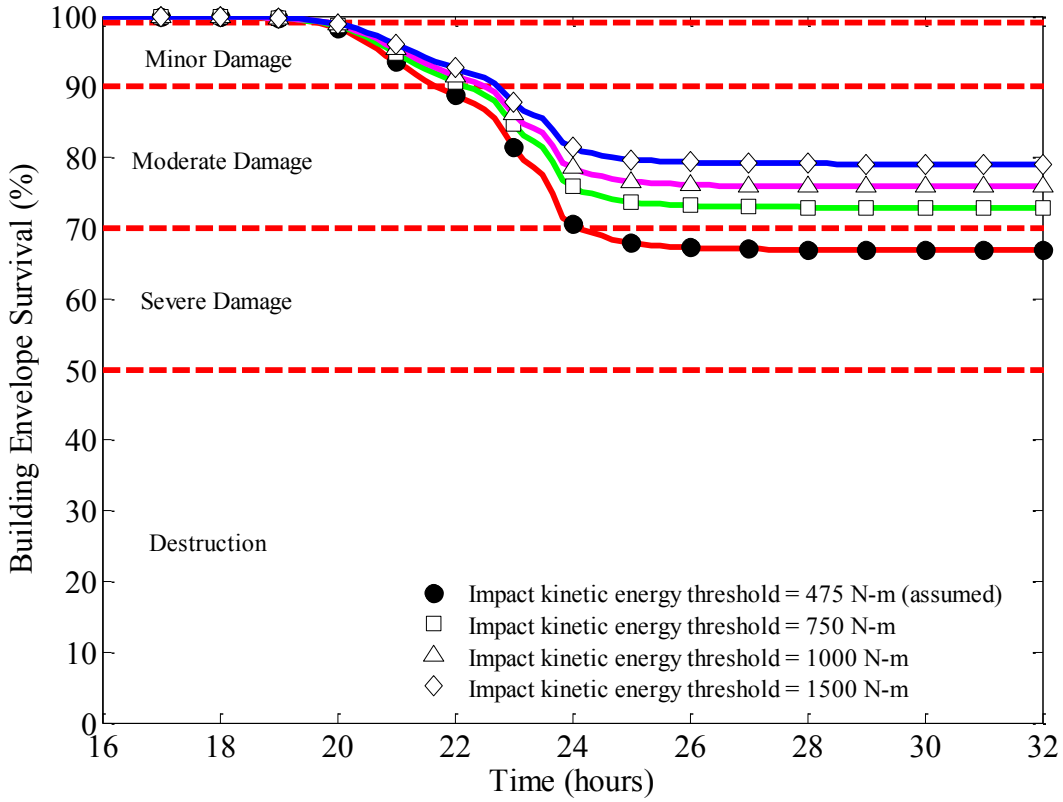

Figure C.3: Sensitivity of the BEFA model output to the impact kinetic energy threshold utilized to calculate the adjusted number of impacts.

Figure C.4 illustrates the sensitivity of the BEFA model output to the maximum impact kinetic energy ratio utilized in the adjusted number of impacts calculation (i.e., assumption #3). It is evident that assuming that the impact kinetic energy ratio is unlimited as implemented within the BEFA model is a conservative assumption. However, there is little illustrated difference in the BEFA output beyond the impact kinetic energy ratio limited at 25; therefore, the slightly more conservative assumption that the impact kinetic energy ratio is unlimited is utilized within the BEFA model.

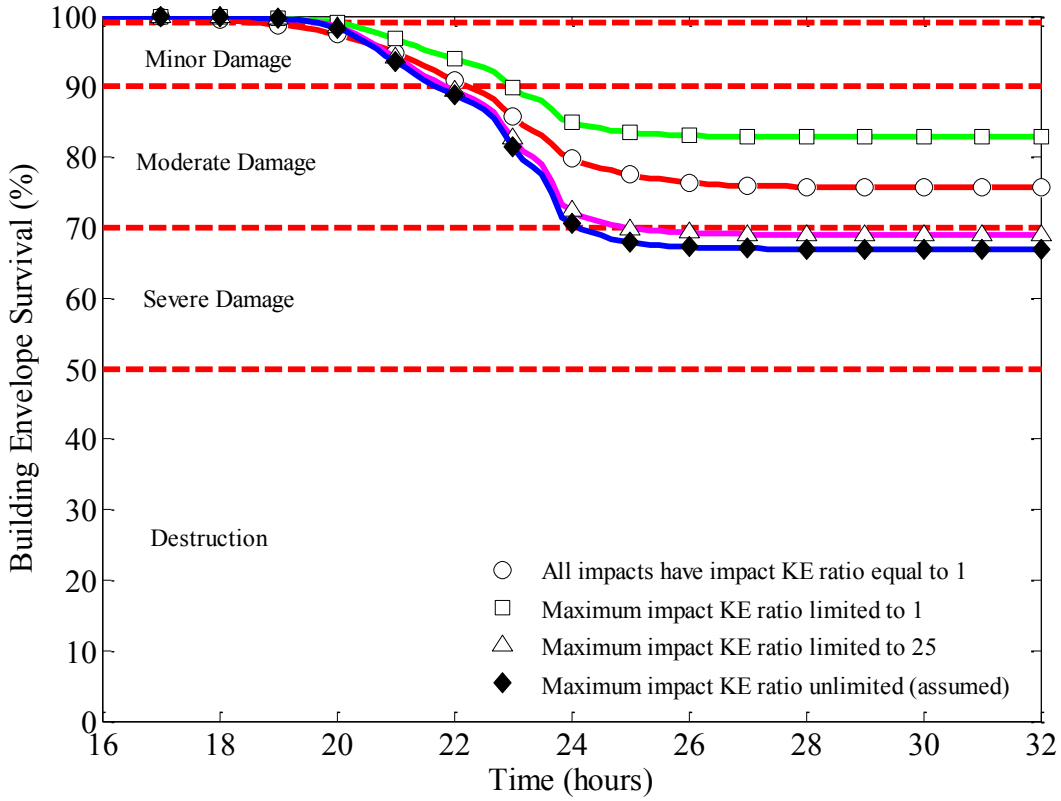

Figure C.4: Sensitivity of the BEFA model output to the maximum impact KE ratio used to determine the *Adjusted Number of Impacts*.

The results of this study illustrate that the BEFA model is highly influenced by the assumptions used to quantify the building envelope damage contributed by wind-borne debris impacts. All three assumptions contribute various levels of uncertainty into the results of the BEFA model. However, the assumption for the total impacts required for a home to attain destruction-level damage appears to be the most volatile. Additionally, it is not a conservative assumption in terms of the damage experienced by the residential development. However, until full-scale research is conducted to determine the cumulative damage effects of a building envelope impacted by wind-borne debris, a more rigorous analysis of the results of this sensitivity study is not possible.

D DATA SUMMARY

Table D.1: Final building envelope survival statistics for the residential development subjected to the aggregate 700-year MRI hurricane event.

Retrofitted (%)	Mean survival (%)	Standard deviation (%)	Damage
0	67.0	21.3	Severe
25	74.7	17.3	Moderate
50	82.1	12.6	Moderate
75	91.1	6.70	Minor
100	99.7	0.400	Very minor

Table D.2: Final building envelope survival statistics for the retrofitted homes subjected to the aggregate 700-year MRI hurricane event.

Retrofitted (%)	Mean survival (%)	Standard deviation (%)	Damage
0	-	-	-
25	88.2	11.0	Moderate
50	91.8	8.05	Minor
75	96.0	3.99	Minor
100	99.7	0.350	Very minor

Table D.3: Final building envelope survival statistics for the unretrofitted homes subjected to the aggregate 700-year MRI hurricane event.

Retrofitted (%)	Mean survival (%)	Standard deviation (%)	Damage
0	67.0	21.3	Severe
25	69.8	19.9	Severe
50	72.4	18.2	Moderate
75	75.4	17.1	Moderate
100	-	-	-

Table D.4: Final building envelope survival statistics for the residential development subjected to the ten individual 700-year MRI hurricane events.

Retrofitted (%)	Event	Mean survival (%)	Standard deviation (%)	Damage
0	1	56.2	17.6	Severe
	2	76.7	8.63	Moderate
	3	31.6	15.2	Destruction
	4	89.7	2.84	Moderate
	5	62.4	10.2	Severe
	6	74.9	8.39	Severe
	7	89.7	4.51	Moderate
	8	40.4	16.1	Destruction
	9	55.1	14.0	Severe
	10	93.0	3.74	Minor
25	1	67.8	12.5	Severe
	2	82.3	6.85	Moderate
	3	45.0	14.8	Destruction
	4	92.5	2.12	Minor
	5	71.8	7.32	Moderate
	6	81.5	6.52	Moderate
	7	92.7	3.35	Minor
	8	52.6	14.5	Severe
	9	65.2	11.1	Severe
	10	95.2	2.36	Minor
50	1	77.8	8.41	Moderate
	2	88.6	4.35	Moderate
	3	59.2	12.1	Severe
	4	94.5	1.65	Minor
	5	80.1	5.97	Moderate
	6	87.3	4.48	Moderate
	7	94.4	2.66	Minor
	8	66.4	13.2	Severe
	9	75.7	9.22	Moderate
	10	97.0	1.76	Minor
75	1	88.9	5.43	Moderate
	2	94.8	2.77	Minor
	3	78.2	8.48	Moderate
	4	97.7	0.756	Minor
	5	90.9	3.15	Minor
	6	93.3	3.10	Minor
	7	97.5	1.45	Minor
	8	83.1	7.19	Moderate
	9	88.4	5.68	Moderate
	10	98.6	0.746	Minor
100	1	99.6	0.196	Very minor

Retrofitted (%)	Event	Mean survival (%)	Standard deviation (%)	Damage
100	2	99.9	0.068	Very minor
	3	98.7	0.969	Minor
	4	99.9	0.062	Very minor
	5	99.8	0.169	Very minor
	6	99.8	0.076	Very minor
	7	99.9	0.043	Very minor
	8	99.7	0.309	Very minor
	9	99.7	0.122	Very minor
	10	99.9	0.032	Very minor

Table D.5: Final building envelope survival statistics for the retrofitted homes subjected to the ten individual 700-year MRI hurricane events.

Retrofitted (%)	Event	Mean survival (%)	Standard deviation (%)	Damage
0	1	-	-	-
	2	-	-	-
	3	-	-	-
	4	-	-	-
	5	-	-	-
	6	-	-	-
	7	-	-	-
	8	-	-	-
	9	-	-	-
	10	-	-	-
25	1	95.6	3.52	Minor
	2	92.2	4.79	Minor
	3	69.9	12.2	Severe
	4	97.7	2.60	Minor
	5	84.2	7.89	Moderate
	6	91.2	6.17	Minor
	7	98.3	1.72	Minor
	8	69.0	11.6	Severe
	9	85.5	7.25	Moderate
	10	98.1	1.73	Minor
50	1	96.8	1.86	Minor
	2	94.5	2.92	Minor
	3	74.9	8.68	Moderate
	4	97.8	1.59	Minor
	5	89.8	5.06	Moderate
	6	94.0	3.03	Minor
	7	98.4	1.46	Minor
	8	80.5	7.32	Moderate
	9	92.1	3.78	Minor
	10	98.9	1.12	Minor
75	1	98.5	1.02	Minor
	2	97.5	1.94	Minor
	3	87.5	4.42	Moderate
	4	99.1	0.770	Very minor
	5	95.7	2.68	Minor
	6	96.6	2.09	Minor
	7	99.3	0.791	Very minor
	8	90.5	3.68	Minor
	9	96.1	2.36	Minor
	10	99.4	0.659	Very minor
100	1	99.6	0.172	Very minor

Retrofitted (%)	Event	Mean survival (%)	Standard deviation (%)	Damage
100	2	99.9	0.081	Very minor
	3	98.7	0.889	Minor
	4	99.9	0.027	Very minor
	5	99.8	0.197	Very minor
	6	99.8	0.061	Very minor
	7	99.9	0.029	Very minor
	8	99.7	0.370	Very minor
	9	99.7	0.062	Very minor
	10	99.9	0.019	Very minor

Table D.6: Final building envelope survival statistics for the unretrofitted homes subjected to the ten individual 700-year MRI hurricane events.

Retrofitted (%)	Event	Mean survival (%)	Standard deviation (%)	Damage
0	1	56.2	3.78	Severe
	2	76.7	3.98	Moderate
	3	31.6	3.10	Destruction
	4	89.7	2.16	Moderate
	5	62.4	4.82	Severe
	6	74.9	4.33	Moderate
	7	89.7	2.17	Moderate
	8	40.4	4.43	Destruction
	9	55.1	3.46	Severe
	10	93.0	1.71	Minor
25	1	57.9	4.63	Severe
	2	78.8	4.49	Moderate
	3	36.1	5.06	Destruction
	4	90.7	2.51	Minor
	5	67.4	4.35	Severe
	6	78.0	3.95	Moderate
	7	90.7	2.66	Minor
	8	46.8	4.32	Destruction
	9	57.9	4.66	Severe
	10	94.2	1.50	Minor
50	1	58.9	5.21	Severe
	2	82.6	3.78	Moderate
	3	43.4	5.26	Destruction
	4	91.1	2.65	Minor
	5	70.5	4.92	Moderate
	6	80.7	4.15	Moderate
	7	90.4	3.13	Minor
	8	52.2	5.29	Severe
	9	59.4	4.82	Severe
	10	95.0	1.93	Minor
75	1	58.2	8.13	Severe
	2	85.9	4.79	Moderate
	3	47.9	5.97	Destruction
	4	93.2	2.63	Minor
	5	75.3	5.77	Moderate
	6	82.6	5.15	Moderate
	7	91.7	2.86	Minor
	8	59.2	6.42	Moderate
	9	63.8	5.98	Moderate
	10	96.0	1.81	Minor
100	1	-	-	-

Retrofitted (%)	Event	Mean survival (%)	Standard deviation (%)	Damage
100	2	-	-	-
	3	-	-	-
	4	-	-	-
	5	-	-	-
	6	-	-	-
	7	-	-	-
	8	-	-	-
	9	-	-	-
	10	-	-	-

REFERENCES

Abdi, H., and Molin, P. (2007). "Lilliefors test for normality." In N. Salkind (Ed.), *Encyclopedia of measurement and statistics.* (pp. 541-545). Thousand Oaks, CA: SAGE Publications, Inc. doi: 10.4135/9781412952644.n256.

American Society of Civil Engineers (1998). *Minimum design loads for buildings and other structures*, ASCE/SEI 7-98, Reston, VA: ASCE.

American Society of Civil Engineers. (2010). *Minimum design loads for buildings and other structures*, ASCE/SEI 7-10, Reston, VA: ASCE.

American Society of Testing and Materials (2011). "D 7158-11: Standard test method for wind resistance of asphalt shingles (uplift force/uplift resistance method)." ASTM International, West Conshohocken, PA, USA.

Ayyub, B. M., and McCuen, R. H. (2002). *Probability, statistics, and reliability for engineers and scientists*. Boca Raton, FL: Chapman & Hall/CRC.

Bruneau, M., Chang, S. E., Eguchi, R. T., Lee, G. C., O'Rourke, T. D., Reinhorn, A. M., Shinozuka, M., Tierney, K., Wallace, W. A., von Winterfeldt, D. (2003). "A framework to quantitatively assess and enhance the seismic resilience of communities." *Earthq. Spectra*, 19 (4), 733-752.

Bruneau, M., and Reinhorn, A. (2007). "Exploring the concept of seismic resilience for acute care facilities." *EERI Spectra J.*, 23 (1), 41-62.

Buckle, P., Marsh, G., and Smale, S. (2000). "New approaches to assessing vulnerability and resilience." *Aust. J. Emer. Manage.*, 15 (2), 8-14.

Cimellaro, G.P., Reinhorn, A.M., and Bruneau, M. (2010). "Seismic resilience of a hospital system." *Struct. Infrastruct. Eng.*, 6 (1-2), 127-144.

Datin, P.L., Prevatt, D.O., and Pang, W. (2011). "Wind-uplift capacity of residential wood roof-sheathing panels retrofitted with insulating foam adhesive." *J. Archit. Eng.*, 17 (4), 144-154.

Dao, T.N., van de Lindt, J.W., Prevatt, D.O., and Gupta, R. (2012). "Probabilistic procedure for wood-frame roof sheathing panel debris impact to windows in hurricanes." *Eng. Struct.*, 35, 178-187.

Ellingwood, B.R., and Tekie, P.B. (1999). "Wind load statistics for probability-based structural design." *J. Struct. Eng.*, 125 (4), 453-463.

Emanuel, K. A. (2013). "Downscaling CMIP5 climate models shows increased tropical cyclone activity over the 21st century." *Proceedings of the National Academy of Sciences*, 110 (30), 12219-12224.

Ewing, L. and Synolakis, C. (2011). "Coastal resilience: Can we get beyond planning the last disaster?" *In the proceedings of the Solutions to Coastal Disasters Conference*, Anchorage, AK. June 26-29, 2011. 936-946.

Federal Emergency Management Agency (2003). *Multi-hazard loss estimation methodology-Hurricane model*. HAZUS-MH Technical Manual.

Florida building code (2001). State of Florida, Tallahassee, Florida.

Gaynor, J., and Simiu, E. (2007). "The NIST-NOAA resilient communities cooperative initiative and its contribution to coastal community resilience." *Marine Tech. Soc. J.*, 41 (1), 26-32.

Georgiou, P.N. (1985). "Design windspeeds in tropical cyclone-prone regions," Doctoral dissertation, Univ of Western Ontario.

Grayson, J.M. (2011). "Development and application of a three-dimensional probabilistic wind-borne debris trajectory model." M.S. thesis. Clemson Univ. Clemson, SC.

Grayson, M., Pang, W, and Schiff, S. (2012). "Three-dimensional probabilistic wind-borne debris trajectory model for building envelope impact risk assessment." *J. Wind Eng. Ind. Aerodyn.*, 102, 22-35.

Grayson, J.M., Pang, W., and Schiff, S. (2013a). "Building envelope failure assessment framework for residential communities subjected to hurricanes." *Eng. Struct.*, 51, 245-258.

Grayson, J. M., Pang, W., and Schiff, S. (2013b). "Statistical development of an exogenous wind-borne debris generator for building envelope failure assessment models." *In the proceedings of 11th International Conference on Structural Safety and Reliability (ICOSSAR 2013)*, New York, New York, USA, June 16-20, 2013.

Grayson, J. M., Pang, W., and Schiff, S. (2013c). Accounting for exogenous wind-borne debris in building envelope failure assessment models. *In the proceedings of the 12th Americas Conference on Wind Engineering (12ACWE)*, Seattle, Washington, USA, June 16-20, 2013.

Gurley, K., Pinelli, J.-P., Subramanian, C., Cope, A., Zhang, L., Murphree, J., et al. (2005). *Florida public hurricane loss projection model engineering team. Final report*, International Hurricane Research Center, Florida International University, Miami, USA.

Harper, B.A., Kepert, J.D., and Ginger, J.D. (2010). "Guidelines for converting between various wind averaging periods in tropical cyclone conditions." Report TD-No. 1555, World Meteorol. Org., Geneva, Switzerland.

Herbin, A.H., and Barbato, M. (2012). "Fragility curves for building envelope components subject to windborne debris impact." *J Wind Eng Ind Aerodyn*, 107-8, 285-298.

Holmes, J.D. (2010). "Windborne debris and damage risk models: a review." *Wind and Struct.*, 13(2), 95-108.

Jain, V.K., and Davidson, R.A. (2007). "Forecasting changes in the hurricane wind vulnerability of a regional inventory of wood-frame houses." *J. Infrastruct. Syst.*, 13 (1), 31-42.

Kopp, G.A., Morrison, M.J., and Henderson, J.D. (2012) "Full-scale testing of low-rise, residential buildings with realistic wind loads." *J. Wind Eng. Ind. Aerodyn.*, 104-106, 25-39.

Lee, K.H., and Rosowsky, D.V. (2005). "Fragility assessment for roof sheathing failure in high wind regions." *Eng. Struct.*, 27, 857-868.

Lee, K.H., and Rosowsky, D.V. (2007). "Synthetic hurricane wind speed records: Development of a database for hazard analyses and risk studies." *Nat. Hazard. Rev.*, 8 (2), 23-34.

Li, Y., and Ellingwood, B.R. (2006). "Hurricane damage to residential construction in the US: Importance of uncertainty modeling in risk assessment." *Eng. Struct.*, 28, 1009-1018.

Li, Y., and Ellingwood, B.R. (2009). "Framework for Multihazard risk assessment and mitigation for wood-frame residential construction." *J. Struct. Eng.*, 135 (2), 159-168.

Lin, N. (2010). "Multi-hazard risk analysis related to hurricanes." Doctoral dissertation, Princeton Univ., Princeton, NJ.

Lin, N., and Vanmarcke, E. (2008). "Windborne debris risk assessment." *Probab. Eng. Mech.*, 23, 523-530.

Lin, N., and Vanmarcke, E. (2010). "Windborne debris risk analysis: Part I. Introduction and methodology." *Wind and Struct.*, 13 (2), 191-206.

Lin, N., Vanmarcke, E., and Yau, S.C. (2010). "Windborne debris risk analysis: Part II. Application to structural vulnerability modeling." *Wind and Struct.*, 13 (2), 207-220.

Liu, F., and Pang, W. (2013). "Projection of Future US Design Wind Speeds due to Changes in Hurricane Activities." *In the proceedings of the 12th Americas Conference on Wind Engineering (12ACWE)*, Seattle, Washington, USA, June 16-20, 2013.

Liu, F. (2014). "Projections of future U.S. design wind speeds and hurricane losses due to climate change." Doctoral Dissertation, Clemson Univ., Clemson, SC.

Masters, F.J., Gurley, K.R., Shah, N., Fernandez, G. (2010). "The vulnerability of residential window glass to lightweight windborne debris." *Eng. Struct.*, 32, 911-921.

McAllister, T. (2013). "Developing guidelines and standards for disaster resilience of the built environment: A research needs assessment." NIST TN-1795.

McDonald, J.R. (1990). "Impact resistance of common building materials to tornado missiles." *J Wind Eng Ind Aerodyn* 36, 717-724.

National Oceanic and Atmospheric Administration (NOAA). (2011). "Communities: The U.S. population living at the coast." <http://stateofthecoast.noaa.gov/population/welcome.html> Last accessed: 4/21/2014.

National Research Council (NRC). (2012). "Disaster resilience: A national imperative." Washington, D.C.: The National Academies Press.

National Science Board (NSB). (2007). "Hurricane warning: The critical need for a national hurricane research initiative." NSB-06-115. National Science Foundation.

National Science and Technology Council (NSTC). (2008). "Grand challenges for disaster reduction implementation plan: Hurricane." Committee on Environmental and Natural resources, Subcommittee on Disaster Reduction.

Olive, D.J. (1998). "Applied robust statistics." Doctoral dissertation, Univ. of Minnesota, Minneapolis, MN.

Pang, W., Liu, F., Fang, S., and Yue, L., (2012). "Spatial Correlation and Wind Speed Uncertainties of Hurricane Wind Field Model," *2012 Joint Conference of the Engineering Mechanics Institute and the11th ASCE Joint Specialty Conference on Probabilistic Mechanics and Structural Reliability*, Notre Dame, IN, June 2012.

Pielke, R.A. Jr., Gratz, J., Landsea, C.W., Collins, D., Saunders, M.A., Musulin, R. (2008). "Normalized hurricane damage in the United States: 1900-2005. *Nat. Hazards Rev.*, 9 (1), 29-42.

Pinelli, J.-P., Simiu, E., Gurley, K., Subramanian, C., Zhang, L., Cope, A., Filliben, J.J., and Hamid, S. (2004). "Hurricane damage prediction model for residential structures." *J. Struct. Eng.*, 130 (11), 1685-1691.

Powell, M.D., Dodge, P.P., and Black, M.L. (1991). "The landfall of Hurricane Hugo in the Carolinas: surface wind distribution." *Weather Forecast.*, 6, 379-399.

Powell, M.D., Murillo, S., Dodge, P., Uhlhorn, E., Gamache, J., Cardone, V., et al. (2010). "Reconstruction of Hurricane Katrina's wind fields for storm surge and wave hindcasting." *Ocean Eng.*, 37, 26-36.

Reinhold, T.A., Schiff, S.D., Rosowsky, D.V., Sill, B.L. (2000) "Enhanced protection from severe wind storms." *Dept. of Civil Engineering Rep. to the Federal Emergency Management Agency, Region IV Mitigation Division*, Clemson Univ., Clemson, S.C.

Reinhold, T.A., Schiff, S.D., Rosowsky, D.V., Sill, B.L. (2002) "Case for enhanced in-home protection from severe winds." *J. Arch. Eng.*, 8: 60-68.

Rosowsky, D.V, and Schiff, S.D. (2003). "What are our expectations, objectives, and performance requirements for wood structures in high wind regions?." *Nat. Hazards Rev.*, 4 (3), 144-148.

Scheer, D.L. (2005). "Large wind missile impact performance of public and commercial building assemblies." MS Thesis, College of Engineering, Florida A&M University-Florida State University, Tallahassee, FL.

Texas Tech University. (2006). "A summary report on debris impact resistance of building assemblies." Wind Science and Engineering Research Center, Texas Tech Univ., Lubbock, Texas.

Tokgoz, B.E., (2012). "Probabilistic resilience quantification and visualization building performance to hurricane wind speeds." Doctoral dissertation, Old Dominion Univ., Norfolk, VA.

Twisdale, L.A., Vickery, P.J. and Steckley, A.C. (1996). "Analysis of hurricane windborne debris impact risk for residential structures." Rpt 5303 Appl. Res. Assoc., Inc. Raleigh, NC.

U.S. Agency for International Development (USAID). (2007). "How resilient is your community? A guide for evaluating coastal community resilience to tsunamis and other hazards." U.S. Indian Ocean Tsunami Warning System Program.

U.S. Census Bureau. (2011). Census 2010. <http://factfinder2.census.gov/faces/nav/jsf/pages/index.xhtml> Last accessed: 4/21/2014.

U.S. Department of Housing and Urban Development (HUD), (2013). "Hurricane Sandy rebuilding strategy: Stronger communities, a resilient region." Hurricane Sandy Rebuilding Task Force.

Vickery, P.J., Skerlj, P.F., and Twisdale, L.A (2000). "Simulation of hurricane risk in the U.S. using empirical track model." *J. Struct. Eng.*, 126 (10), 1222-1237.

Vickery, P.J., Lin, J., Skerlj, P.F., Twisdale, L.A., and Huang, K. (2006a). "HAZUS-MH hurricane model methodology I: Hurricane hazard, terrain, and wind load modeling." *Nat. Hazards Rev.*, 7 (2), 82-93.

Vickery, P.J., Skerlj, P.F., Lin, J., Twisdale, L.A., Young, M.A., and Lavelle, F.M. (2006b). "HAZUS-MH hurricane model methodology II: Damage and loss estimation," *Nat. Hazards Rev.*, 7 (2), 94-103.

Vickery, P.J., Wadhera, D., Twisdale, L. A., and Lavelle, F. M. (2009). "U.S. hurricane wind speed risk and uncertainty." *J. Struct. Eng.*, 135 (3), 301-320.

Yau, S.C., Lin, N. and Vanmarcke, E. (2011). "Hurricane damage and loss estimation using an integrated vulnerability model." *Nat. Hazards Rev.*, 12 (4), 184-189.

Yazdani, N., Green, P., and Haroon, S. (2004). "Large wind missile performance of public and commercial building assemblies." Florida Dept. of Community Affairs, Division of Emergency Management.

Yazdani, N., Green, P. S., Haroon, S. A. (2006). "Large wind missile impact capacity of residential and light commercial buildings." *Pract. Period. Struct. Des. Constr.* 11: 206-217.